Inhomogeneous chiral symmetry breaking in isospin-asymmetric strong-interaction matter

Vom Fachbereich Physik
der Technischen Universität Darmstadt

zur Erlangung des Grades
eines Doktors der Naturwissenschaften
(Dr. rer. nat.)

genehmigte Dissertation von
M. Sc. Daniel Nowakowski
aus Heidelberg

Darmstadt 2017
D17

Inhomogeneous chiral symmetry breaking
in isospin-asymmetric strong-interaction matter

Inhomogene Chirale Symmetrie-brechende Phasen
in isospin-asymmetrischer stark-wechselwirkender Materie

Referent: Priv. Doz. Dr. Michael Buballa
Korreferent: Prof. Dr. Jochen Wambach

Tag der Einreichung: 06.04.2016
Tag der Prüfung: 25.04.2016

Abstract

In this thesis we investigate the effects of an isospin asymmetry on inhomogeneous chiral symmetry breaking phases, which are characterized by spatially modulated quark-antiquark condensates. In order to determine the relevance of such phases for the phase diagram of strong-interaction matter, a two-flavor Nambu–Jona-Lasinio model is used to study the properties of the ground state of the system. Confirming the presence of inhomogeneous chiral symmetry breaking in isospin-asymmetric matter for a simple Chiral Density Wave, we generalize the modulation of the quark-antiquark pairs to more complicated shapes and study the effects of different degrees of flavor-mixing on the inhomogeneous phase at non-zero isospin asymmetry. Then, we investigate the occurrence of crystalline chiral symmetry breaking phases in charge-neutral matter, from which we determine the influence of crystalline phases on a quark star by calculating mass-radius sequences. Finally, our model is extended through color-superconducting phases and we study the interplay of these phases with inhomogeneous chiral-symmetry breaking at non-vanishing isospin asymmetry, before we discuss our findings.

Zusammenfassung

In dieser Arbeit betrachten wir das Phasendiagram stark-wechselwirkender Materie bei nichtverschwindender Isospin-Asymmetrie und untersuchen im Rahmen eines Zwei-Flavor-Nambu–Jona-Lasinio Modells die Relevanz von inhomogenenen Phasen, in denen der chirale Ordnungsparameter räumlich variiert. Zuerst zeigen wir für eine einfache Chiral Density Wave-Modulation der Quark-Antiquark–Paare, dass inhomogene chiral-gebrochene Phasen in isospin-asymmetrischer Materie auftreten können. Im nächsten Schritt verallgemeinern wir die räumliche Modulation der Ordnungsparameter auf kompliziertere Formen und untersuchen im Detail den Einfluss des Flavor-Mixing–Grades auf die inhomogene Phase. Dabei konzentrieren wir uns auf eindimensionale räumliche Modulationen des Ordnungsarameters und analysieren zusätzlich die Auswirkungen der Forderung nach elektrischer Ladungsneutralität auf die inhomogenen chiral gebrochenen Phasen. Als Anwendung bestimmen wir daraus Masse-Radius–Beziehungen für einen Quark-Stern. Zuletzt erweiteren wir unser Modell um farbsupraleitende Phasen und studieren das Zusammenspiel zwischen solchen Phasen und inhomogen chiral-gebrochenen Phasen bei endlichen Werten der Isospin-Asymmetrie. Abschließend diskutieren und interpretieren wir unsere Ergebnisse.

Contents

1. Introduction

To understand "whatever holds the world together in its inmost folds" [1], one needs to study the properties of the four fundamental interactions in nature: gravitation, the electromagnetic, the weak and the strong interaction. Besides gravity, this was accomplished in terms of the standard model of particle physics. In the following we focus on Quantum Chromodynamics (QCD), which is believed to be the fundamental theory describing the strong interaction within the standard model. It consists of quarks and spin 1 bosons, called gluons, and is a gauge theory based on the SU(3) color group. From a theoretical point, due to complicated non-perturbative processes at low energies, it is so far not completely understood and one commonly tries to solve it by numerical ab-initio methods, although they are in general restricted in their application. Another helpful tool are effective models, which describe only few aspects of the theory and allow to understand certain aspects of QCD in a simpler way. In particular, our focus is on chiral symmetry breaking, where this symmetry is a global symmetry of QCD on the Lagrangian level. Through the breaking of the symmetry in the ground state of QCD in vacuum this allows to explain the dynamical mass generation by non-perturbative phenomena.

The phase structure of strong-interaction matter is still largely unknown and many investigations are dedicated to map out the actual phase structure. Here we will provide only an overview of the features of QCD, while the details are presented later. Until recently the phase diagram of strong interaction was believed to basically consist of two regions: one region at low temperatures and density with a confined and chirally broken phase and one at high densities and temperatures with deconfinement and chiral restoration. It was established in [2] that at least for vanishing density the deconfinement and chiral phase transition coincide. In analogy to solid state physics or more prominently the phase diagram of water, one may ask if crystalline structures are present in the phase diagram of strong-interaction matter. For the appearance of such inhomogeneous phases, fermions may condense into pairs with non-zero net momentum – which is not possible for purely homogeneous phases, where condensing fermion pairs need to have vanishing net momentum. This non-zero momentum dependence of inhomogeneous phases leads to a non-trivial spatial dependence of the condensates in position space. For chiral symmetry breaking the condensates consist of quarks and antiquarks and their spatial dependencies have so far not intensively been discussed. Only recently it gained increased attention again, although the concept of crystalline order-parameters was for example investigated by Overhauser in 1960 in the context of density waves in nuclear matter [3] or for crystalline phases in "ordinary" superconductivity by Fulde and Ferrell [4] as well as by Larkin and Ovchinnikov [5]. For color-superconductivity, model calculations confirmed that crystalline phases may be the ground state of strong-interaction

matter (e. g. [6, 7], for a review see also [8] and [9]) when (isospin) non-degenerate quark flavors are considered. In particular, only for a finite difference between the Fermi surfaces of different quark flavors, leading to a pairing stress for the quark-quark pairs, inhomogeneous color-superconducting phases are eventually energetically favored over homogeneous phases (see also [10]).

In contrast for chiral symmetry breaking it was found that even for degenerate quark flavors, inhomogeneous phases can appear. Here, a baryon-chemical potential leads to a pairing stress for the chiral condensates until at some point the condensation becomes energetically disfavored, leading to chiral restoration. Allowing for crystalline order-parameters may stabilize chiral-symmetry breaking phases against the pairing stress in comparison to constant-in-space order-parameters. Model results suggest for this case that the characteristic length-scale of the crystalline structure is directly related to the baryon-chemical potential.

Realistic descriptions of astrophysical situations or heavy-ion collision experiments require non-vanishing baryon-chemical potential and non-zero differences between the chemical potentials for different quark flavors at the same time. This is for example relevant in the context of astrophysical environments, where electric charge-neutrality for quark matter in β-equilibrium is necessary. This requires an imbalance between the quark chemical potentials for different flavors, characterized by an isospin-chemical potential. Also for experiments exploring the QCD phase diagram, model calculations with non-zero chemical potentials could provide pre- and postdictions for experimental observations that allow in turn to deepen the knowledge about the QCD phase structure at non-zero densities. Another interesting application within effective models would be to study the simultaneous appearance of inhomogeneous chiral-symmetry breaking and inhomogeneous color-superconducting phase, which implies an isospin imbalance and a non-zero baryon-chemical potential at the same time.

In this thesis the main goal is to extend the analysis of inhomogeneous chiral condensates to non-degenerate quark flavors. Since characteristic properties of the crystal lattice depend on the quark chemical potentials, it is an interesting question to study how inhomogeneous phases are affected when non-degenerate quark flavors are allowed. For this we concentrate on the formation of crystalline structures for chiral-symmetry breaking within a Nambu–Jona-Lasinio model. In contrast to former investigations we consider explicitly non-degenerate quark flavors, allowing for non-zero baryon- and isospin-chemical potentials and use a generalized four-fermion interaction, which allows to control the degree of flavor mixing explicitly. In particular, we investigate if and how different shapes for the modulation of the order-parameters are changing the phase structure, which was not possible before for isospin-symmetric strong-interaction matter where the spatial modulation of the order-parameters is identical for both quark flavors.

Since the generalized interaction of our model allows to change the degree of flavor mixing, a discussion about the influence of different degrees of flavor mixing on inhomogeneous chiral-symmetry breaking phases will also be given in this work. As a special case a realistic degree of flavor mixing is used in our approach to obtain a more realistic description of the model's phase structure at non-zero isospin-chemical potentials and allowing for inhomogeneous chiral symmetry breaking.

As an application for the resulting model phase structure at non-vanishing isospin imbalance, we consider charge-neutral quark matter in β-equilibrium, while we allow for crystalline phases. Since the core of compact stars may consist of quark matter at finite densities, inhomogeneous phases might be the energetically favored ground state there. To investigate this we apply our equation of state for charge-neutral matter to determine the mass-radius sequence for pure quark stars. Although concentrating on stars consisting purely of quark matter is too simplistic in comparison to realistic conditions for neutron stars, this nevertheless allows to gain insight about the influence of crystalline chiral-symmetry breaking to a realistic description.

Since there may be an interplay between color-superconductivity and chiral symmetry breaking, we study the effects of such a scenario for a simple modulation of the effective quarks masses and assume the quark-quark pairs associated with color superconductivity to be constant-in-space. Within this we investigate which pairing pattern is realized in the ground state and further determine the effects of an isospin-asymmetry on the system; previous investigations showed for isospin-symmetric matter already the relevance of phases where both quark-antiquark and quark-quark pairs are simultaneously present [11]. As expected quark-antiquark and quark-quark condensates are affected in different ways by an isospin-asymmetry. The resulting phase structure depends on the exact value of the isospin-chemical potential and a phase diagram is presented for vanishing temperatures.

This thesis is organized as follows: In chapter 2 we review the basics of QCD, which is the theory our model is based on. Then the details of the Nambu–Jona-Lasinio model are explained in chapter 3, while in chapter 4 we present the formalism and resulting phase structure for allowing spatially-modulated order-parameters in isospin-asymmetric matter for chiral-symmetry breaking. After this we present in chapter 5 possible applications of our results, like the phase structure for electric charge-neutral quark matter and derive mass-radius sequences for pure quark stars. In chapter 6 we study the interplay of chiral symmetry breaking and color superconductivity and present the phase structure at vanishing temperature for this configuration. Finally, we summarize our results and give an outlook on future developments in chapter 7.

2. Quantum Chromodynamics

Quantum Chromodynamics is a quantum field theory (QFT) incorporating quarks and gluons as the fundamental degrees of freedom. The quarks come in six different flavors, have spin 1/2 and carry fractional electric and baryonic charge. Gluons are characterized by carrying momentum, spin and a color degree of freedom.

QCD is a non-abelian SU(3) gauge theory constrained by renormalizability, local gauge symmetry, locality and Poincaré invariance. Its Lagrangian is defined up to gauge-fixing terms (with implicitly summing over same indices and using natural units for the ongoing discourse) by

$$\mathcal{L}_{\text{QCD}} = \overline{\psi}\left(i\gamma^{\mu}D_{\mu} - \hat{m}\right)\psi - \frac{1}{4}F^{a}_{\mu\nu}F^{\mu\nu}_{a}, \tag{2.1}$$

where ψ denotes a fermionic quark field with four Dirac-, $N_f = 6$ flavor- and $N_c = 3$ (fundamental[1]) color-degrees of freedom. $\hat{m}$ is the (diagonal) current quark mass matrix with dimension $N_f \times N_f$, describing the bare masses of the quarks generated by the electroweak interaction. The covariant derivative

$$D_{\mu} = \partial_{\mu} - ig\frac{\lambda^{a}}{2}A^{a}_{\mu} \tag{2.2}$$

represents the minimal coupling of the quarks to the gluon field A^{a}_{μ}, with λ^{a} being the a-th generator of SU(3) (the so called Gell-Mann matrices) and the gluon field strength tensor is given by

$$F^{a}_{\mu\nu} = \partial_{\mu}A^{a}_{\nu} - \partial_{\nu}A^{a}_{\mu} + gf^{abc}A^{b}_{\mu}A^{c}_{\nu}. \tag{2.3}$$

Here, f^{abc} are the (totally anti-symmetric) structure constants of the SU(3) gauge group defined by

$$[\lambda^{a}, \lambda^{b}] = if^{abc}\lambda^{c} \tag{2.4}$$

with $[\cdot,\cdot]$ being the commutator and g denotes the (unrenormalized) coupling constant of QCD (related to α_s by $g^2 = 4\pi\alpha_s$).

[1] The elements of the SU(3) gauge group of QCD are the set of unitary 3×3 matrices with determinant one and correspondingly eight (different) generators. In the fundamental representation we may represent the generators of the gauge group as a set of eight trace-less and hermitian 3×3 matrices where we refer to the rows and columns of these matrices by using so called fundamental indices, ranging from 1 to 3. In contrast, the adjoint indices enumerate the generators, ranging from 1 to 8. Quarks are in the fundamental representation of the $\text{SU}_c(3)$ color group, while gluons transform under the adjoint representation.

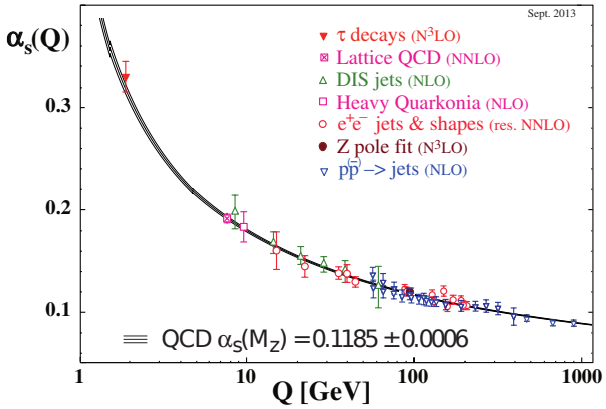

Figure 2.1.: The running coupling of QCD α_s as a function of the energy scale Q (taken from [12]). The points which are shown, were determined from different methods (for details cf. the reference).

The field strength tensor describes the kinetics of the gluons and the interaction of the gluons with each other. This is in contrast to QED possible in QCD due to the non-abelian nature of the gauge group (mirrored by the last term in Eq. (2.3)) and the gluons themselves carry color. Thus a 2-gluon term, but as well a 3-gluon and a 4-gluon vertex are contained in the theory.

Besides that QCD also features other interesting properties. For example, the Lagrangian of QCD has only one parameter besides the quark masses; namely, the dimensionless coupling g, which is actually not 'constant' but scale-dependent, as can be seen in Fig. 2.1. This quantity scales as $g^2(Q) \propto \log^{-1}(Q)$ with the characteristic momentum transfer Q of the process considered and for $Q \to \infty$ the so called asymptotic freedom shows up, which means that the coupling vanishes at large momentum transfers resp. short distances. The coupling constant rises strongly in the opposite limit at low energies resp. large distances, rendering a perturbative treatment of QCD impossible and complicating theoretical approaches. In this low energy regime also confinement prevents the appearance of colored objects: trying to separate two quarks over large distances requires large amounts of energy such that new quark pairs can be created out of the vacuum, forming new hadrons with the initial quarks. Since these hadrons are color-singlets, no colored objects are observable in QCD, which is also supported by experimental evidence and is known as confinement. In general QCD is so far not completely understood and many ongoing investigations are dedicated to gain insight on the properties of this theory.

2.1. Symmetries and properties

Of great importance are the symmetries of QCD since they allow to obtain significant information, restrictions and insights on the theory. In this section we will focus on the – for us – most important symmetries and review the connected properties and phenomena.

The QCD Lagrangian Eq. (2.1) is invariant under $\mathrm{SU}_c(3)$ gauge transformations, which is evident from the transformation laws of the different parts

$$\psi(x) \to U(x)\psi(x) \tag{2.5}$$
$$F_{\mu\nu} \to U(x)F_{\mu\nu}U^\dagger(x) \tag{2.6}$$
$$D_\mu \to U(x)D_\mu U^\dagger(x) \tag{2.7}$$
$$gA_\mu(x) \to U(x)\left(gA_\mu(x) - i\partial_\mu\right)U^\dagger(x) \tag{2.8}$$

under those local gauge transformations of the form

$$U(x) = \exp\left[i\Theta_a(x)\,\frac{\lambda^a}{2}\right] \tag{2.9}$$

that are unitary with $\Theta_a(x) \in \mathbb{R}$ being a rotation angle in color space.

Furthermore the QCD Lagrangian in the (theoretical) limit of massless quarks $\hat{m} = 0$ is invariant under global $\mathrm{SU}_V(N_f) \times \mathrm{SU}_A(N_f)$ transformations, which are defined by

$$\mathrm{SU}_V(N_f): \quad \psi \to \exp\left(\frac{\mathrm{i}}{2}\theta_a\tau^a\right)\psi \tag{2.10}$$

and

$$\mathrm{SU}_A(N_f): \quad \psi \to \exp\left(\frac{\mathrm{i}}{2}\tilde{\theta}_a\gamma_5\tau^a\right)\psi. \tag{2.11}$$

Here τ^a are unitary $N_f \times N_f$ matrices acting on flavor space[2] and γ_5 is the fifth Dirac matrix. Only for the case of massless quarks, this is an exact symmetry. However, especially in the light quark sector with up and down quarks, the symmetry turns out to be a rather good approximation because of the small bare quark masses $m_{u,d} \ll \Lambda_{\mathrm{QCD}}$, where Λ_{QCD} is a characteristic scale of QCD.

Concentrating on the chiral limit, defined by considering massless quark flavors with $m_f = 0$, the QCD Lagrangian is invariant under combined global $\mathrm{SU}_V(N_f)$ and $\mathrm{SU}_A(N_f)$ transformation (cf. Eq. (2.10) and Eq. (2.11)). In particular for $N_f = 2$ quark flavors, the Lagrangian is invariant under combined global $\mathrm{SU}_V(2)$ and $\mathrm{SU}_A(2)$ transformations and this symmetry is isomorphic to $\mathrm{SU}_L(2) \times \mathrm{SU}_R(2)$, where L/R indicates the chirality. This combined symmetry is also called the chiral symmetry and corresponds to independent SU(2) flavor rotations of the doublets (u_L, d_L) and (u_R, d_R). For a small difference between the non-vanishing quark masses $m_u - m_d \neq 0$, the chiral symmetry turns out to be still a very good approximation. In general the chiral condensate $\langle\bar{\psi}\psi\rangle$ is not invariant under $\mathrm{SU}_A(2)$ transformations and therefore serves as an associated order-parameter, indicating the breaking ($\langle\bar{\psi}\psi\rangle \neq 0$) or restoration ($\langle\bar{\psi}\psi\rangle = 0$) of the chiral symmetry. Since experimentally degenerate chiral partners are not observed, one thus concludes that the symmetry must be spontaneously broken in nature.

[2]For $N_f = 2$ the unitary 2×2 matrices are the Pauli matrices.

The ground state of QCD in the chiral limit (at vanishing density) indeed breaks the chiral symmetry spontaneously and three massless Goldstone pseudoscalar bosons are generated, since the vacuum is symmetric under $\mathrm{SU}_V(N_f) \times \mathrm{U}_V(1)$ transformations and the symmetry group of the QCD Lagrangian $\mathrm{SU}_V(N_f) \times \mathrm{SU}_A(N_f) \times \mathrm{U}_V(1)$ is larger. On the other hand, for sufficiently high temperatures a perturbative treatment of QCD as a gas of free quarks and gluons should become valid, due to asymptotic freedom of QCD. In this regime chiral symmetry is not spontaneously broken any more. Therefore one expects a transition from the region of broken chiral symmetry to a region with a chirally symmetric ground state at some critical temperature T_c. For two light quark flavors in the chiral limit, the transition can be either first or second order (see e. g. [13] and references therein). In contrast, for "real" QCD (with $N_f = 2 + 1$ flavors) the transition from broken to restored chiral symmetry at vanishing chemical potential was found to be of a rapid crossover-type and happens around a critical temperature[3] of $T_c \approx 155$ MeV [14, 15, 16].

In general massless Nambu–Goldstone bosons appear due to the spontaneous breaking of a continuous global symmetry [17, 18]. For the chiral symmetry in the light quark sector, the associated pseudoscalar bosons are the pions. These are however no real Goldstone but pseudo Goldstone bosons, since the chiral symmetry is only an approximate symmetry and thus the pions become massive, but still their masses are small compared to the scale of the strong interaction or to the masses of other hadrons.

For $N_f = 3$ flavors one would expect due to the spontaneous breaking of $\mathrm{U}_L(3) \times \mathrm{U}_R(3)$ to $\mathrm{U}_V(3)$ nine Goldstone bosons. Indeed all pions, kaons and the eta in the pseudoscalar octet are light and correspond to Goldstone bosons. However, the η' mass is not small as the others, as expected for a Goldstone boson. This was puzzling since the η' mass is associated with the $\mathrm{U}_A(1)$ symmetry. To solve this puzzle, one finally realized that there exists an axial anomaly that does not render the mass of the η' small [19] – as one would (naively) expect from the spontaneous breaking of the $\mathrm{U}_A(1)$ symmetry. In particular, the $\mathrm{U}_A(1)$ symmetry is violated on the quantum level, while quantizing QCD where the symmetry becomes explicitly broken by the axial anomaly. Assuming that the semi-classical limit is a good approximate description of QCD, instantons play a crucial role. They are semi-classical objects present due to the tunneling between infinite numbers of topologically distinct vacuum configurations, where each vacuum is defined by a parameter θ. Instantons can be regarded as effective vertices for quarks, mediating a $\mathrm{SU}_L(N_f) \times \mathrm{SU}_R(N_f)$ symmetric interaction, which breaks the $\mathrm{U}_A(1)$ symmetry [20].

For finite temperatures the thermodynamics of QCD is accessible by first-principle lattice methods, where a discretized space-time is used to simulate the action of QCD. In general one is restricted by these approaches to vanishing chemical potentials, but there exist few cases that allow to explore QCD in certain limits. This is possible, for example for $N_f = 2$ and the special case of a pure isospin chemical potential characterized

[3] Since the crossover-transition is rapid, it is still meaningful to associate a critical temperature with it.

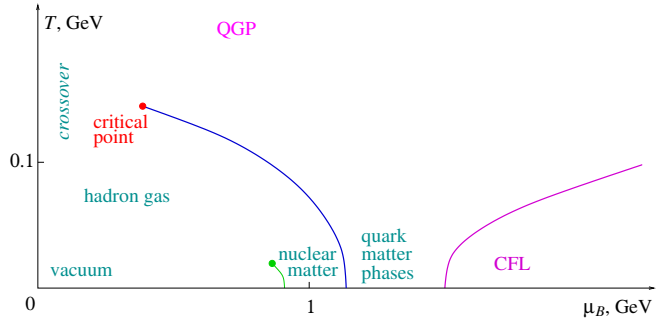

Figure 2.2.: Sketch of the QCD phase diagram (taken from [13]).

by (see e. g. [21])

$$\mu_u - \mu_d \neq 0 \tag{2.12}$$

$$\mu_u + \mu_d = 0 \tag{2.13}$$

where $\mu_{u,d}$ are the quark chemical potentials. However the major drawback of this powerful ab-initio approach of simulating full QCD, is in general the limitation to zero baryon densities, because of the sign problem due to non-vanishing chemical potentials.

Due to the conceptual problem or the lack of other first-principle results for this region of interest, most predictions of QCD for finite, non-zero densities[4] are based on effective models. For the models used, one concentrates on sharing important symmetries and aspects with QCD, which allow to make predictions for non-zero densities from the models while not considering the full underlying theory. Since there are many different models available with different predictions concerning the chiral phase transition, the nature of the phase transition is still under debate. Most model results suggest that for two quark flavors in the chiral limit the chiral phase transition is of second-order for sufficiently small baryon chemical potential, which is in accordance with lattice simulations at vanishing chemical potential and universality arguments. For intermediate densities and low temperatures many models predict a discontinuous jump of the chiral condensates from a region with broken chiral symmetry to a region with restored symmetry through a first-order phase transition. Within these models it was mostly assumed so far that $\langle\bar{\psi}\psi\rangle$ is constant in space, but also more "exotic" phases, like color-superconducting ones are possible and need to be considered for a sophisticated description.

As already mentioned in the introduction, recently different predictions for intermediate densities, like Dyson-Schwinger studies [22] or qualitative arguments based on the study of QCD in the limit of a large number of colors [23], suggest that this assumption may be too restrictive and they confirmed the relevance of spatially modulated chiral condensates. This is also supported by the findings in effective quark models [24, 25, 26].

Complementary to that, from a weak coupling analysis, it is expected that for low temperatures and very high densities the ground state of QCD should become color-

[4]Often non-zero baryon chemical potential and non-zero densities are used equivalently, although non-zero baryon chemical potential not always implies non-zero density. Hence, here we distinguish between non-zero densities and chemical potential explicitly.

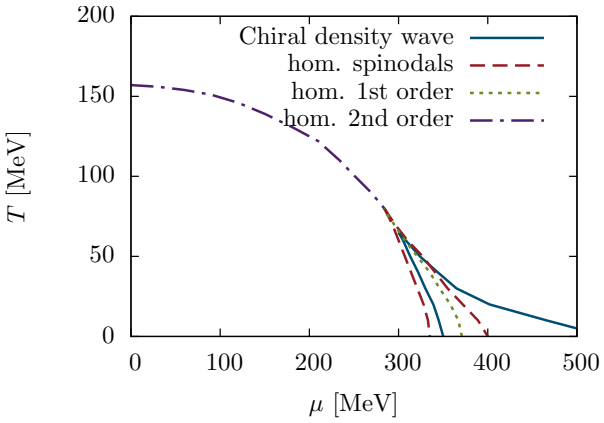

Figure 2.3.: Phase diagram from Dyson-Schwinger equations, when focusing on intermediate densities and allowing for crystalline condensates (taken from [22]).

superconducting. For intermediate densities it is however not clear, how exactly the ground state of QCD matter looks like. Current experiments have so far not proved to be very helpful to reveal details of the phase structure for this region. Future facilities like FAIR in Darmstadt and NICA at JINR [27] may explore the region at low temperatures and intermediate densities, which is of special interest for us, but also from compact stars, properties of cold and dense quark matter may be inferred.

The phase structure of QCD is in any case believed to be very rich and a large variety of predictions for the phase diagrams are available. The first conjecture goes back to Cabibbo and Parisi in 1975 [28]. They identified two regions in the temperature T-baryon density n_B plane, where quarks are confined or unconfined. In the following decades the picture of possible phases evolved and for example regions with broken or restored chiral symmetry were predicted in the QCD phase diagram. A typical sketch of the phase diagram in the $\mu_B - T$-plane is shown in Fig. 2.2, where the chiral phase transition coincides with the confinement-deconfinement transition and there is a first-order phase transition for low temperatures going up to a critical point. First, the possible existence of a QCD critical point was pointed out in 1989 within an effective model [29] and it is still not clear, if a critical point exists in QCD or not. At zero temperature the phase transition is located around baryon densities of about a few times nuclear matter density. For large baryon chemical potentials QCD matter is believed to be color-superconducting and is in the color-flavor locked (CFL) phase (see e. g. [30] for details). Focusing on the intermediate density regions, more recent results indicate a richer and potentially more complicated phase structure for the chiral symmetric resp. broken region, as seen in Fig. 2.3. Around the former first-order phase transition, the region in the QCD phase diagram may be characterized by the formation of crystalline structures, which has mostly been neglected so far. Therefore we will investigate the occurrence of such structures in the context of an effective model of QCD, which will be presented in the following chapter in detail.

3. Nambu–Jona-Lasinio model

Since in QCD non-zero baryon chemical potential poses a severe conceptual or computational problem for ab-initio methods, mostly effective models are used to explore the intermediate density region. Here we will make use of a Nambu–Jona-Lasinio (NJL) model, as an effective model of strong-interaction matter with point-like four-fermion interactions (see e. g. [31, 32, 33, 34] for a review) and concentrate on the breaking and restoration of the chiral symmetry.

Originally developed to describe field-theoretically properties of nucleons by Nambu and Jona-Lasinio [35, 36], it was after the formulation of QCD reinterpreted to incorporate quark degrees of freedoms instead of nucleons by extending the model through e. g. additional quantum numbers like color. In this model only quarks are the fundamental degrees of freedom and interact locally via n-point vertices. The interaction can be modeled to share the relevant global symmetries with QCD. For us the most important symmetry will be the chiral symmetry. The NJL model is not able to reproduce the running of the coupling or to have confinement, because of the lack of gluonic degrees of freedom in the model. To model the latter it is however possible to extend the NJL model by the Polyakov loop (see e. g. [37]), which serves as an approximate order parameter for confinement. Because the NJL model may share all (or most of) the symmetries of QCD, while being computationally much simpler, it allows to investigate non-perturbative effects of QCD in the low-energy regime and long wavelength limit and to clarify the relevant degrees of freedom. For example, since interactions of the NJL model are attractive in the quark-antiquark channel, the NJL model exhibits spontaneous symmetry breaking for small densities and temperatures, through which the quarks acquire a large effective mass.

For completeness we mention that recently it was recognized that the chiral phase transition of the NJL model is of a liquid-gas transition type, while it is not clear at present what kind of phase transition the QCD transition should be (see e. g. [38, 39, 40]).

3.1. The model

In this section we will introduce the details of our NJL model, where the focus is on chirally-invariant four-fermion interactions, that are non-renormalizable. Specifically, here we employ the two-flavor Nambu–Jona-Lasinio model in $3+1$ dimensions, defined by the Lagrangian [29, 41]

$$\mathcal{L} = \mathcal{L}_0 + \mathcal{L}_A + \mathcal{L}_B, \tag{3.1}$$

consisting of a free Dirac-part

$$\mathcal{L}_0 = \bar{\psi}(\mathrm{i}\partial\!\!\!/ - \hat{m})\psi$$

with $\partial\!\!\!/ = \gamma^\mu \partial_\mu$ and the current mass matrix $\hat{m} = \mathrm{diag}\,(m_u, m_d)$ containing the bare quark masses of up and down quarks. The two interaction parts, describing the four-fermion interaction, are given by

$$\mathcal{L}_A = G_1 \left(\left(\bar{\psi}\psi\right)^2 + \left(\bar{\psi}\vec{\tau}\psi\right)^2 + \left(\bar{\psi}\mathrm{i}\gamma_5\psi\right)^2 + \left(\bar{\psi}\mathrm{i}\gamma_5\vec{\tau}\psi\right)^2 \right), \tag{3.2}$$

$$\mathcal{L}_B = G_2 \left(\left(\bar{\psi}\psi\right)^2 - \left(\bar{\psi}\vec{\tau}\psi\right)^2 - \left(\bar{\psi}\mathrm{i}\gamma_5\psi\right)^2 + \left(\bar{\psi}\mathrm{i}\gamma_5\vec{\tau}\psi\right)^2 \right) \tag{3.3}$$

and are a linear combination of scalar $(\bar{\psi}\,\Gamma_f\,\psi)$ and pseudoscalar $(\bar{\psi}\,i\gamma_5\Gamma_f\,\psi)$ terms. $\Gamma_f \in \{1, \vec{\tau}\}$ is here an operator and τ^a denotes the Pauli matrices, both acting in the $N_f = 2$-dimensional flavor space. Here the index a runs from 1 to 3. By this, the scalar and pseudoscalar terms have contributions from iso-singlet and iso-triplett parts. In our formalism, the field ψ denotes a $4N_fN_c$-Dirac spinor, representing the quarks in our model and we will only consider $N_c = 3$ color-degrees of freedom. Furthermore γ_μ are the Dirac matrices and G_1 and G_2 are dimensionful couplings.

The two interaction parts $\mathcal{L}_A$ and $\mathcal{L}_B$ share an $\mathrm{SU}_L(2) \times \mathrm{SU}_R(2) \times \mathrm{U}(1)$ symmetry. The Lagrangian $\mathcal{L}_A$ given by Eq. (3.2) is invariant under $\mathrm{U}_A(1)$ transformations, whereas $\mathcal{L}_B$ explicitly breaks this symmetry. The two coupling constants $G_1 \geq 0$ and $G_2 \geq 0$ allow to control, if or how strongly the $U_A(1)$ symmetry is broken or – in other words – if or how strong the up- and down-quarks are coupled and interact with each other, as will become clear later on. The second interaction term Eq. (3.3) is also called 't Hooft interaction, since it is of an instanton interaction-type [42, 20]. For the special case $G_1 = G_2 = G/2$ the interaction considered, reduces to the commonly used standard interaction in NJL models

$$\mathcal{L}_{\mathrm{int}} = G \left(\left(\bar{\psi}\psi\right)^2 + \left(\bar{\psi}\mathrm{i}\gamma^5\tau^a\psi\right)^2 \right). \tag{3.4}$$

As the couplings are dimensionful with the unit of an inverse energy squared, the NJL model is non-renormalizable (at least for 3+1 dimension, as we consider it), which is due to the nature of the point-like four-fermion interaction. The model therefore needs to be regularized to render quantities finite.

3.2. Mean-field Lagrangian

To proceed, we need to derive an explicit expression for the thermodynamic potential from which we can determine all thermodynamically relevant quantities. This will be done in the so called Hartee approximation, which is equivalent to substituting the field bilinears in our model with mean fields and neglecting second-order fluctuations around the expectation values of these classical fields. For this approximation the resulting mean-field Lagrangian becomes easier, allowing us to integrate the fields out.

Writing the free part of the Lagrangian Eq. (3.1) in terms of the up and down-quark spinors u and d with $\psi = (u, d)^T$ yields

$$\mathcal{L}_0 = \bar{u}\left(\mathrm{i}\partial\!\!\!/ - m_u\right) u + \bar{d}\left(\mathrm{i}\partial\!\!\!/ - m_d\right) d \tag{3.5}$$

and analogously we arrive for the interaction parts Eq. (3.2) and Eq. (3.3) at

$$\begin{aligned}\mathcal{L}_A = 2G_1\Big(&(\bar{u}u)^2 + \left(\bar{d}d\right)^2 + (\bar{u}\mathrm{i}\gamma_5 u)^2 + \left(\bar{d}\mathrm{i}\gamma_5 d\right)^2 \\ &+ 2\left(\bar{u}d\right)\left(\bar{d}u\right) + 2\left(\bar{u}\mathrm{i}\gamma_5 d\right)\left(\bar{d}\mathrm{i}\gamma_5 u\right)\Big)\end{aligned} \tag{3.6}$$

as well as

$$\mathcal{L}_B = 4G_2\left(\left(\bar{u}u\right)\left(\bar{d}d\right) - \left(\bar{u}d\right)\left(\bar{d}u\right) - \left(\bar{u}\mathrm{i}\gamma_5 u\right)\left(\bar{d}\mathrm{i}\gamma_5 d\right) + \left(\bar{u}\mathrm{i}\gamma_5 d\right)\left(\bar{d}\mathrm{i}\gamma_5 u\right)\right). \tag{3.7}$$

Linearizing around the expectation values of the condensates, yields in a mean-field approximation

$$\begin{aligned}\mathcal{L}_{\mathrm{MF}} =&\bar{u}\left(\mathrm{i}\partial\!\!\!/ - m_u + 4G_1\left\langle\bar{u}u\right\rangle + 4G_1\mathrm{i}\gamma_5\left\langle\bar{u}\mathrm{i}\gamma_5 u\right\rangle + 4G_2\left\langle\bar{d}d\right\rangle - 4G_2\mathrm{i}\gamma_5\left\langle\bar{d}\mathrm{i}\gamma_5 d\right\rangle\right) u + \\ &\bar{u}\left(4G_1\left\langle\bar{d}u\right\rangle + 4G_1\mathrm{i}\gamma_5\left\langle\bar{d}\mathrm{i}\gamma_5 u\right\rangle - 4G_2\left\langle\bar{d}u\right\rangle + 4G_2\mathrm{i}\gamma_5\left\langle\bar{d}\mathrm{i}\gamma_5 u\right\rangle\right) d + \\ &\bar{d}\left(\mathrm{i}\partial\!\!\!/ - m_d + 4G_1\left\langle\bar{d}d\right\rangle + 4G_1\mathrm{i}\gamma_5\left\langle\bar{d}\mathrm{i}\gamma_5 d\right\rangle + 4G_2\left\langle\bar{u}u\right\rangle - 4G_2\mathrm{i}\gamma_5\left\langle\bar{u}\mathrm{i}\gamma_5 u\right\rangle\right) d \\ &\bar{d}\left(4G_1\left\langle\bar{u}d\right\rangle + 4G_1\mathrm{i}\gamma_5\left\langle\bar{u}\mathrm{i}\gamma_5 d\right\rangle - 4G_2\left\langle\bar{u}d\right\rangle + 4G_2\mathrm{i}\gamma_5\left\langle\bar{u}\mathrm{i}\gamma_5 d\right\rangle\right) u - \\ &2G_1\left(\left\langle\bar{u}u\right\rangle^2 + \left\langle\bar{d}d\right\rangle^2 + \left\langle\bar{u}\mathrm{i}\gamma_5 u\right\rangle^2 + \left\langle\bar{d}\mathrm{i}\gamma_5 d\right\rangle^2\right) - 4G_1\left(\left\langle\bar{u}d\right\rangle\left\langle\bar{d}u\right\rangle + \left\langle\bar{d}\mathrm{i}\gamma_5 u\right\rangle\left\langle\bar{u}\mathrm{i}\gamma_5 d\right\rangle\right) - \\ &4G_2\left(\left\langle\bar{d}d\right\rangle\left\langle\bar{u}u\right\rangle + \left\langle\bar{d}\mathrm{i}\gamma_5 u\right\rangle\left\langle\bar{u}\mathrm{i}\gamma_5 d\right\rangle\right) + 4G_2\left(\left\langle\bar{u}d\right\rangle\left\langle\bar{d}u\right\rangle + \left\langle\bar{u}\mathrm{i}\gamma_5 u\right\rangle\left\langle\bar{d}\mathrm{i}\gamma_5 d\right\rangle\right),\end{aligned} \tag{3.8}$$

where quadratical fluctuations were neglected.

Furthermore restricting our analysis to flavor-diagonal condensates

$$\left\langle\bar{u}\Gamma u\right\rangle \quad \text{and} \quad \left\langle\bar{d}\Gamma d\right\rangle, \tag{3.9}$$

where Γ is an arbitrary operator and assuming vanishing flavor–non-diagonal condensates

$$\left\langle\bar{f}\Gamma h\right\rangle = 0, \quad f, h \in \{u, d\},\ f \neq h \tag{3.10}$$

the mean-field Lagrangian Eq. (3.8) simplifies to

$$\begin{aligned}\mathcal{L}_{\mathrm{MF}} =&\bar{u}\left(\mathrm{i}\partial\!\!\!/ - m_u + 4G_1\left\langle\bar{u}u\right\rangle + 4G_1\mathrm{i}\gamma_5\left\langle\bar{u}\mathrm{i}\gamma_5 u\right\rangle + 4G_2\left\langle\bar{d}d\right\rangle - 4G_2\mathrm{i}\gamma_5\left\langle\bar{d}\mathrm{i}\gamma_5 d\right\rangle\right) u + \\ &\bar{d}\left(\mathrm{i}\partial\!\!\!/ - m_d + 4G_1\left\langle\bar{d}d\right\rangle + 4G_1\mathrm{i}\gamma_5\left\langle\bar{d}\mathrm{i}\gamma_5 d\right\rangle + 4G_2\left\langle\bar{u}u\right\rangle - 4G_2\mathrm{i}\gamma_5\left\langle\bar{u}\mathrm{i}\gamma_5 u\right\rangle\right) d + \\ &2G_1\left(\left\langle\bar{u}u\right\rangle^2 + \left\langle\bar{d}d\right\rangle^2 + \left\langle\bar{u}\mathrm{i}\gamma_5 u\right\rangle^2 + \left\langle\bar{d}\mathrm{i}\gamma_5 d\right\rangle^2\right) - 4G_2\left(\left\langle\bar{d}d\right\rangle\left\langle\bar{u}u\right\rangle\left\langle\bar{u}\mathrm{i}\gamma_5 u\right\rangle\left\langle\bar{d}\mathrm{i}\gamma_5 d\right\rangle\right).\end{aligned} \tag{3.11}$$

In particular Eq. (3.10) means that the possibility of charged pion condensation is neglected, which is related to the non-vanishing expectation values $\langle\bar{u}i\gamma_5 d\rangle$ and $\langle\bar{d}i\gamma_5 u\rangle$.

Since the focus is on inhomogeneous chiral symmetry breaking, we retain an explicit spatial dependence of the mean fields and follow the formalism reviewed in [43], generalizing it to isospin-asymmetric matter. By defining

$$S_u(\vec{x}) = \langle \bar{u}u \rangle \quad \text{and} \quad S_d(\vec{x}) = \langle \bar{d}d \rangle \tag{3.12}$$

for the scalar and

$$P_u(\vec{x}) = \langle \bar{u}i\gamma_5 u \rangle \quad \text{and} \quad P_d(\vec{x}) = \langle \bar{d}i\gamma_5 d \rangle \tag{3.13}$$

for the pseudoscalar mean fields, the Lagrangian Eq. (3.11) then formally has the form

$$\mathcal{L}_{\text{MF}} = \sum_{f=u,d} \mathcal{L}_f + \mathcal{L}_{\text{cond}} \tag{3.14}$$

with

$$\mathcal{L}_f = \bar{f}\Big\{ i\partial\!\!\!/ - m_f + \big[\, (4G_1 S_f(\vec{x}) + 4G_2 S_h(\vec{x})) + i\gamma_5 \,(4G_1 P_f(\vec{x}) - 4G_2 P_h(\vec{x}))\,\big] \Big\} f \tag{3.15}$$

and

$$\begin{aligned} \mathcal{L}_{\text{cond}} = -2G_1 \left(S_u(\vec{x})^2 + S_d(\vec{x})^2 + P_u(\vec{x})^2 + P_d(\vec{x})^2 \right) \\ -4G_2 \left(S_u(\vec{x}) S_d(\vec{x}) - P_u(\vec{x}) P_d(\vec{x}) \right). \end{aligned} \tag{3.16}$$

At this point it is useful to rewrite the mean-field Lagrangian as

$$\mathcal{L}_{\text{MF}} = \bar{\psi} \mathcal{S}^{-1}(\vec{x}) \psi + \mathcal{L}_{\text{cond}}, \tag{3.17}$$

where $\mathcal{S}^{-1}$ denotes the inverse propagator and is given in our approximation by

$$\mathcal{S}^{-1}(x) = \text{diag}_f \left(\mathcal{S}_u^{-1}(x), \mathcal{S}_d^{-1}(x) \right) \tag{3.18}$$

in flavor space. One component of the inverse propagator reads

$$\mathcal{S}_f^{-1}(x) = i\partial\!\!\!/ \; - m_f + 4\Big[G_1 S_f(\vec{x}) + G_2 S_h(\vec{x}) + i\gamma_5 \left(G_1 P_f(\vec{x}) - G_2 P_h(\vec{x}) \right) \Big] \tag{3.19}$$

and contains a linear combination of condensates associated with both flavors.

From these expressions, it turns out to be practical to introduce

$$\hat{M}_f(\vec{x}) = m_f - 4\big[\, (G_1 S_f(\vec{x}) + G_2 S_h(\vec{x})) + i\gamma_5 \left(G_1 P_f(\vec{x}) - G_2 P_h(\vec{x}) \right) \big], \tag{3.20}$$

as the mass function of one quark flavor, which can, after a rearrangement of the terms, also be expressed as

$$\hat{M}_f(\vec{x}) = m_f - 4 \left\{ G_1 \left[S_f(\vec{x}) + i\gamma_5 P_f(\vec{x}) \right] + G_2 \left[S_h(\vec{x}) - i\gamma_5 P_h(\vec{x}) \right] \right\}. \tag{3.21}$$

Then Eq. (3.21) shows that G_2 indeed controls the degree of flavor mixing, as for $G_2 = 0$ the mass of one flavor solely depends on the scalar and pseudoscalar condensates of the same flavor. In contrast this is not true for $G_2 \neq 0$, where the condensates of the other flavor also contribute to the mass. For $G_1/G_2 < 1$ the thermodynamic potential is unbound from below, as detailed in Appendix A.1.

As already mentioned, Eq. (3.1) reduces for equal couplings $G_1 = G_2$ to the standard NJL Lagrangian, where both quark flavors are maximally coupled.

3.3. Thermodynamic potential

To determine the thermodynamically favored ground state of the system, the grand potential per unit volume needs to be evaluated. In this section we will derive an expression for the thermodynamic potential associated with the model Lagrangian while not specifying an exact ansatz for the modulation of the condensates which will be done for several shapes of the modulation later. Since we are interested in the phase structure of the model this will be done for vanishing as well as for non-vanishing temperatures and densities.

After introducing a chemical potential matrix $\hat{\mu}$ in flavor space

$$\hat{\mu} = \mathrm{diag}_f\left(\mu_u, \mu_d\right), \tag{3.22}$$

with the quark chemical potential μ_f of flavor f on the diagonal, we can formally evaluate the grand potential per unit volume Ω, since in contrast to the original Lagrangian the mean-field Lagrangian is bilinear in the quark fields. Namely, the grand potential per volume V at a given temperature T reads in the path-integral formulation

$$\Omega_{\mathrm{MF}}(T,\hat{\mu}) = -\frac{T}{V}\log\left(\int \mathcal{D}\overline{\psi}\mathcal{D}\psi \exp\left(\int_{[0,\frac{1}{T}]\times V} d^4x_E \, \left(\mathcal{L}_{\mathrm{MF}} + \overline{\psi}\hat{\mu}\gamma^0\psi\right)\right)\right), \tag{3.23}$$

where the integral in the exponent is performed in Euclidean space-time $x_E = (\tau, \vec{x})$ with imaginary time $\tau = \mathrm{i}t$.

Performing the path integral in Eq. (3.23) by using

$$\begin{aligned}\log\int \mathcal{D}\overline{\psi}\mathcal{D}\psi \exp\left(\int_{[0,\frac{1}{T}]\times V} d^4x_E \, \left(\mathcal{L}_{\mathrm{MF}} + \overline{\psi}\hat{\mu}\gamma^0\psi\right)\right) \\ = \log\det\tilde{\mathcal{S}}^{-1}(x) + \int_{[0,\frac{1}{T}]\times V} d^4x_E \, \mathcal{L}_{\mathrm{cond}}\end{aligned} \tag{3.24}$$

for the Grassmann-valued fields ψ, $\overline{\psi}$ and the inverse propagator $\tilde{\mathcal{S}}^{-1}$ incorporating the chemical potential matrix $\hat{\mu}$, results in

$$\begin{aligned}\Omega_{\mathrm{MF}}(T,\{\mu_f\}) &= -\frac{T}{V}\mathrm{Tr}\left(\log\left(\frac{\tilde{\mathcal{S}}^{-1}(x)}{T}\right)\right) - \frac{T}{V}\int_{[0,\frac{1}{T}]\times V} d^4x_E \, \mathcal{L}_{\mathrm{cond}} \\ &= -\frac{T}{V}\mathrm{Tr}\left(\log\left(\frac{\tilde{\mathcal{S}}^{-1}(x)}{T}\right)\right) + \frac{2T}{V}\int_{[0,\frac{1}{T}]\times V} d^4x_E \, \Big(G_1\left[S_u(\vec{x})^2 + S_d(\vec{x})^2 + P_u(\vec{x})^2 + P_d(\vec{x})^2\right] \\ &\qquad + 2G_2\left[S_u(\vec{x})S_d(\vec{x}) - P_u(\vec{x})P_d(\vec{x})\right]\Big)\end{aligned} \tag{3.25}$$

for the mean-field thermodynamic potential, where the trace (indicated by Tr) runs over $[0,\frac{1}{T}]\times V$ and the color-, flavor- and Dirac-degrees of freedom.

Making the flavor structure explicit, by inserting Eq. (3.14) in Eq. (3.23), yields

$$\begin{aligned}&\Omega_{\mathrm{MF}}(T,\{\mu_f\};\{S_f\},\{P_f\}) \\ &= -\frac{T}{V}\sum_{f=u,d}\mathrm{tr}\left(\log\left(\frac{\tilde{\mathcal{S}}_f^{-1}(x)}{T}\right)\right)+\frac{2T}{V}\int_{[0,\frac{1}{T}]\times V}d^4x_E\,\big(G_1\big[S_u(\vec{x})^2+S_d(\vec{x})^2 \\ &\qquad +P_u(\vec{x})^2+P_d(\vec{x})^2\big]+2G_2\left[S_u(\vec{x})S_d(\vec{x})-P_u(\vec{x})P_d(\vec{x})\right]\big),\end{aligned} \tag{3.26}$$

where the trace does not include flavor degrees of freedom any more.

Here we used the notation $\{\mu_f\}$, $\{S_f\}$ and $\{P_f\}$ to indicate the dependence of the thermodynamic potential on the two quark chemical potentials resp. the scalar and pseudoscalar condensates per flavor. Instead, we could also rewrite the dependence of the thermodynamic potential as

$$\Omega_{\mathrm{MF}}(T,\{\mu_f\};\{S_f\},\{P_f\})\equiv\Omega_{\mathrm{MF}}(T,\{\mu_f\};\{\hat{M}_f\}), \tag{3.27}$$

since $\hat{M}_f$ is a linear combination of the scalar and pseudoscalar condensates. In general the notation on the r. h. s. of Eq. (3.27) will be our preferred method to indicate the dependence of the thermodynamic potential on the quark condensates resp. mean-fields. Furthermore we will suppress from now on the subscript of the thermodynamic potential $\Omega_{\mathrm{MF}}\equiv\Omega$.

At this point we are not really able to evaluate the thermodynamic potential and to determine the condensates or quark masses self-consistently. It turns out that the practical evaluation of the inverse propagator, entering the thermodynamic potential, is still very difficult and thus we proceed further with simplifying the expression for Ω_{MF}. By separating the time derivative of the inverse propagator $\tilde{\mathcal{S}}^{-1}(x)$ according to

$$\tilde{\mathcal{S}}^{-1}(x)\equiv\gamma^0(i\partial\!\!\!/_0-(\mathcal{H}(\vec{x})-\hat{\mu})) \tag{3.28}$$

we can identify an effective mean-field Dirac Hamiltonian

$$\mathcal{H}(\vec{x})=\mathrm{diag}_f\left(\mathcal{H}_u(\vec{x}),\mathcal{H}_d(\vec{x})\right) \tag{3.29}$$

with components

$$\mathcal{H}_f(\vec{x})=-i\gamma^0\gamma^i\partial_i+\gamma^0\hat{M}_f(\vec{x})=\begin{pmatrix}i\sigma^i\partial_i & M_f(\vec{x})\\ M_f^*(\vec{x}) & -i\sigma^i\partial_i\end{pmatrix} \tag{3.30}$$

in flavor space, where we introduced an effective quark mass

$$M_f(\vec{x})=m_f-4\left[G_1\left(S_f(\vec{x})+iP_f(\vec{x})\right)+G_2\left(S_h(\vec{x})-iP_h(\vec{x})\right)\right] \tag{3.31}$$

and used the chiral representation for gamma matrices in Eq. (3.30) to explicit the Dirac structure. Here, the mean-field Hamiltonian is hermitian and its components are time-independent, so that the Hamiltonian can in principle be diagonalized. The time-component of the functional trace of Eq. (3.25) can then be evaluated by summing

Matsubara frequencies. For this, it is convenient to switch to momentum space and expand the fields and the condensates as a Fourier series. Doing this for a system with finite volume V yields

$$\begin{aligned}\psi(x) &= \frac{1}{\sqrt{V}} \sum_{p_n} \psi_{p_n} \exp\left(-ip_n x\right) \\ &= \frac{1}{\sqrt{V}} \sum_{\omega_n} \sum_{\vec{p}_n} \psi_{p_n} \exp\left(-i\left(\omega_n \tau - \vec{p}_n \cdot \vec{x}\right)\right),\end{aligned} \tag{3.32}$$

and

$$\begin{aligned}\overline{\psi} &= \frac{1}{\sqrt{V}} \sum_{p_n} \overline{\psi}_{p_n} \exp\left(ip_n x\right) \\ &= \frac{1}{\sqrt{V}} \sum_{\omega_n} \sum_{\vec{p}_n} \overline{\psi}_{p_n} \exp\left(i\left(\omega_n \tau - \vec{p}_n \cdot \vec{x}\right)\right)\end{aligned} \tag{3.33}$$

with $\tau \in [0, T]$. Here we assumed anti-periodic boundary conditions for the time-direction and expanded the fields with respect to 4-momenta p_n given by

$$p_n = \begin{pmatrix} i\omega_n \\ \vec{p}_n \end{pmatrix}$$

with discrete Matsubara frequencies ω_n and spatial three-momenta $\vec{p}_n$. For static condensates we analogously obtain with $k_n = (0, \vec{k}_n)^\mathsf{T}$

$$M_f(\vec{x}) = \sum_{k_n} M^f_{k_n} \exp\left(-ik_n x\right) = \sum_{\vec{k}_n} M^f_{\vec{k}_n} \exp\left(i\vec{k}_n \cdot \vec{x}\right) \tag{3.34}$$

and the inverse propagator in momentum space reads (cf. Appendix A.2 for details)

$$\left(\tilde{\mathcal{S}}_f^{-1}\right)_{p_m, p_n} = \gamma^0 \left(i\omega_n \delta_{\vec{p}_n, \vec{p}_m} - \gamma^0 \vec{\gamma} \cdot \vec{p}_n \delta_{\vec{p}_n, \vec{p}_m} - \gamma^0 \sum_{\vec{k}_n} M^f_{\vec{k}_n} \delta_{\vec{p}_n, \vec{p}_m + \vec{k}_n} + \mu_f \delta_{\vec{p}_n, \vec{p}_m} \right) \delta_{\omega_m, \omega_n}, \tag{3.35}$$

which is diagonal in the Matsubara frequencies. This, in turn, also determines the component of the mean-field Hamiltonian in momentum space, where an element is given by

$$\left(\mathcal{H}_f\right)_{\vec{p}_m, \vec{p}_n} = \begin{pmatrix} -\vec{p}_m \cdot \vec{\sigma}\, \delta_{\vec{p}_m, \vec{p}_n} & M_f^+ \\ M_f^- & \vec{p}_m \cdot \vec{\sigma}\, \delta_{\vec{p}_m, \vec{p}_n} \end{pmatrix}, \tag{3.36}$$

where we defined

$$M_f^+ = \sum_{\vec{q}_k} M^f_{\vec{q}_k}\ \delta_{\vec{p}_m, \vec{p}_n + \vec{q}_k}, \tag{3.37}$$

$$M_f^- = \sum_{\vec{q}_k} (M^f_{\vec{q}_k})^*\ \delta_{\vec{p}_m, \vec{p}_n - \vec{q}_k}, \tag{3.38}$$

which are specific for a chosen ansatz of the modulation of the quark masses or condensates.

Then the thermodynamic potential can be formally expressed as

$$\Omega(T, \{\mu_f\}; \{M_f\}) = \Omega_{\text{kin}} + \Omega_{\text{cond}}\,, \tag{3.39}$$

where the condensate part is given by

$$\begin{aligned}\Omega_{\text{cond}} = \frac{2}{V}\int d^3x \,\big(G_1\left[S_u(\vec{x})^2 + S_d(\vec{x})^2 + P_u(\vec{x})^2 + P_d(\vec{x})^2\right] \\ + 2G_2\left[S_u(\vec{x})S_d(\vec{x}) - P_u(\vec{x})P_d(\vec{x})\right]\big).\end{aligned} \tag{3.40}$$

The part Ω_{kin} is given by

$$\Omega_{\text{kin}} = \sum_{f=u,d} \Omega^f_{\text{kin}}, \tag{3.41}$$

with Ω^f_{kin} being the kinetic contribution of flavor f

$$\Omega^f_{\text{kin}} = -\frac{TN_c}{V}\sum_n \text{tr}\left(\log\left(\frac{1}{T}\left(i\omega_n - \mathcal{H}_f + \hat{\mu}_f\right)\right)\right). \tag{3.42}$$

Here, the trace in color space was already performed and we are left with a sum over Matsubara frequencies and a trace over Dirac and three-momentum space.

Since the inverse propagator is diagonal in the Matsubara frequencies and as already mentioned the mean-field Hamiltonian is in principle diagonalizable, the sum over these ω_n's can be evaluated (see e. g. [44]) and finally gives

$$\Omega^f_{\text{kin}} = -\frac{N_c}{V}\sum_{\lambda_f}\left[\frac{|E_{\lambda_f} - \mu_f|}{2} + T\log\left(1 + \exp\left(-\frac{|E_{\lambda_f} - \mu_f|}{T}\right)\right)\right] + \text{const.} \tag{3.43}$$

Here we introduced λ_f as a label for the eigenstates of the Hamiltonian per flavor, E_{λ_f} are the associated eigenvalues of $\mathcal{H}_f$ and the kinetic part is only determined up to a temperature-independent constant, which we will omit in the following. Further rewriting Eq. (3.43), yields

$$\Omega^f_{\text{kin}} = -\frac{T}{V}N_c\sum_{\lambda_f}\log\left(2\cosh\left(\frac{E_{\lambda_f} - \mu_f}{2T}\right)\right). \tag{3.44}$$

Now the problem of calculating the thermodynamic potential is reduced to determining the eigenvalue spectrum of the mean-field Hamiltonian $\mathcal{H}_f$ for a given ansatz for the mass functions $M_f(\vec{x})$ or the condensates $S_f(\vec{x})$ and $P_f(\vec{x})$, which we will discuss in detail in the next chapter, where different ansätze for the mass- or condensate-modulations will be evaluated.

Figure 3.1.: Diagrammatic representation of the gap-equation. Solid lines denote the full propagator and dashed ones the bare propagator for quarks in the NJL model.

3.4. Self-consistency and gap equations

At this stage, we are in principle ready to calculate the thermodynamic potential for a given ansatz M_f (or S_f and P_f), but we need to determine the variational parameters associated to the ansatz, that enter the thermodynamic potential. In the following we will show, how to determine these parameters self-consistently in our model.

As already mentioned, chiral symmetry can be spontaneously broken in the NJL model due to the – in the scalar and pseudoscalar channel attractive – four-fermion quark-antiquark interaction (cf. Eq. (3.1)). By this symmetry breaking, large constituent quark (fermion) masses are generated and the system develops a gap in the spectrum. Energetically it is favorable for the system to display a gap in the excitation spectrum, because this leads to an overall lower energy of the system for sufficiently low temperatures $T < T_C$ and chemical potentials $\mu_f < \mu_f^c$ by lowering the negative energy branch of the dispersion relations for massive quarks. This effect, present in the form of Eq. (3.42), is counteracted by the condensate part Eq. (3.40) and the overall favored value of the gap is determined by the relative weights of the two terms.

In general the quasi-particles obtain dynamically their effective masses through the interaction with the background mean-field condensates, as schematically depicted in Fig. 3.1, which is also analogous to the BCS theory for superconductivity.

In order to determine the thermodynamically favored shape of the mass functions $\{M_f\}$ we must find the minimum of the thermodynamic potential with respect to the masses. This can be done directly by searching the minimum of the grand potential or in terms of the gap-equations, where the problem of solving self-consistently the gap-equations can be mapped to finding roots. In particular, to determine the yet unknown mean-fields $\{M_f\}$ we address a system of coupled equations

$$\frac{\partial\Omega(T,\{\mu_f\})}{\partial\{M_f\}} \stackrel{!}{=} 0, \tag{3.45}$$

from which the energetically favored shape of the mass functions can be determined. By rewriting the mass functions M_f in terms of their Fourier coefficients, one easily sees that there are infinitely many coupled equations with an in-general complicated matrix structure, which need to be solved to determine $\{M_f\}$.

Through the relation Eq. (3.20) also $\{S_f\}$ and $\{P_f\}$ can be determined by solving the gap-equations. In analogy to the stationary constraints Eq. (3.45), the condensates can

be obtained from a set of equations

$$\frac{\partial\Omega(T,\{\mu_f\})}{\partial\{S_f,P_f\}} \stackrel{!}{=} 0 \tag{3.46}$$

which needs to be solved together with Eq. (3.45) self-consistently to obtain the energetically favored shape of the condensates.

Since the gap equations exhibit a rather complicated structure, we mainly minimize the thermodynamic potential to determine the preferred value of the variational parameters.

3.5. Regularization

In general the thermodynamic potential Eq. (3.39) is quartically divergent due to the summation over all single particle energies including contributions from the vacuum state of the model. Since the NJL model is not renormalizable, we need to regularize the diverging terms in the thermodynamic potential. Unlike in renormalizable models a regularization scheme in the NJL model ultimately affects the details of the model. There exists no unique procedure to regularize model quantities (for an overview see [32]) and results will depend on the regularization scheme employed (for more details also see the appendix A.4). Furthermore the NJL model, as an effective low-energy model of QCD, is in general only applicable up to a certain energy scale, which is set by the cutoff parameter of the regularization scheme.

Also the proper choice of the regularization scheme is important when allowing for crystalline order-parameters, since otherwise unphysical or unwanted artifacts can occur, like the violation of the Silver-Blaze property through the regularized thermodynamic potential.

In the following the details of the regularization procedure will be presented. In order to prevent unwanted artifacts we follow [26] (and partly [7]) and use a covariant regularization scheme for our model. For this we need to identify the vacuum contributions in the thermodynamic potential and apply our regularization scheme only to these, as we will show in this section.

To start with regularizing the thermodynamic potential, we use that the energy spectrum of the quarks is symmetric around zero[1] and the kinetic part of the thermodynamic potential Eq. (3.43) can be rewritten as (see Appendix A.3 for details)

$$\Omega^f_{\text{kin}} = -\frac{1}{V}\sum_{E_{\lambda_f}>0}\Bigg[E_{\lambda_f} + T\ln\left(1+\exp\left(-\frac{E_{\lambda_f}+\mu_f}{T}\right)\right) + T\ln\left(1+\exp\left(-\frac{E_{\lambda_f}-\mu_f}{T}\right)\right)\Bigg], \tag{3.47}$$

[1] This is at least true for the modulations we consider throughout this work, if not otherwise stated.

where we only sum over the positive eigenenergies E_{λ_f}. This allows to identify the divergent vacuum contributions by writing

$$\Omega^f_{\text{kin}} \equiv -\frac{1}{V}\sum_{E_{\lambda_f}>0}\Big[\omega_{\text{vac}}(E_{\lambda_f}) + \omega_{\text{med}}(E_{\lambda_f};T,\mu_f)\Big]\,, \tag{3.48}$$

with the vacuum and medium contributions given by

$$\omega_{\text{vac}}(E) = E \tag{3.49}$$

and

$$\omega_{\text{med}}(E;T,\mu) = T\ln\left(1+\exp\left(-\frac{E+\mu}{T}\right)\right) + T\ln\left(1+\exp\left(-\frac{E-\mu}{T}\right)\right). \tag{3.50}$$

Only the vacuum term Eq. (3.49) generates the quartic divergencies. To remove those, we choose a Pauli-Villars regularization scheme (see [32] and Appendix A.4 for details) where $\omega_{\text{vac}}(E)$ is replaced by

$$\omega_{\text{vac}}(E) \to \omega_{\text{PV}}(E) = \sum_j c_j\sqrt{E^2+j\Lambda^2} \tag{3.51}$$

with coefficients c_j fulfilling $\sum_j c_j = 0$ and a regulator cutoff Λ. In order to remove the divergencies completely we further have to require that $\sum_j c_j(E^2+j\Lambda^2) = 0$ and $\sum_j c_j(E^2+j\Lambda^2)^2 = 0$.

The medium term Eq. (3.50) is finite and thus does not need to be regularized. If one regularizes this part also, the correct Stefan-Boltzmann limit for the grand potential will not be obtained. The thermodynamic potential in its regularized form is given by

$$\Omega(T,\{\mu_f\};\,\{M_f\}) = -\frac{1}{V}\sum_{f=u,d}\left(\sum_{E_{\lambda_f}>0}\Big[\omega_{\text{PV}}(E_{\lambda_f}) + \omega_{\text{med}}(E_{\lambda_f};T,\mu_f)\Big]\right) + \Omega_{\text{cond}}\,. \tag{3.52}$$

where Ω_{cond} is given by Eq. (3.40). Here, the final task before evaluating Ω is to determine the so far unknown model parameters (Λ, G_1, G_2) at given bare quark masses $\{m_f\}$.

To do so, we fix the parameters by fitting our model results to vacuum phenomenology for a given homogeneous, constant-in-space quark mass in vacuum M_{vac}. Parametrizing the two couplings G_1 and G_2 in terms of a 'common' coupling G and a parameter $\alpha \in [0;0.5]$[2] as

$$G_1 = (1-\alpha)\,G, \quad G_2 = \alpha\,G \tag{3.53}$$

[2] In general α may range from $-\infty$ to ∞, but as we have seen before, for $G_1/G_2 < 1$ the thermodynamic potential is unbound from below. This condition translates for our parameterization to a range of $\alpha \in (0.5;1]$.

we can obtain the parameters (Λ, G, α) instead of (Λ, G_1, G_2). Inserting Eq. (3.53) in Eq. (3.15) and Eq. (3.16) yields

$$\begin{aligned}\mathcal{L}_f =& \bar{f}\Big\{ i\partial\!\!\!/ - \Big[m_f - 4G\Big(\big(S_f(\vec{x}) + i\gamma_5 P_f(\vec{x})\big) \\ & - \alpha\big[(S_f(\vec{x}) - S_h(\vec{x})) + i\gamma_5(P_f(\vec{x}) + P_h(\vec{x}))\big]\Big)\Big]\Big\} f \end{aligned} \tag{3.54}$$

and

$$\begin{aligned}\mathcal{L}_{\text{cond}} =& -2G\Big\{ \big[S_u^2(\vec{x}) + S_d^2(\vec{x}) + P_u^2(\vec{x}) + P_d^2(\vec{x})\big] \\ & - \alpha\left[(S_u(\vec{x}) - S_d(\vec{x}))^2 + (P_u(\vec{x}) + P_d(\vec{x}))^2\right]\Big\}. \end{aligned} \tag{3.55}$$

Then for the special case of $S_u(\vec{x}) = S_d(\vec{x})$ and $P_u(\vec{x}) = -P_d(\vec{x})$, which is the usual condition realized in isospin-symmetric matter, the mean-field Lagrangian and consequently the thermodynamic potential is independent of α, from which the remaining model parameters G and Λ are determined using standard procedures (cf. Appendix A.4 for details). The remaining parameter α is (if not otherwise mentioned) treated as a free parameter and allows to control – in analogy to the former discussion – the degree of flavor mixing. The case of maximal coupling of up and down quarks corresponds to $\alpha = 0.5$, while we have $\alpha = 0$ for uncoupled quark flavors.

In the following we restrict our calculations to the chiral limit $m_f = 0$ and, if not indicated otherwise, use a Pauli-Villars regularization scheme where we require a vacuum quark mass of $M_{\text{vac}} = 300\,\text{MeV}$ and the pion decay constant (in the chiral limit) to be $f_\pi = 88$ MeV, yielding $\Lambda = 757.05\,\text{MeV}$ and $G\Lambda^2 = 6.002$ in our regularization scheme for $n_{PV} = 3$ regulators.

4. Spatially-modulated condensates

As seen in the previous chapter, the evaluation of the thermodynamic potential essentially reduces to the determination of the eigenvalue spectrum of the model by diagonalizing the Hamiltonian $\mathcal{H}$. However, this is a very demanding task when allowing for arbitrary spatial dependencies of the mean fields and thus simplifications are required. Here, our aim is to investigate periodic modulations of the order-parameter in our model, since then the approach turns out to be more tractable. As a starting point, we consider constant-in-space order parameters and derive the thermodynamic potential for this ansatz.

For convenience we introduce a flavor-averaged chemical potential

$$\bar{\mu} = \frac{1}{2}\left(\mu_u + \mu_d\right) \tag{4.1}$$

and an isospin-chemical potential

$$\mu_I = \mu_u - \mu_d, \tag{4.2}$$

which allow to parameterize the up and down quark chemical potentials as

$$\mu_u = \bar{\mu} + \frac{\mu_I}{2}, \tag{4.3}$$

$$\mu_d = \bar{\mu} - \frac{\mu_I}{2}. \tag{4.4}$$

Note that the difference between the two flavor chemical potentials can also be expressed as $\mu_u - \mu_d = 2\delta\mu$. In the literature also $\mu_I = (\mu_u - \mu_d)/2$ is used, which differs by a factor of two from our definition Eq. (4.2).

Although in astrophysical situations μ_I usually takes negative values due to the requirement of electric charge neutrality (see e. g. [45]), here we will only consider non-negative values of the isospin-chemical potential $\mu_I \geq 0$ for the following discussions. Changing the sign of μ_I only interchanges the roles of up and down quarks and therefore this presents no restriction (if $m_u = m_d$), since only the two different quark chemical potentials differentiate up from down quarks from each other (for $m_u = m_d$).

For simplicity we restrict our calculations to the chiral limit $m_u = m_d = 0$. We are aware that charged pion condensation sets in as soon as $\mu_I > m_\pi$, which in the chiral limit would correspond to $\mu_I > 0$. Here, however, the limit $m_f = 0$ will only be regarded as a useful approximation to evaluate the thermodynamic potential and we assume that charged pions do not condense below the physical pion mass.

4.1. Constant-in-space condensates

The simplest case, where chiral symmetry breaking occurs in our framework, is when the chiral condensate is spatially constant. This well-known case will be our starting point to obtain and compare results for inhomogeneous phases in the chiral limit.

For homogeneous condensates

$$S_f(\vec{x}) = S_f, \quad P_f(\vec{x}) = P_f \tag{4.5}$$

the Fourier-expanded masses Eq. (3.34) contains only the zeroth coefficient

$$\begin{aligned} M^f_{k_n} &= M^f_0 \, \delta_{\vec{k}_n,0} \\ &= \big(-4G\big[\,((1-\alpha)S_f + \alpha S_h) + i\gamma_5\,((1-\alpha)P_f - \alpha P_h)\,\big]\big)\ \delta_{\vec{k}_n,0} \end{aligned} \tag{4.6}$$

and the eigenvalues of the Hamiltonian $\mathcal{H}_f$ can be easily determined, since it is diagonal in momentum space. A generic element on the diagonal reads

$$(\mathcal{H}_f)_{\vec{p},\vec{p}} = \left(\gamma^0\vec{\gamma}\cdot\vec{p} + \gamma^0 M^f_0\right) \tag{4.7}$$

and is a 4×4 block in momentum space whose eigenvalues are twice degenerate and are given by

$$E_{\lambda_f}(\vec{p}) = \pm\sqrt{\vec{p}^2 + \left(M^f_0\right)^2}. \tag{4.8}$$

All eigenstates of the Hamiltonian can be labeled by a momentum component $\vec{p}$, which will in general not be possible any more for inhomogeneous chiral condensates.

For this ansatz the (unregularized) thermodynamic potential Eq. (3.39) reads

$$\begin{aligned} \Omega(T,\{\mu_f\};\{S_f\},\{P_f\}) = &-\frac{N_c T}{V}\sum_{f=u,d}\sum_{E_{\lambda_f}(\vec{p})}\log\left(2\cosh\left(\frac{E_{\lambda_f}-\mu_f}{2T}\right)\right) \\ &+ 2G\big((1-\alpha)\left[S_u^2+S_d^2+P_u^2+P_d^2\right] + 2\alpha\left[S_uS_d - P_uP_d\right]\big), \end{aligned} \tag{4.9}$$

which can be rewritten as

$$\begin{aligned} &\Omega(T,\{\mu_f\};\{S_f\},\{P_f\}) = \\ &-2N_c\sum_{f=u,d}\int\frac{d^3p}{(2\pi)^3}\left[\sqrt{\vec{p}^2+{M_f}^2} + T\log\left(1+\exp\left(-\frac{\sqrt{\vec{p}^2+{M_f}^2}-\mu_f}{T}\right)\right)\right. \\ &\qquad\left. + T\log\left(1+\exp\left(-\frac{\sqrt{\vec{p}^2+{M_f}^2}+\mu_f}{T}\right)\right)\right] \\ &+ 2G\big((1-\alpha)\left[S_u^2+S_d^2+P_u^2+P_d^2\right] + 2\alpha\left[S_uS_d - P_uP_d\right]\big), \end{aligned} \tag{4.10}$$

by switching from the energy summation to a momentum integral. Here we replaced M_0^f with M_f for better readability.

By changing the integration variable from momentum to energy $E = (\vec{p}^2 + M_f^2)^{1/2}$ the thermodynamic potential can also be expressed in terms of an effective density of states per flavor $\rho_f(E)$ as

$$\begin{aligned}\Omega(T, \{\mu_f\}; \{S_f\}, \{P_f\}) = -N_c \sum_{f=u,d} \int_0^\infty dE\, \rho_f(E) \big(\omega_{\text{vac}}(E) + \omega_{\text{med}}(E; T, \mu_f)\big) \\ + 2G\big((1-\alpha)\left[S_u^2 + S_d^2 + P_u^2 + P_d^2\right] + 2\alpha\left[S_u S_d - P_u P_d\right]\big),\end{aligned} \tag{4.11}$$

which is possible since an analytical expression for the eigenvalues of the mean-field Hamiltonian is known. Formally the effective density of states can be determined from its definition

$$\rho_f(E) = \frac{1}{V} \sum_{\lambda_f} \delta(E - E_{\lambda_f}), \tag{4.12}$$

which in particular reads here

$$\rho_f^{\text{hom}}(E) = \frac{1}{\pi^2} E \sqrt{E^2 - M_f^2}\, \Theta(E - M_f), \tag{4.13}$$

where the Heaviside theta function is present due to the gap of magnitude M_f in the energy spectrum (for details see also Appendix B.1).

For isospin-symmetric matter $\mu_u = \mu_d = \bar{\mu}$ the masses M_f are independent of α and become equal $M_u = M_d = M$, consequently the effective densities of state are also not dependent on the parameter α and the two kinetic parts are degenerate. This allows to perform the sum over the two flavors in Eq. (4.11) trivially; resulting in a factor N_f for the thermodynamic potential

$$\Omega(T, \mu; S, P) = -N_c N_f \int_0^\infty dE\, \rho^{\text{hom}}(E) \big[\omega_{\text{vac}}(E) + \omega_{\text{med}}(E; T, \mu)\big] + \frac{M^2}{4G}, \tag{4.14}$$

where $\pi^2 \rho^{\text{hom}}(E) = E(E^2 - M^2)^{1/2}\, \Theta(E - M)$.

The self-consistently obtained values for M at different chemical potentials are shown for the isospin-symmetric case and zero temperature in Fig. 4.1 on the left. For sufficiently small $\mu < \mu_c$ we find that a chirally broken state, indicated by a large effective mass M, is energetically favored over the restored phase (with $M = 0$) in our model. The transition from the homogeneous phase with $M \neq 0$ to the restored phase with $M = 0$ is discontinuous, i. e. of first order, at $T = 0$ (while restricting to homogeneous condensates), as can also be seen from the relative differences of the free energies in Fig. 4.1 on the right, where the homogeneous phase crosses at $\bar{\mu} = \mu_c$ the restored phase. For our special choice of model-parameters in the Pauli-Villars regularization scheme, the critical chemical potential is larger than the vacuum quark mass, namely

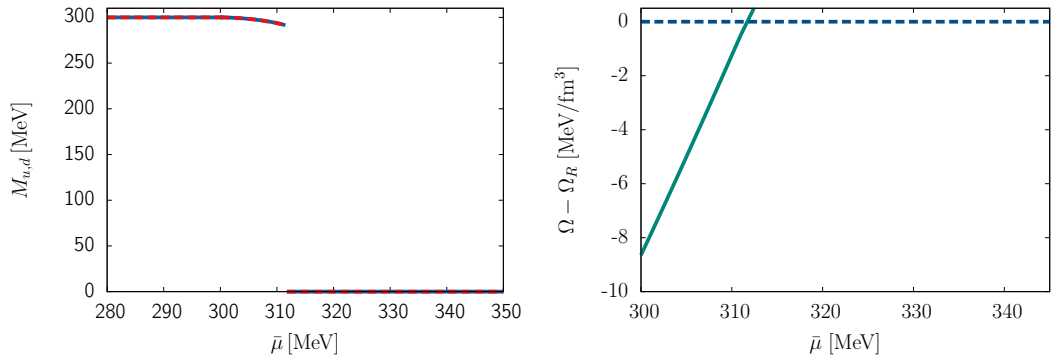

Figure 4.1.: *(Left):* Effective mass of up (solid blue) and down (dashed red) quarks against the quark chemical potential $\mu_u = \mu_d = \bar{\mu}$ at $T = 0$ for constant-in-space condensates. *(Right):* Thermodynamic potential relative to the thermodynamic potential of the restored phase against the average quark chemical potential at $T = 0$ and $\mu_u = \mu_d = \bar{\mu}$ for solutions with constant-in-space mass (solid) and vanishing mass (dashed).

$\mu_c > M_{\text{vac}} = 300\,\text{MeV}$. Thus for $\bar{\mu} \geq M_{\text{vac}}$, the effective mass begins to decrease and then drops to zero at $\bar{\mu} \geq \mu_c$. By allowing non-zero temperatures the nature of the phase transition from the homogeneous chirally broken to the restored phase changes to second order above a critical temperature $T > T_{TCP}$. In particular, at the so called tricritical point the order of the phase transition changes. This is evident in Fig. 4.2 where two distinct regions can be identified in the $\bar{\mu} - T$-plane; one with spontaneous broken chiral symmetry and one with restored chiral symmetry connected by a phase transition of first order (for $T < T_{TCP}$) resp. second order above $T \geq T_{TCP}$.

At non-vanishing isospin-chemical potential a richer phase structure emerges, since an additional dependence on the degree of flavor mixing α is present. Dependent on the value of α one flavor could, for instance, have major influence on the mass function of the other flavor (see the definition Eq. (3.31)). For zero temperature and fixed μ_I the effects of varying α are illustrated in Fig. 4.3. At $\alpha = 0$ both mass functions are only sensitive to their respective flavor chemical potential and are completely independent on the other flavor. Hence, when plotted against $\bar{\mu}$ this results in a trivial shift by $\pm\mu_I/2$ along the $\bar{\mu}$-axis with two separate first-order phase transitions, while when plotted against the respective flavor-chemical potential the order parameter of the flavor looks identical to the one of the other flavor.

On the other hand even for small $\alpha = 0.05$ the effect of one flavor on the other flavor's mass is non-negligible, as can be seen in the middle panel of Fig. 4.3, where still two first-order phase transitions are present, but not as strong as in the decoupled-flavor case. Increasing the degree of flavor mixing further results at some $\alpha \geq \alpha_c$ in the joining of the two phase-transitions, as can be seen in Fig. 4.3 for $\alpha = 0.5$. Focusing only on down quarks now (which have for $\mu_I > 0$ the smaller chemical potential than up quarks), the corresponding $\bar{\mu} - \mu_I$-phase diagram allows to discuss the influence of the up quarks on the down quarks at $T = 0$, as can be seen in Fig. 4.4. Below a critical isospin chemical

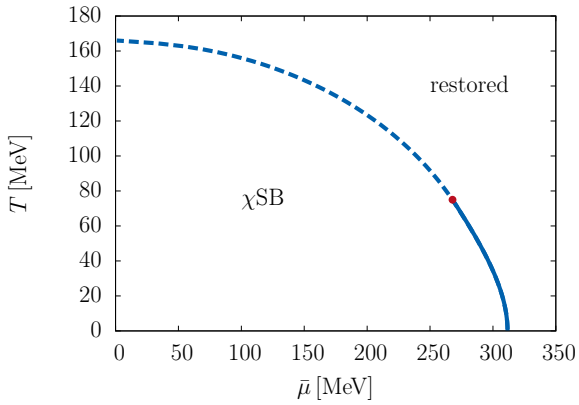

Figure 4.2.: Phase diagram at $\mu_u = \mu_d = \bar{\mu}$ for homogeneous condensates. The region with spontaneous broken chiral symmetry is indicated by χSB. Both regions are connected through a phase transition, which is of first-order (solid blue) below the critical point (red dot) and turns second-order (dashed blue) above.

Table 4.1.: Phases and corresponding order parameters for homogeneous condensates. For the pseudoscalar condensates P_f without loss of generality one always can assume $P_f = 0$ due to the chiral symmetry.

Phase	Amplitudes
(r, r)	$S_u = S_d = 0$
(r, h)	$S_u = 0, \quad S_d \neq 0$
(h, r)	$S_u \neq 0, \quad S_d = 0$
(h, h)	$S_u,\ S_d \neq 0$

potential μ_I^c the position of the down quark phase transition coincides with the phase transition for maximally coupled quarks, while for $\alpha = 0$ it agrees just for $\mu_I = 0$.

For $\alpha = 0$ the phase structure in the $\bar{\mu} - T$-plane is shown in Fig. 4.5. The phase transitions of up and down quarks do not coincide for any temperature and chemical potential except for $\mu_I = 0$, while several regions with different realizations of chiral symmetry exists. For an overview, we list all combinations in Tab. 4.1, which do not necessarily need to be realized. The different realizations of the chiral symmetry are denoted by (κ_u, κ_d), where the first column refers to up and the second one to down quarks and κ_f can label homogeneous breaking (h) or the restoration (r) of chiral symmetry. For small values of the flavor-averaged chemical potentials at fixed temperature both quarks have a large dynamically created mass, while after the phase transition of up quarks only the down quark condensates break chiral symmetry. The chiral symmetry of down quarks subsequently also gets restored for increasing chemical potential. The whole phase structure at $\alpha = 0$ can again be mapped to the phase structure of $\alpha = 0.5$ at $\mu_I = 0$, shown in Fig. 4.2, by applying a trivial shift of $\pm\delta\mu$ along the $\bar{\mu}$-axis.

Concentrating on a realistic degree of flavor mixing, which was found to be in the range

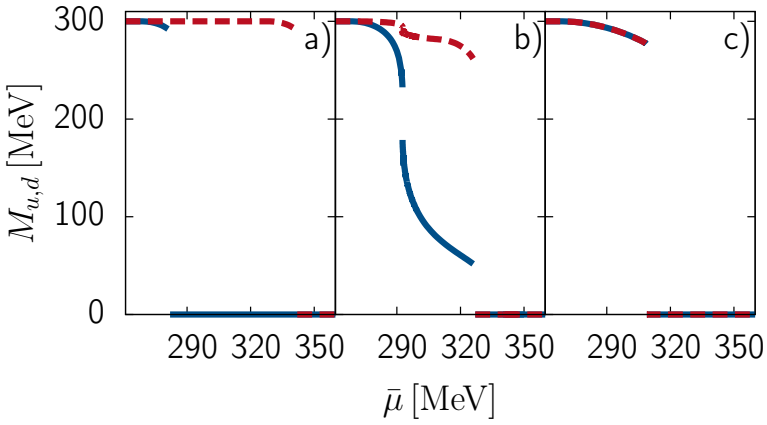

Figure 4.3.: Effective mass of up (solid blue) and down (dashed red) quarks against the average quark chemical potential at $T = 0$ and $\mu_I = 60\,\mathrm{MeV}$ for a constant-in-space chiral condensate at varying degree of flavor-mixing: a) $\alpha = 0$, b) $\alpha = 0.05$ and c) $\alpha = 0.5$.

$\alpha \approx 0.1-0.2$ [41], we choose $\alpha = 0.2$ for our purposes as a realistic degree of flavor mixing. For this degree of flavor mixing the temperature dependence of the mass functions is shown in Fig. 4.6 for two fixed values of the isospin-chemical potential. There the second-order phase transition for small enough $\bar{\mu}$ (at fixed μ_I) is easily recognized since the mass functions continuously approach zero with increasing temperature. This 'melting' of the condensates happens for larger chemical potentials instead in a discontinuous way and the phase transition to the chirally restored phase is of first order. Although the magnitudes of the mass modulations are different at non-zero μ_I – as can be seen from the figure – the phase transition of up and down quarks happen at the same chemical potential $\bar{\mu}$ and the same temperature T. In the $\bar{\mu} - T$-plane this is also true and both phase-transition lines coincide. The general behavior can be seen for the quarks in Fig. 4.7; for up quarks at $\alpha = 0.1$ and $\alpha = 0.2$ the phase transition would happen at the same line as for down quarks at the particular value of μ_I. It was found by Frank et al. [41] for a three-momentum cutoff regularization that in general already for relatively small values of α both phase-transition lines coincide, which is confirmed by our calculations.

4.2. Spatially-varying order-parameters

Turning now to the investigation of the occurrence of spatially modulated phases in isospin-asymmetric matter, where an imbalance between the quark occupation numbers is present, we are faced with the diagonalization of the mean-field Hamiltonian for spatially modulated condensates. This is a highly non-trivial task. In particular, when evaluating the Hamiltonian in momentum space one has is in general to deal with infinitely many momenta connected through the chiral condensates, which in principle require to diagonalize an infinite matrix with a continuous set of elements. To circum-

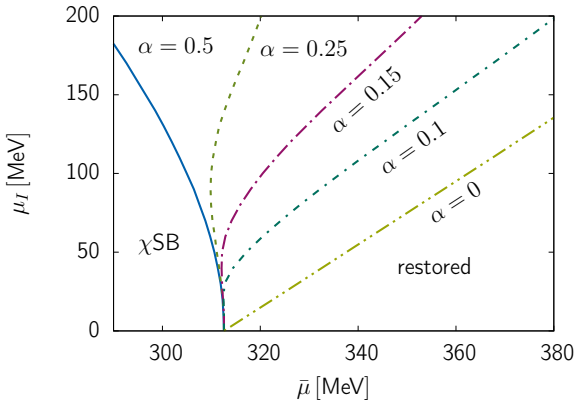

Figure 4.4.: Phase structure for down quarks at $T = 0$ for homogeneous quark masses. The lines indicate the phase boundary of down quarks for given α. Left of these lines chiral symmetry is homogeneously broken, while to the right it is restored.

vent this very complicated task, we assume periodic structures in coordinate space for the condensates, which allows to follow the formalism developed in Refs. [7, 26, 46]. There, a phase structure similar to the depicted phase diagram of QCD in Fig. 2.3 was found, as can be seen in Fig. 4.8, where a ground state with a spatially modulated order-parameter is seen in the $\mu - T$-plane. In this section we aim at generalizing the approach for crystalline structures to account for non-zero isospin-chemical potentials, allow a generalized quark-antiquark interaction and study the resulting phase structure.

In particular we require for applying the formalism, the condensate functions to be periodic, i. e. for $\vec{a}_i$ with $i = 1, 2, 3$ being linear independent vectors

$$S_f(\vec{x}) = S_f(\vec{x} + \vec{a}_i), \quad P_f(\vec{x}) = P_f(\vec{x} + \vec{a}_i) \tag{4.15}$$

or on the level of the quark masses

$$M_f(\vec{x}) = M_f(\vec{x} + \vec{a}_i) \tag{4.16}$$

holds. With this, the momenta $\vec{k}_n$ of the Fourier decomposition form a reciprocal lattice (RL) and fulfill the condition $(\vec{k}_n \cdot \vec{a}_i)/(2\pi) \in \mathbb{Z}$. From Eq. (3.36) and (3.37) one can see, that Fourier modes with $\vec{q}_k \neq 0$ couple unequal momenta and the Hamiltonian becomes non-diagonal in momentum space, as then also the inverse propagator Eq. (3.35) is. Since the condensates are non-uniform in space and thus carry non-vanishing momentum, it is possible for the quarks to change their momenta by scattering off the condensates.

Due to the restriction of allowed momenta the set of $\vec{k}_n$'s becomes discrete but still infinite. Using Bloch's theorem, all momenta can be decomposed as

$$\vec{p}_n = \vec{k}_n + \vec{q}_n, \tag{4.17}$$

where $\vec{q}_n$ belongs to the RL and $\vec{k}_n$ is an element of the Brillouin zone (BZ). Momenta $\vec{p}_m$ and $\vec{p}_n$ are only coupled if $\vec{k}_m = \vec{k}_n$ and therefore the effective mean-field Hamiltonian

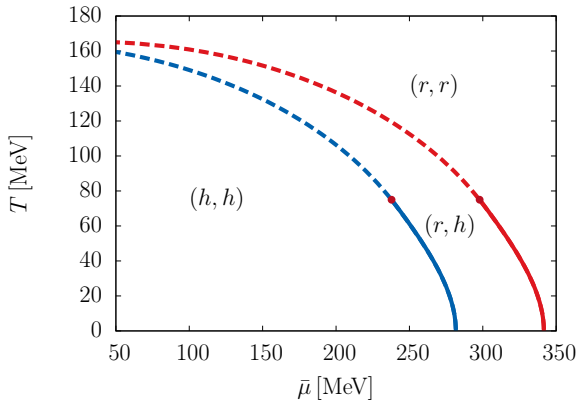

Figure 4.5.: Phase structure of up (blue) and down (red) quarks for $\alpha = 0$ at $\mu_I = 60\,\mathrm{MeV}$ and homogeneous quark masses. Solid lines indicate a first-order phase transition, while dashed lines represent second-order transitions.

Eq. (3.30) can be written as a direct product in terms of blocks associated with the momentum $\vec{k}_n = \vec{k}_m = \vec{k}$ in the BZ as

$$\mathcal{H}_f = \sum_{\vec{k}\in \mathrm{BZ}} \mathcal{H}_f(\vec{k}). \tag{4.18}$$

Since now the Hamiltonian is block-diagonal, the kinetic part of the thermodynamic potential Eq. (3.43) becomes

$$\Omega^f_{\mathrm{kin}} = -N_c \int_{\mathrm{BZ}} \frac{d^3k}{(2\pi)^3} \sum_{\lambda_f} \left(\frac{E_{\lambda_f}(\vec{k}) - \mu_f}{2} + T \log\left(1 + \exp\left(-\frac{E_{\lambda_f}(\vec{k}) - \mu_f}{T}\right)\right)\right), \tag{4.19}$$

where λ_f here labels eigenstates of $\mathcal{H}_f(\vec{k})$ and $E_{\lambda_f}(\vec{k})$ are the corresponding eigenvalues. Here we were able to transform the sum over all eigenvalues of $\mathcal{H}_f$ with a continuous set of eigenvalues into a discrete set of eigenvalues of $\mathcal{H}_f(\vec{k})$ times an integration over momentum space, rendering the numerical evaluation of the mean-field Hamiltonian and its eigenvalue spectrum in principle straightforward. Exploiting the fact that the energy spectrum is symmetric around zero again, the kinetic part can be rewritten further as

$$\begin{aligned}\Omega^f_{\mathrm{kin}} = -N_c \int_{\mathrm{BZ}} \frac{d^3k}{(2\pi)^3} \sum_{E_{\lambda_f}>0} \Bigg[& E_{\lambda_f}(\vec{k}) + T \log\left(1 + \exp\left(-\frac{E_{\lambda_f}(\vec{k}) + \mu_f}{T}\right)\right) \\ & + T \log\left(1 + \exp\left(-\frac{E_{\lambda_f}(\vec{k}) - \mu_f}{T}\right)\right)\Bigg].\end{aligned} \tag{4.20}$$

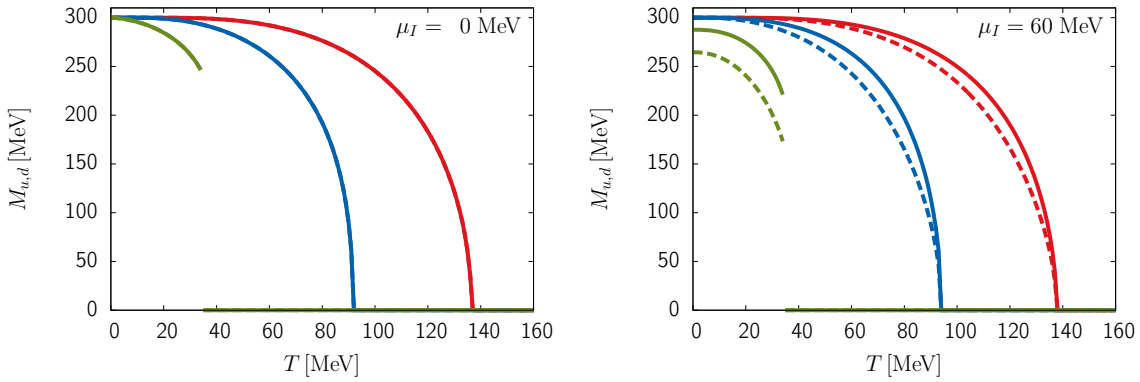

Figure 4.6.: Mass amplitudes M_f of up (solid) and down (dashed) quarks for three flavor-averaged chemical potentials: $\bar{\mu} = 170\,\text{MeV}$ (red), $\bar{\mu} = 250\,\text{MeV}$ (blue) and $\bar{\mu} = 300\,\text{MeV}$ (green) at zero temperature, $\alpha = 0.2$ and two values of μ_I for constant-in-space condensates.

The condensate part is given by

$$\Omega_{\text{cond}} = \frac{2G}{V}\int_V d^3x \Big[\left(S_u(\vec{x})^2 + S_d(\vec{x})^2 + P_u(\vec{x})^2 + P_d(\vec{x})^2\right) - \alpha\left(\left(S_u(\vec{x}) - S_d(\vec{x})\right)^2 + \left(P_u(\vec{x}) + P_d(\vec{x})\right)^2\right)\Big]. \tag{4.21}$$

4.3. Chiral Density Wave

To have a well-defined starting point, we need to specify the characteristic shape of the modulations of the condensates or mass functions. The simplest periodic ansatz for the spatial modulation of the order-parameters corresponds to a single plane wave for the modulation of the quark masses given by

$$\hat{M}(\vec{x}) = \Delta \exp\left(\mathrm{i}\gamma^5\tau^3\vec{q}\cdot\vec{x}\right), \tag{4.22}$$

which is also equivalent to limiting the number of Fourier coefficient in the Fourier transformed version of Eq. (3.30) to one (while identifying $\hat{M}_1 = \Delta$). Here Δ and $\vec{q}$ are variational parameters of the ansatz, characterizing the amplitude and the wave vector of the modulation. Specifically for this ansatz, the up and down quarks have same amplitudes and equal wave-vectors, which is often called the (Dual) Chiral Density Wave (CDW) [25].

As an alternative, but equivalent formulation, the CDW can also be written in terms of a sinusoidal modulation of the scalar and pseudoscalar condensate functions given by

$$S_f(\vec{x}) = -\frac{\Delta}{4G}\cos\left(\vec{q}_f\cdot\vec{x}\right), \quad P_f(\vec{x}) = -\frac{\Delta}{4G}\sin\left(\vec{q}_f\cdot\vec{x}\right). \tag{4.23}$$

Here we have to require the flavor-dependent wave vectors $\vec{q}_f$ to reproduce Eq. (4.22), to be of the same magnitude $|\vec{q}_u| = |\vec{q}_d| = |\vec{q}| = q$ but opposite sign $\vec{q}_u = -\vec{q}_d = \vec{q}$. The

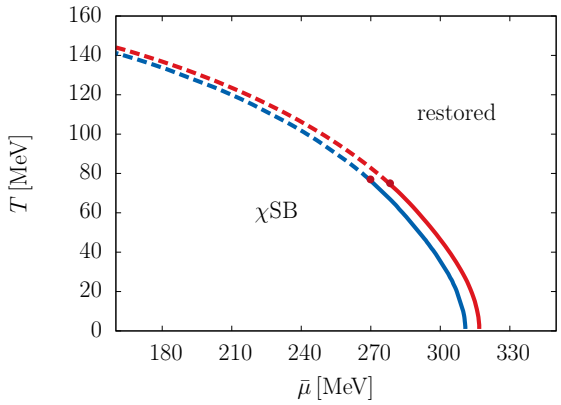

Figure 4.7.: Phase structure for $\alpha = 0.2$ (blue) and $\alpha = 0.1$ (red) at $\mu_I = 60\,\mathrm{MeV}$ and homogeneous quark masses. Here the transitions for up and down quarks coincide. Solid lines indicate a first-order phase transition, while dashed lines represent second-order transitions between the regions with broken chiral symmetry (χSB) and chiral restoration.

minus sign arises as a consequence of the isovector nature of the pseudoscalar interaction used in Eq. (3.1), which can also be seen by rewriting Eq. (4.22) as

$$\hat{M}(\vec{x}) = \Delta \left(\cos\left(\vec{q}\cdot\vec{x}\right) + \mathrm{i}\gamma^5\tau^3 \sin\left(\vec{q}\cdot\vec{x}\right)\right), \tag{4.24}$$

where the presence of τ^3 enforces $\vec{q}_u = -\vec{q}_d = \vec{q}$.

The associated effective Hamiltonian (in position space) for the CDW ansatz can be obtained from Eq. (4.22) (together with Eq. (3.29)) and is given by

$$\mathcal{H}(\vec{x}) = -i\gamma^0\gamma^i + \gamma^0\Delta \exp\left(i\gamma^5\tau^3\vec{q}\cdot\vec{x}\right). \tag{4.25}$$

The eigenvalue spectrum needs to be determined for the evaluation of the thermodynamic potential and then, in turn, the variational parameters of this ansatz (Δ, q) can be determined from minimizing Ω.

A big advantage of this approach is, that it is still possible to obtain an analytical expression for the eigenvalue spectrum [47]. For this we consider local chiral rotations per flavor to eliminate the spatial dependence from $\mathcal{H}_f$, from which the eigenvalues can be easily determined (see Appendix B.1 for a detailed discussion)

$$E^{\pm\,2} = \vec{p}^{\,2} + \Delta^2 + \frac{\vec{q}^{\,2}}{4} \pm \sqrt{\Delta^2\,\vec{q}^{\,2} + \left(\vec{p}\cdot\vec{q}\right)^2}. \tag{4.26}$$

The kinetic part of the thermodynamic potential is given by

$$\Omega^f_{\mathrm{kin}} = -N_c \sum_{\ell=\pm} \int \frac{d^3p}{(2\pi)^3} \left[E^\ell + T\log\left(1+\exp\left(-\frac{E^\ell-\mu_f}{T}\right)\right)\right. \tag{4.27}$$
$$\left. + T\log\left(1+\exp\left(-\frac{E^\ell+\mu_f}{T}\right)\right)\right]$$

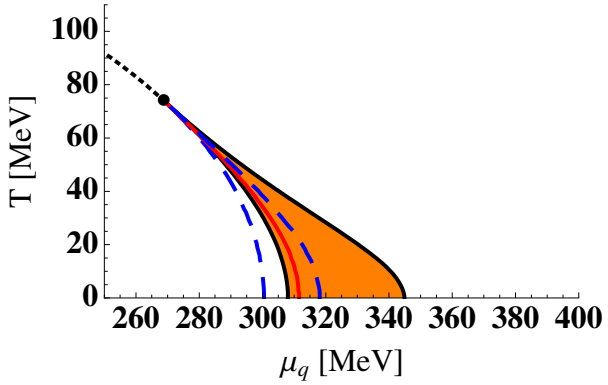

Figure 4.8.: Phase diagram of the NJL model for isopin-symmetric matter, when allowing for crystalline structures (taken from [26]). The shaded area indicates where an inhomogeneous phase is energetically favored.

and can be written in terms of an effective density of states

$$\begin{aligned}\rho^{\mathrm{CDW}}(E) =& \frac{E}{2\pi^2}\Bigg[\sqrt{\left(E-\frac{q}{2}\right)^2-\Delta^2}\,\theta\left(E-\frac{q}{2}-\Delta\right)\\ &+\sqrt{\left(E+\frac{q}{2}\right)^2-\Delta^2}\,\theta\left(E-\frac{q}{2}+\Delta\right)\theta\left(E+\frac{q}{2}-\Delta\right)\\ &+\left(\sqrt{\left(E+\frac{q}{2}\right)^2-\Delta^2}-\sqrt{\left(E-\frac{q}{2}\right)^2-\Delta^2}\right)\theta\left(\frac{q}{2}-\Delta-E\right)\Bigg]\end{aligned} \tag{4.28}$$

as

$$\begin{aligned}\Omega^f_{\mathrm{kin}} = -N_c\int_0^\infty dE\;\rho^{\mathrm{CDW}}(E)\Bigg[E+T\log\left(1+\exp\left(-\frac{E-\mu_f}{T}\right)\right)\\ +T\log\left(1+\exp\left(-\frac{E+\mu_f}{T}\right)\right)\Bigg].\end{aligned} \tag{4.29}$$

The condensate part can be obtained by inserting Eq. (4.23) into Eq. (3.40) and is explicitly given by

$$\Omega_{\mathrm{cond}} = \frac{\Delta^2}{4G}. \tag{4.30}$$

For isospin-symmetric matter the amplitude Δ and the wave number q are shown in the left panel of Fig. 4.9. First, a homogeneous phase with $q = 0$ is favored, then at intermediate values of $\bar{\mu}$ the amplitude has smaller values and at the same time the wave number becomes non-zero, indicating the favorisation of the inhomogeneous phase. The phase transition from the homogeneous broken to the inhomogeneous phase is of first order and there the amplitude drops in a discontinuous way. The onset of the spatially modulated phase is located at smaller values of $\bar{\mu}$ than the critical chemical potential for homogeneous condensates only. The wave number jumps at the onset from zero to

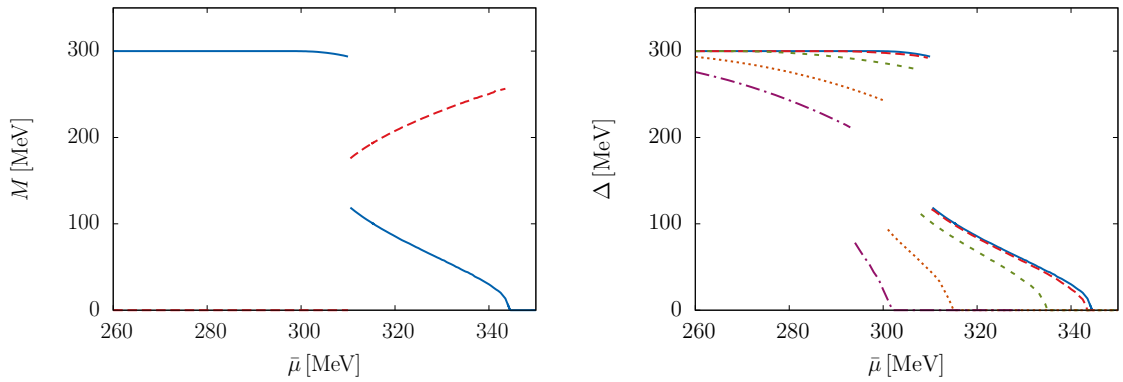

Figure 4.9.: Variational parameters allowing for a CDW at $T = 0$ against the flavor-averaged chemical potential $\bar{\mu}$. *(Left):* Amplitude (solid blue) and wave number (dashed red) at $\mu_I = 0$. *(Right):* Amplitude at $\mu_I = 0$ (solid blue), $\mu_I = 20\,\text{MeV}$ (long-dashed red), $\mu_I = 60\,\text{MeV}$ (dashed green), $\mu_I = 100\,\text{MeV}$ (dotted orange) and $\mu_I = 120\,\text{MeV}$ (dash-dotted purple).

a non-zero value and grows when the chemical potential is increased. In particular, it is found that the wave number is approximately proportional to the chemical potential $\bar{\mu}$. For even larger $\bar{\mu}$, the amplitude Δ continuously approaches zero in a second-order phase transition and the inhomogeneous chiral symmetry-breaking solution becomes disfavored against the restored phase with intact chiral symmetry. The phase diagram in the $\bar{\mu} - T$-plane is similar to the one in Fig. 4.8 and is shown together with the phase diagrams at non-zero μ_I in the upper left panel of Fig. 4.11. The chiral phase boundary for homogeneous condensates only, is completely covered by the inhomogeneous region. For large temperatures the phase boundaries of the CDW region meet in a critical point, marking the upper end of the inhomogeneous region along the temperature axis.

For the CDW the thermodynamic potential is the same for every degree of flavor-mixing, even in isospin-asymmetric matter, since the kinetic part Eq. (4.29) and the condensate part Eq. (4.30) are independent of the degree of flavor mixing α for this type of modulation. Thus, the CDW solutions are relevant for all degrees of flavor mixing, but not necessarily the most favored one, as we will see later.

The results at $T = 0$ for isospin-asymmetric matter are shown in the right panel of Fig. 4.9. One sees that the transition from the homogeneous phase with $q = 0$ to the inhomogeneous phase with $q \neq 0$ is still of first order and the amplitude drops there too. For increasing μ_I, the onset and the upper end of the inhomogeneous window shift along the $\bar{\mu}$-axis to lower values. Because the upper critical chemical potential $\bar{\mu}_{c,2}$ is shifted to smaller values more rapidly than the lower one $\bar{\mu}_{c,1}$, the size of the inhomogeneous window is effectively decreasing for increasing μ_I. The spatially modulated phase is connected to the restored phase via a second-order phase-transition and for increasing $\bar{\mu}$ the CDW amplitude is continuously approaching zero, as in isospin-symmetric matter.

Energetically the CDW is favored at $T = 0$ and fixed $\bar{\mu}$ below a critical isospin chemical potential μ_I^c, as can be seen for $\bar{\mu} = 320\,\text{MeV}$ in Fig. 4.10. At small μ_I the

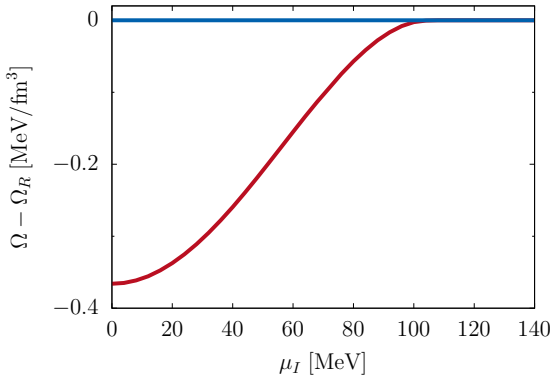

Figure 4.10.: Thermodynamic potential for a CDW modulation (solid red) relative to the thermodynamic potential of the restored phase (blue) against the isospin-chemical potential μ_I at zero temperature and $\bar{\mu} = 320\,\mathrm{MeV}$.

CDW solution has a larger pressure than the restored phase, but for increasing μ_I the difference between the two pressures continuously gets smaller, until the CDW solution reaches a critical isospin chemical potential and vanishes.

As can be seen for four values of μ_I in Fig. 4.11, the inhomogeneous phases in the $\bar{\mu} - T$-plane exist around intermediate chemical potentials resp. densities and low temperatures. For $\mu_I \neq 0$, although the inhomogeneous region in the $\bar{\mu} - T$-plane shrinks for increasing isospin-chemical potential, an inhomogeneous chiral-symmetry breaking phase is present in the phase diagram. Like for $\mu_I = 0$, the phase transition at $\mu_I \neq 0$ from the homogeneous to the inhomogeneous phase is of first-order and from the inhomogeneous to the restored phase is of second order. At a critical temperature T_c the boundaries of the inhomogeneous phase coincide and above an inhomogeneous solution is not favored any more.

Since we have seen that the amplitude of the modulation depends on the chemical potential and the values of the wave vector are approximately proportional to the chemical potential, it is clear that providing the same wave vector for up and down quarks or equal amplitudes may present a severe restriction in isospin-asymmetric matter, because of the two flavors favoring different wave vectors or amplitudes. Therefore, as a next step, we need to check if inhomogeneous solutions with different amplitudes and unequal wave vectors can occur and if they are more favored than the CDW.

4.4. Plane-wave modulation for the quark masses

To relax the requirement of equal amplitudes and wave vectors for the two flavors, we study now a plane wave modulation of the mass functions according to

$$\hat{M}_f(\vec{x}) = \Delta_f \exp\left(\mathrm{i}\gamma^5 \vec{q}_f \cdot \vec{x}\right), \tag{4.31}$$

where the up and down quark masses are allowed to have different amplitudes Δ_f and wave vectors. For simplicity we will refer to this ansatz as the "mass ansatz". By

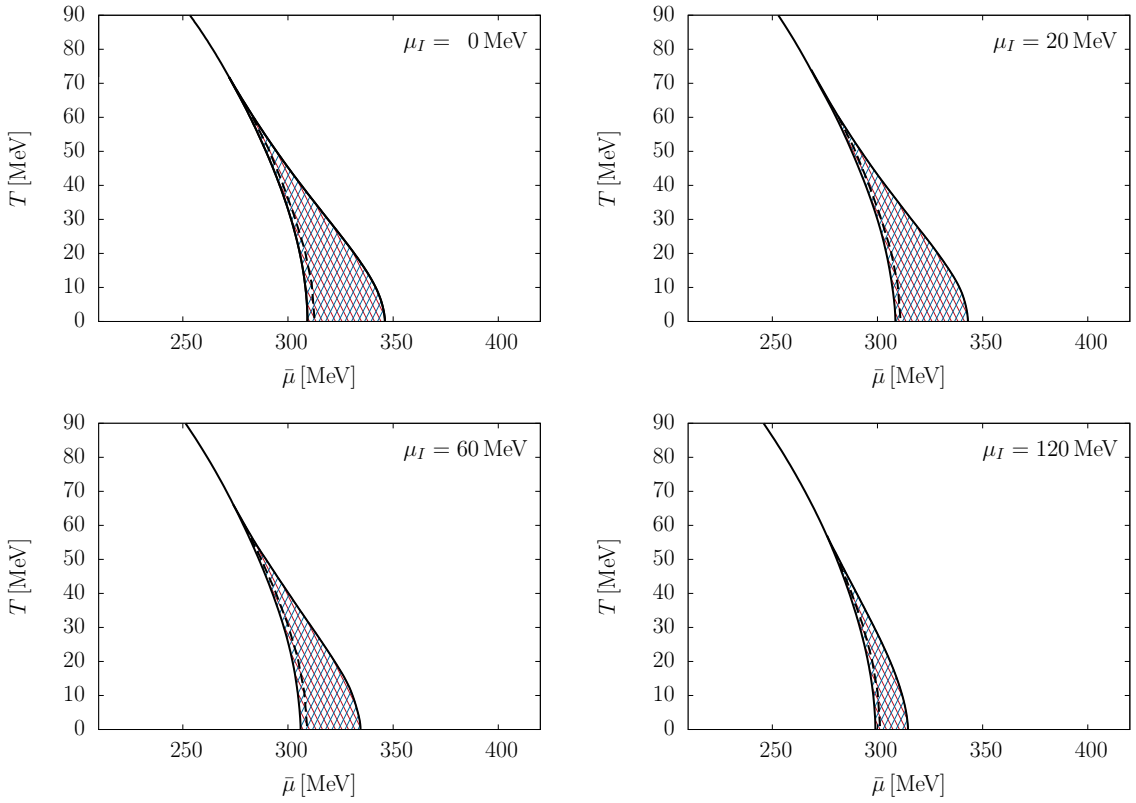

Figure 4.11.: Phase structure allowing for a CDW modulation in the $\bar{\mu} - T$-plane for four values of the isospin-chemical potential. In the shaded region an inhomogeneous region is favored. To the left (right) of the inhomogeneous phases, homogeneous broken (restored) solutions are favored. For reference the chiral phase boundaries of homogeneous matter are also shown (dashed lines).

enforcing the amplitudes and the wave vectors of up and down quarks to be equal by requiring $\Delta_u = \Delta_d = \Delta$ and $\vec{q}_u = -\vec{q}_d = \vec{q}$, we recover the CDW given in Eq. (4.22) from the mass ansatz.

The condensate functions can be determined for this ansatz by rewriting the mass functions

$$\hat{M}_f(\vec{x}) \equiv -4G\left(X_f(\vec{x}) + i\gamma^5 Y_f(\vec{x})\right), \tag{4.32}$$

in terms of a real and imaginary part. The condensates are given (see Appendix B.2 for a derivation) by

$$S_f(\vec{x}) = \frac{1}{4G\,(2\alpha - 1)}\left[(1-\alpha)\Delta_f \cos\left(\vec{q}_f \cdot \vec{x}\right) - \alpha\Delta_h \cos\left(\vec{q}_h \cdot \vec{x}\right)\right], \tag{4.33}$$

and

$$P_f(\vec{x}) = \frac{1}{4G\,(2\alpha - 1)}\left[(1-\alpha)\Delta_f \sin\left(\vec{q}_f \cdot \vec{x}\right) + \alpha\Delta_h \sin\left(\vec{q}_h \cdot \vec{x}\right)\right]. \tag{4.34}$$

In analogy to the former section, the eigenvalue spectrum can be still determined by applying local chiral rotations (see Appendix B.1 for a detailed discussion) to eliminate the space-dependence of $\mathcal{H}$. In contrast to the CDW case, this needs to be done on the level of the flavor components of the mean-field Hamiltonian

$$\mathcal{H}_f(\vec{x}) = -i\gamma^0\gamma^i + \gamma^0\Delta_f \exp\left(i\gamma^5\vec{q}_f\cdot\vec{x}\right). \tag{4.35}$$

After applying the chiral rotation, the eigenvalues associated with flavor f can be easily determined and they are given by

$$E_f^{\pm\,2} = \vec{p}^{\,2} + \Delta_f^2 + \frac{\vec{q}_f^{\,2}}{4} \pm \sqrt{\Delta_f^2\,\vec{q}_f^{\,2} + \left(\vec{p}\cdot\vec{q}_f\right)^2}. \tag{4.36}$$

These eigenvalues can be encoded in a flavor-dependent density of states

$$\begin{aligned}\rho_f^{\mathrm{mpw}}(E) =& \frac{E}{2\pi^2}\Big[\sqrt{\left(E-\frac{q_f}{2}\right)^2-\Delta_f^2}\;\theta\left(E-\frac{q_f}{2}-\Delta_f\right)\\ &+\sqrt{\left(E+\frac{q_f}{2}\right)^2-\Delta_f^2}\;\theta\left(E-\frac{q_f}{2}+\Delta_f\right)\theta\left(E+\frac{q_f}{2}-\Delta_f\right)\\ &+\left(\sqrt{\left(E+\frac{q_f}{2}\right)^2-\Delta_f^2}-\sqrt{\left(E-\frac{q_f}{2}\right)^2-\Delta_f^2}\right)\theta\left(\frac{q_f}{2}-\Delta_f-E\right)\Big],\end{aligned} \tag{4.37}$$

from which we can generalize the kinetic part Eq. (4.27) of the CDW grand potential to account for the mass ansatz according to

$$\begin{aligned}\Omega_{\mathrm{kin}}^f = -N_c\int_0^\infty dE\;\rho_f^{\mathrm{mpw}}(E)\Bigg[E + T\log\left(1+\exp\left(-\frac{E-\mu_f}{T}\right)\right)\\ + T\log\left(1+\exp\left(-\frac{E+\mu_f}{T}\right)\right)\Bigg].\end{aligned} \tag{4.38}$$

To arrive at an expression for the condensate part, we insert Eqn. (4.33) and (4.34) in Eq. (3.40), which yields

$$\Omega_{\mathrm{cond}} = \frac{1}{8GV\left(1-2\alpha\right)}\int_V d^3x\,\Big[\left(1-\alpha\right)\left(\Delta_u^2+\Delta_d^2\right) - 2\alpha\Delta_u\Delta_d\cos\left(\left(\vec{q}_u+\vec{q}_d\right)\cdot\vec{x}\right)\Big]. \tag{4.39}$$

Since here $\vec{q}_u = -\vec{q}_d$ or $\vec{q}_u \neq -\vec{q}_d$ is possible, we need to distinguish between these two cases in the condensate part. For the first case $\vec{q}_u = -\vec{q}_d$, the integration over the sum in Eq. (4.39) can be performed trivially, because the summands have no space-dependence. The condensate part for this case then reads

$$\Omega_{\mathrm{cond}} = \frac{1}{8G}\,\frac{1}{1-2\alpha}\left[\left(1-\alpha\right)\left(\Delta_u^2+\Delta_d^2\right) - 2\alpha\Delta_u\Delta_d\right]. \tag{4.40}$$

For $\vec{q}_u \neq \vec{q}_d$ in contrast, we need to integrate over the oscillating cosine function. Since we integrate over a Wigner-Seitz cell[1], this basically amounts to integrate the function over one period, so that in the end the integral over the cosine vanishes. Then, the condensate part is given for $\vec{q}_u \neq -\vec{q}_d$ by

$$\Omega_{\text{cond}} = \frac{1}{8G}\frac{1}{1-2\alpha}\left[(1-\alpha)\left(\Delta_u^2+\Delta_d^2\right)\right] \tag{4.41}$$

and we have in general for the condensate part of the mass ansatz

$$\Omega_{\text{cond}} = \frac{1}{8G}\frac{1}{1-2\alpha}\begin{cases}\left[(1-\alpha)\left(\Delta_u^2+\Delta_d^2\right)-2\alpha\Delta_u\Delta_d\right], & \vec{q}_u=-\vec{q}_d\\ \left[(1-\alpha)\left(\Delta_u^2+\Delta_d^2\right)\right], & \vec{q}_u\neq-\vec{q}_d\end{cases}. \tag{4.42}$$

Considering different amplitudes, the thermodynamic potential does depend on the degree of flavor mixing. In particular for this case, the α-dependence is present solely in the condensate part Eq. (4.42), which for $\alpha = 0.5$ diverges, unless $\Delta_u = \Delta_d$ and $\vec{q}_u = -\vec{q}_d$. In order to allow to investigate the mass ansatz and not only the CDW case, we will limit ourselves to $\alpha \neq 0.5$ first, but later take the limit $\alpha \to 1/2$ for the condensate part (see also Appendix B.2 for details).

Since the kinetic part of the thermodynamic potential is independent of α, the flavor mixing of the two flavors happens solely through the condensate part. Inspecting the two expressions for the condensate part, we note that for $0 < \alpha < 0.5$ the condensate part Eq. (4.40) is energetically favored over Eq. (4.41). The condensate part prefers $\vec{q}_u = -\vec{q}_d$, while the kinetic part favors wave-numbers $|\vec{q}_f|$ of the order μ_f – irrelevant of the direction of $\vec{q}_f$. Then, the decision if equal or unequal wave vectors are favored during the minimization of the grand potential, depends only on the relative weight of the kinetic against the condensate part of the thermodynamic potential.

In the following the variational parameters of the ansatz are determined for different degrees of flavor mixing and the resulting phase structure is studied. We start with completely decoupled quark flavors, since this allows to perform the study at $\mu_I \neq 0$ in a well-defined way; namely, the results for isospin-symmetric matter can be related to $\mu_I \neq 0$, as it was the case for homogeneous condensates. In analogy to former results we distinguish between different phases, dependent on which of the order-parameter is zero or non-zero. These are listed for inhomogeneous chiral-symmetry breaking phases in Tab. 4.2. Besides the indication whether chiral symmetry is homogeneously broken (h) or restored (r), we need to introduce a third label to show that the chiral symmetry for this flavor is inhomogeneously broken (i). In the following we discuss the dependence of flavor mixing for the mass ansatz and analyze if unequal amplitudes or wave vectors are favored.

4.4.1. Completely decoupled quark flavors

For $\alpha = 0$ both quark flavors are completely decoupled and the two cases Eq. (4.40) and Eq. (4.41) for the condensate part become equivalent. As a consequence, visible

[1] A Wigner-Seitz cell is a primitive cell in the crystalline lattice formed by the condensates. From this unit cell the entire direct space can be constructed and corresponds to the first Brillouin zone in reciprocal space.

Table 4.2.: Phases and corresponding order parameters for a plane wave modulation.

Phase	Amplitudes	Wave numbers
(r,r)	$\Delta_u = \Delta_d = 0$	—
(r,h)	$\Delta_u = 0, \quad \Delta_d \neq 0$	$q_d = 0$
(r,i)	$\Delta_u = 0, \quad \Delta_d \neq 0$	$q_d \neq 0$
(h,r)	$\Delta_u \neq 0, \quad \Delta_d = 0$	$q_u = 0$
(i,r)	$\Delta_u \neq 0, \quad \Delta_d = 0$	$q_u \neq 0$
(h,h)	$\Delta_u,\ \Delta_d \neq 0$	$q_u = q_d = 0$
(i,h)	$\Delta_u,\ \Delta_d \neq 0$	$q_u \neq 0, \quad q_d = 0$
(h,i)	$\Delta_u,\ \Delta_d \neq 0$	$q_u = 0, \quad q_d \neq 0$
(i,i)	$\Delta_u,\ \Delta_d \neq 0$	$q_u,\ q_d \neq 0$

in Fig. 4.12 at $T = 0$ and several values of μ_I, the up and down quark amplitudes can also here be mapped to the result at $\mu_I = 0$ by applying a trivial shift of $\pm\mu_I/2$ when plotted against $\bar{\mu}$, as already seen for the amplitudes in the homogeneous case. In particular, since the thermodynamic potential separates into two independent parts associated with the respective quark flavor, unequal amplitudes and wave vectors become always preferred at $\mu_I \neq 0$ for the inhomogeneous phases in this scenario.

For $\mu_I = 0$ we recover the CDW phase structure in the $\bar{\mu} - T$-plane, which is not surprising since for isospin-symmetric matter up and down quarks are degenerate and they prefer to have the same amplitudes and wave vectors.

In Fig. 4.13 the $\bar{\mu} - T$ phase structure for $\alpha = 0$ is shown. In general we find that the phase boundaries of up and down quarks are simply shifted with respect to each other, when plotted against the averaged chemical potential. For small values of μ_I the inhomogeneous phases associated with up and down quarks partially overlap in a coexistence region. Increasing the isospin-asymmetry, leads to a shrinking of the size of the coexistence region until it vanishes at $\mu_I \approx 38\,\mathrm{MeV}$ and then two separate inhomogeneous regions with no overlap are present in the phase diagram. In contrast to the CDW case, inhomogeneous phases are present in a larger region of the phase diagram for $\mu_I \neq 0$ (and unequal wave vectors for up and down quarks are present at the same time). At fixed temperatures the inhomogeneous phases extend in the $\bar{\mu} - \mu_I$-plane to arbitrarily large isospin-chemical potentials as seen in Fig. 4.14 for $T = 0$, although we should be aware that charged pion condensation should become relevant at some point, which we however do no include in the present approach. For the completely decoupled case, the existence of inhomogeneous regions up to arbitrarily large μ_I's can be interpreted as that the up and down quarks are allowed to have their preferred values of Δ and q in the inhomogeneous phase, while they are not affected by the other flavor.

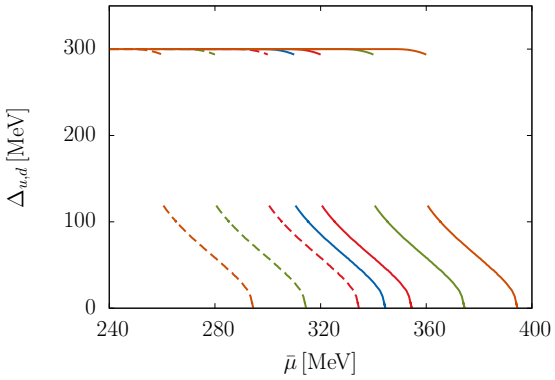

Figure 4.12.: Amplitudes when allowing for a plane wave modulation of the masses at $T = 0$ against the flavor-averaged chemical potential $\bar{\mu}$ at $\mu_I = 0$ (blue), $\mu_I = 20\,\mathrm{MeV}$ (red), $\mu_I = 60\,\mathrm{MeV}$ (green) and $\mu_I = 100\,\mathrm{MeV}$ (orange) for up quarks (dashed) and down quarks (solid) at $\alpha = 0$.

4.4.2. Small degree of flavor mixing

In general, the inhomogeneous solutions can have equal or unequal periodicities, where the periodicity of flavor f is defined by

$$L_f = 2\pi/|\vec{q}_f|. \tag{4.43}$$

As a first step, we discuss the phase structure at small degrees of flavor mixing, when enforcing equal periodicities (corresponding to $|q_u| = |q_d| = q$) while we still aim at investigating if unequal periodicities are favored or not in the end. For this setup, we determine (Δ_u, Δ_d, q) by addressing the extremal condition of the grand potential. In general we may expect that the influence of one flavor on the other is rather small but non-negligible, as we have already found for purely homogeneous condensates.

In Fig. 4.15 the variational parameters (Δ_u, Δ_d, q) are shown at $T = 0$ and fixed isospin-chemical potential for $\alpha = 0.01$, where equal magnitude of the wave vectors, but opposite sign was assumed. Again we recognize the influence of one flavor on the other, that is depicted for $\mu_I = 20\,\mathrm{MeV}$ in the left panel of the figure. There, first both quark flavors prefer homogeneous solutions and the up quarks' amplitude undergoes a significant drop for increasing $\bar{\mu}$ while the amplitude of the down quarks is only weakly affected by the phase transition of the up quarks. In a second jump, the amplitude of the up quarks rises again and at the same time the down quarks' amplitude drops. Both flavors become inhomogeneous, indicated by the wave number q becoming non-zero, until both amplitudes continuously approach zero. For $\mu_I = 60\,\mathrm{MeV}$ (right panel in the figure) the transition to inhomogeneous quark matter is shifted to larger values of the averaged chemical potential and the influence of the down quarks' phase transition on the up quarks is barely visible in the amplitudes. Also the value of Δ_u does not become larger in the inhomogeneous phase. In contrast to $\alpha = 0$ we never find solutions like (i, r) or (r, i), where one flavor is completely chirally restored while the other flavor is not.

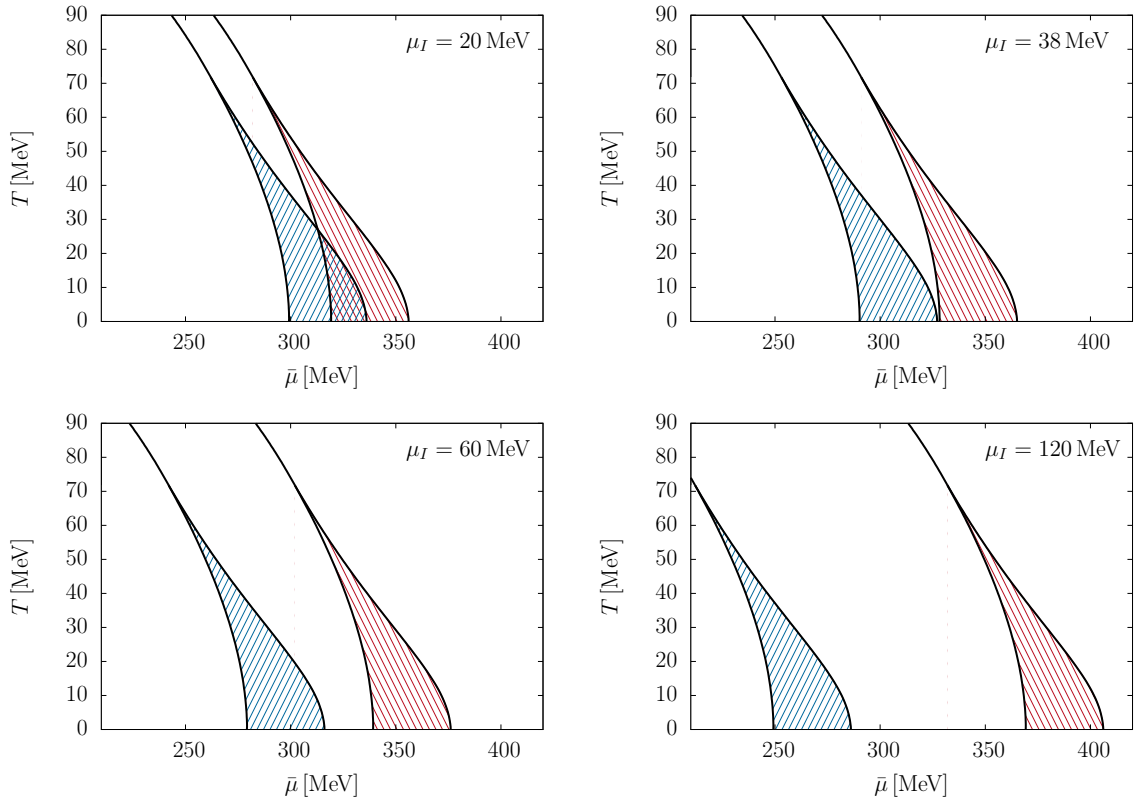

Figure 4.13.: Phase structure allowing for a plane-wave modulation of the mass functions in the $\bar{\mu}-T$-plane for four values of the isospin-chemical potential at $\alpha = 0$. In the shaded region an inhomogeneous solution for the up (blue) or down (red) quarks is favored over a homogeneous solution. To the left (right) of the inhomogeneous phases, homogeneous broken (restored) solutions are favored.

Next we allow for unequal periodicities in our framework, i. e. $q_u \neq q_d$. There we need to determine the set $(\Delta_u, \Delta_d, q_u, q_d)$ as the variational parameters for our ansatz. In particular, we want to clarify if enforcing equal wave numbers is too restrictive.

Before, we turn to very small degrees of flavor mixing, where unequal periodicities $L_u \neq L_d$ are favored for a large enough isospin-asymmetry. This is illustrated in Fig. 4.16, where the amplitudes and wave numbers for each flavor are shown for fixed isospin-chemical potential and $\alpha = 0.0001$ at zero temperature. For $\alpha = 0.0001$ the two quark flavor amplitudes do not fall on top of each other around the onset of the inhomogeneous phases, even if we plot them against the respective quark chemical potential. There Δ_u and Δ_d differ at the lower end of the inhomogeneous window (evaluated at the same quark chemical potential with $\mu_I \neq 0$) and the difference is of the order of approximately one MeV. This is due to the influence of one flavor on the others amplitude. Also the amplitude of one flavor jumps when the phase transition of the other flavor happens, but since this effect is very small due to the tiny amount of flavor mixing, this is not visible

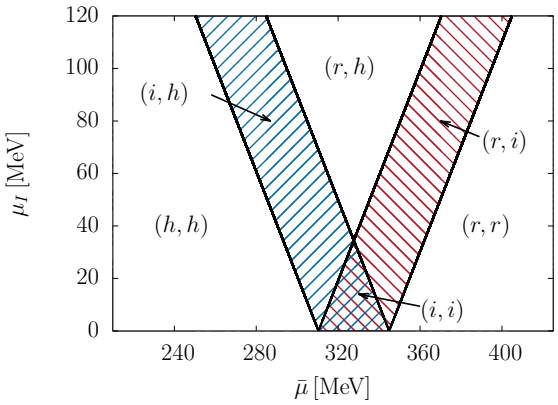

Figure 4.14.: Phase structure allowing for plane-wave modulations of the quark masses in the $\bar{\mu}-\mu_I$-plane at $T = 0$ for $\alpha = 0$. In the shaded region inhomogeneous solutions are favored over a homogeneous solution.

in the figure. For larger flavor-averaged chemical potentials the difference between the two quark flavors becomes smaller at fixed μ_I and thus the two amplitudes fall on top at the upper end of the inhomogeneous window, when plotted against μ_f.

Studying further the possibility of unequal periodicities, the thermodynamic potentials of different types of solutions at $T = 0$ and $\bar{\mu} = 320\,\mathrm{MeV}$ are shown for $\alpha = 0.01$ in Fig. 4.17. Here we allow restored, homogeneous and inhomogeneous solutions. For clarity, we do not show the CDW solution in the following figures, which is always present and is independent of α.

One can see from the figure, that inhomogeneous solutions with equal periodicities are favored for small values of the isospin-chemical potential. At small μ_I, the thermodynamic potential for a solution with unequal periodicities is larger than the one for equal periodicities, which is mainly due to the lack of the term proportional to $\Delta_u\Delta_d$ in the condensate part Eq. (4.41). For non-zero values of μ_I the kinetic part prefers wavenumbers of the order of μ_f and an inhomogeneous phase with unequal periodicities may be energetically favored over the inhomogeneous phase with equal periodicities. The details depend on the actual degree of flavor mixing and in particular on the relative weight of the kinetic and condensate part of the grand potential. For non-zero flavor-mixing, the inhomogeneous phase becomes disfavored at very large values of μ_I against a homogeneous solution and there is a first-order phase transition from the spatially modulated to the spatially homogeneous phase.

Already at relatively small degrees of flavor mixing, unequal periodicities become more and more disfavored against the other types of phases. For $\alpha = 0.03$, $T = 0$ and $\bar{\mu} = 320\,\mathrm{MeV}$ the inhomogeneous solution with unequal periodicities is always disfavored against the inhomogeneous phase with equal periodicities resp. against the homogeneous broken solution, as illustrated in Fig. 4.18. Around $\mu_I = 0$ there exists no favored inhomogeneous solution with $\vec{q}_u \neq -\vec{q}_d$ until for large enough isospin-imbalance there is a second order phase transition from the restored phase to an inhomogeneous solution with unequal periodicities.

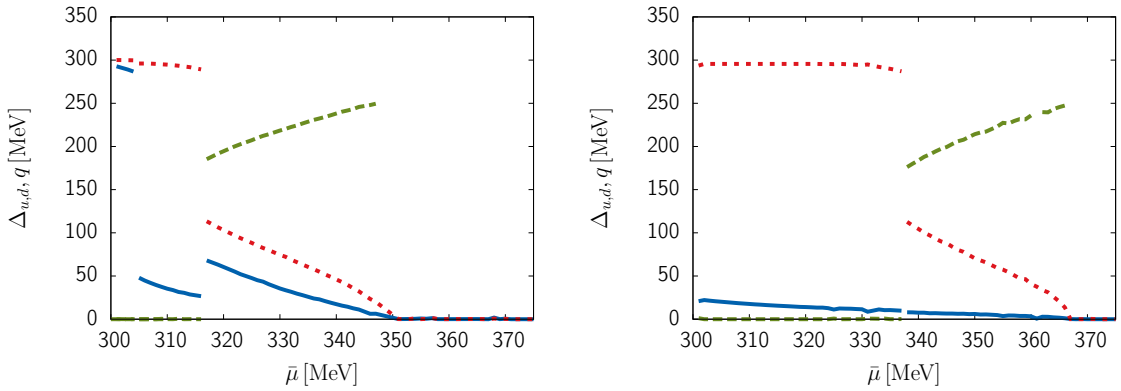

Figure 4.15.: Amplitudes of up (solid blue) and down (dotted red) quarks for a plane wave modulation with $\vec{q}_u = -\vec{q}_d$ and $|\vec{q}_u| = |\vec{q}_d| = q$ (dashed green) against the averaged chemical potential for $\alpha = 0.01$ at $T = 0$ for two isospin-chemical potentials: $\mu_I = 20\,\mathrm{MeV}$ (left) and $\mu_I = 60\,\mathrm{MeV}$ (right).

4.4.3. Maximally coupled quark flavors

Turning now to maximally coupled quark flavors, we are also interested in the question, if unequal periodicities can occur for this case.

For our chosen ansatz one can see that the condensate part of the thermodynamic potential Eq. (4.42) does diverge at $\alpha = 0.5$, unless $\Delta_u = \Delta_d$ and $\vec{q}_u = -\vec{q}_d$. This is precisely, what we required for the CDW case. Thus at $\alpha = 0.5$ no unequal periodicities are possible for the plane-wave modulations specified by Eq. (4.31) and we obtain the same phase structure as in section 4.3. It may present a first hint, that the plane-wave ansatz we have chosen is too restrictive to allow the emergence of unequal periodicities at $\alpha = 0.5$.

4.4.4. Realistic degree of flavor mixing

For a realistic degree of flavor mixing unequal periodicities are not energetically favored over a large parameter range, although an inhomogeneous phase is present.

For $\bar{\mu} = 320\,\mathrm{MeV}$, $T = 0$ and varying isospin imbalance this is evident in Fig. 4.19, where no solutions with unequal periodicities are present. For comparison, we show the CDW case in this figure. Clearly, an inhomogeneous phase with 'unrestricted' amplitudes and $\vec{q}_u = -\vec{q}_d$ is the preferred ground state against the CDW-case, the homogeneous broken or restored phase, except for $\mu_I = 0$ where the CDW and the general solution are identical. The curvature of the free energy of the inhomogeneous phase first is positive along the μ_I-axis, but then the slope alters its sign for relatively large μ_I, indicating that the inhomogeneous phase with $\Delta_u \neq \Delta_d$ and $\vec{q}_u = -\vec{q}_d$ becomes more favored again when the two quark flavors get more non-degenerate.

For a fixed value of the isospin chemical potential, the amplitudes of the two quark flavors are depicted in Fig. 4.20. If the temperature is vanishing and small average chemical potentials are considered, the two amplitudes are identical until they split due

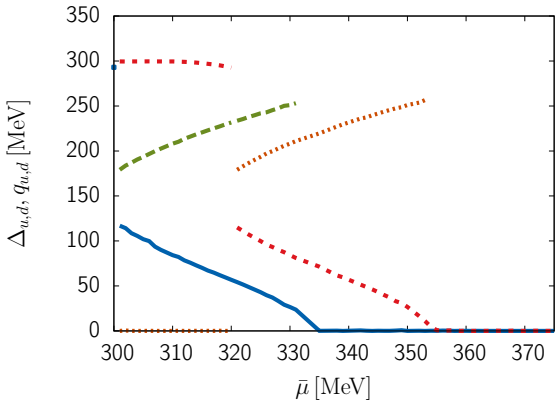

Figure 4.16.: Amplitudes $\Delta_{u,d}$ of up (solid blue) and down (dotted red) quarks and wave numbers q_u (dashed green) and q_d (dotted orange) against the flavor-averaged chemical potential at $T = 0$ and $\mu_I = 20\,\mathrm{MeV}$ for $\alpha = 0.0001$ and a plane-wave modulation of the quark masses.

to the isospin-chemical potential. For increasing values of $\bar{\mu}$ the splitting between the two amplitudes gets larger, until the quark flavors undergo a transition from the homogeneous to the inhomogeneous phase, where the two quantities still do not agree, but the difference becomes smaller when approaching the upper end of the inhomogeneous window and vanishes exactly there. The same behavior can be observed, when the temperature is increased at fixed $\bar{\mu}$. Over the whole temperature range, the amplitudes of the different quark flavors do not coincide except when the two amplitudes become zero in a second order phase transition. The wave number q is for both cases monotonously increasing, which is already the case in isospin-symmetric matter.

In the $\bar{\mu} - T$ plane at fixed μ_I the phase structure linked to up and down quarks is shown in Fig. 4.21. Here the size of the inhomogeneous region is for this realistic degree of flavor mixing larger than for the CDW[2], which might allow to detect inhomogeneous phases in future experiments or in natural environments with a large imbalance more easily. For larger μ_I the lower end of the inhomogeneous window shifts to larger values of $\bar{\mu}$ while at the same time also the upper end shifts to lower values. This is not the case for the CDW, where the lower end moves to lower $\bar{\mu}$ for increasing isospin-imbalance and the inhomogeneous region extends to lower maximal temperatures if the asymmetry becomes larger. Since the shifts occur more rapidly when μ_I is increasing than for inhomogeneous phases at $\alpha = 0.2$, the CDW window effectively shrinks faster.

To summarize the main results of this section, we have seen that for a realistic degree of flavor mixing and a plane-wave modulation for the quark masses, unequal periodicities in the inhomogeneous phase are energetically disfavored against inhomogeneous phases with equal wave vectors but different signs. In contrast for no flavor mixing, unequal periodicities naturally arise at $\mu_I \neq 0$ and are the energetically preferred ground state.

[2] At $T = 0$ the inhomogeneous window extends along the $\bar{\mu}$-window and its size is given by $\Delta\bar{\mu}(\mu_I = 60\,\mathrm{MeV}) = 28.3\,\mathrm{MeV}$ versus $\Delta\bar{\mu}(\mu_I = 80\,\mathrm{MeV}) = 32.1\,\mathrm{MeV}$ for $\mu_I = 80\,\mathrm{MeV}$.

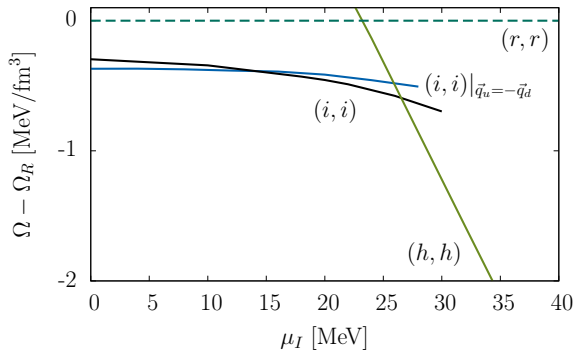

Figure 4.17.: Thermodynamic potential for different plane wave modulations relative to the restored phase against the isospin chemical potential at $T = 0$ and $\bar{\mu} = 320\,\mathrm{MeV}$ for $\alpha = 0.01$.

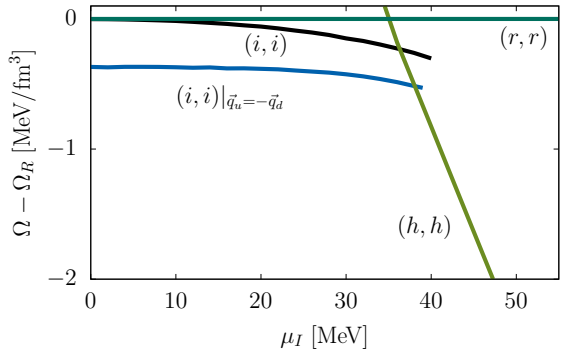

Figure 4.18.: Thermodynamic potential for different plane wave modulations relative to the restored phase against the isospin chemical potential at $T = 0$ and $\bar{\mu} = 320\,\mathrm{MeV}$ for $\alpha = 0.03$.

For a maximal amount of flavor mixing however, no inhomogeneous phase with unequal periodicities at all can occur for the given ansatz.

4.5. One-dimensional spatial modulation of the condensates

So far we have only discussed the simplest possible shape of the modulation for the quark masses, when requiring periodic condensates. We have seen that inhomogeneous phases allowing for unequal amplitudes in the two quark mass functions are favored over spatially-modulated order-parameters with enforced equal amplitudes (except special cases like $\alpha = 0.5$). On the other hand allowing for unequal periodicities $\vec{q}_u \neq -\vec{q}_d$

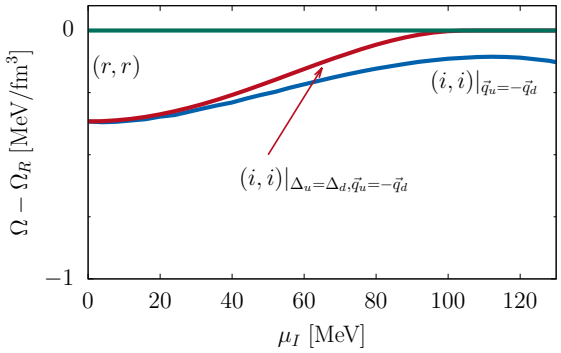

Figure 4.19.: Thermodynamic potential for different plane wave modulations relative to the restored phase against the isospin chemical potential at $T = 0$ and $\bar{\mu} = 320\,\mathrm{MeV}$ for $\alpha = 0.2$.

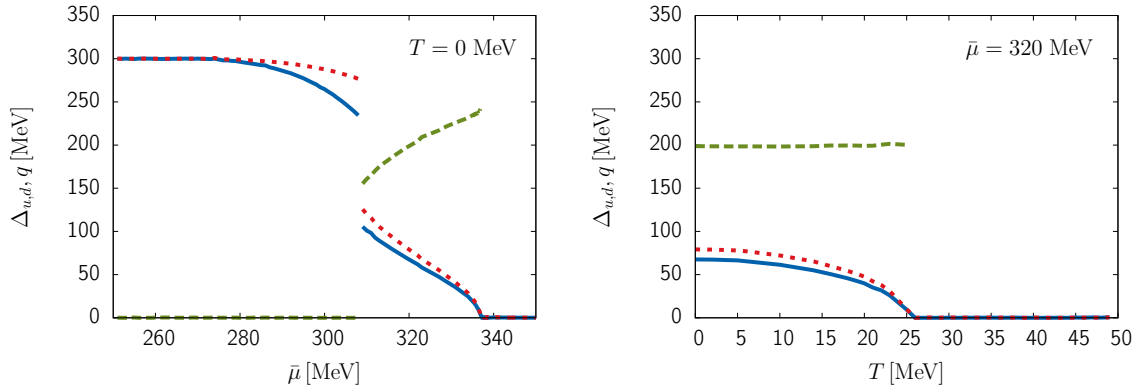

Figure 4.20.: Amplitudes of up (solid blue) and down (dotted red) quarks and the wave-number q (dashed green) for a plane wave modulation of the quark masses at $\alpha = 0.2$, an isospin-chemical potential of $\mu_I = 60\,\mathrm{MeV}$ and as functions of flavor-averaged chemical potentials at $T = 0$ (*left*) and temperatures at $\bar{\mu} = 320\,\mathrm{MeV}$ (*right*).

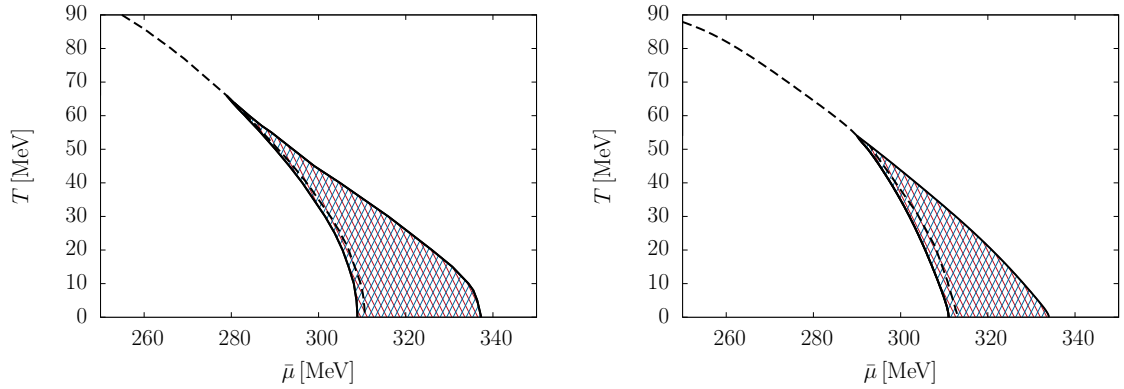

Figure 4.21.: Phase structure allowing for a plane-wave modulation of the quark masses in the $\bar{\mu} - T$-plane at $\mu_I = 60\,\mathrm{MeV}$ (left) and $\mu_I = 80\,\mathrm{MeV}$ (right) at $\alpha = 0.2$. In the shaded region an inhomogeneous solution is favored over a homogeneous solution. For reference the phase transition of purely homogeneous quark matter is also indicated (dashed black).

resulted in the favorisation of such types of phases only for very small degrees of flavor-mixing, but not at a realistic degree of flavor mixing.

At this point we want to extend our approach to a more general setup. This can be done in multiple directions: we could, for example, consider modulations of the condensate instead of the mass functions or allow a general structure for the order-parameters. For these general structures, the evaluation of the thermodynamic potential is still extremely challenging since the numerical implementation turns out to be rather complicated. However, by limiting ourselves to lower-dimensional modulations of the order-parameters and assuming periodicity, the evaluation of the grand potential for a more general shape of the modulation becomes feasible. Therefore we pursue this direction for the ongoing discussion, while specifying the shape of condensate instead of the mass functions will be discussed in the next section.

Since for isospin-symmetric matter it was found that one-dimensional modulations are favored over two-dimensional modulations [48], we restrict our analysis to one-dimensional modulations, although it may be interesting to investigate higher-dimensional modulations with unequal periodicities in isospin-asymmetric matter.

In particular, when restricting to such one-dimensional modulations, it was shown for the isospin-symmetric case that the analytically known solutions from the 1+1 dimensional Gross-Neveu model can be mapped to our 3+1 dimensional NJL model and these results from the lower-dimensional model can be used to construct solutions for our higher-dimensional model [26]. With this, the task of determining the eigenvalue spectrum of the Hamiltonian can be dimensionally reduced [26] and thus simplified. In the following we discuss the details of the simplifications and extend it to isospin-asymmetric matter.

4.5.1. Boosted eigenvalues

For modulations of the masses or condensates in only one or two spatial directions, the system is translationally invariant in the transverse direction along which the condensates are spatially constant. Then the problem of determining the eigenvalue spectrum can be performed on a dimensionally-reduced Hamiltonian [26]. By assuming that the condensates, entering the Hamiltonian, vary only in $d_\parallel$ dimensions and in turn do not depend on the remaining $d_\perp = 3 - d_\parallel$ transverse coordinates, the quark momenta transverse to the modulation-direction are conserved. The Hamiltonian formally commutes then with the transverse momentum operator, which means we can choose a frame where $\vec{p}_\perp = 0$ and solve the dimensionally reduced eigenvalue problem. In the following, this will be shown explicitly for a modulation in one spatial direction.

The momentum integration in the thermodynamic potential factorizes for this kind of modulation according to [26]

$$\Omega^f_{\text{kin}} = -N_c \int \frac{d^2p_\perp}{(2\pi)^2} \frac{1}{V_\parallel} \sum_{E_f} T \log \left[2\cosh\left(\frac{E_f(\vec{p}_\perp) - \mu_f}{2T} \right) \right], \tag{4.44}$$

in a part along the direction of the modulation $\vec{p}_\parallel$ and perpendicular to it. Here $V_\parallel$ is the 1-dimensional "volume" of the unit cell along the direction of the one-dimensional modulation.

More importantly, the diagonalization of a dimensionally-reduced Hamiltonian becomes possible instead of diagonalizing the full Hamiltonian. Here, we follow [26] and furthermore assume without loss of generality that the condensates vary only along the z-direction and do not depend on the transverse coordinates in the $x-y$-plane. For convenience we label these coordinates as $\vec{p}_{xy}$ instead of $\vec{p}_\perp$. Formally due to the translational invariance, the Hamiltonian commutes with the transverse momentum operator

$$[\mathcal{H}_f, \vec{P}_{xy}] = 0 \tag{4.45}$$

and we may find common eigenfunctions of both operators, enabling us to consider only the simpler problem of determining the eigenvalues of $\mathcal{H}_f(\vec{p}_{xy}, \vec{p}_z)$ at $\vec{p}_{xy} = 0$. With this, the eigenvalue problem we have to solve, reads

$$\mathcal{H}_f \, \psi_{\epsilon_f,\, \vec{p}_{xy}=0} = \epsilon_f \, \psi_{\epsilon_f,\, \vec{p}_{xy}=0}, \tag{4.46}$$

where $\psi_{\epsilon_f, \vec{p}_{xy}=0}$ are the simultaneous eigenfunctions of $\mathcal{H}_f$ and $\vec{p}_{xy}$ with eigenvalues evaluated at $\vec{p}_{xy} = 0$. Here, the transverse momenta do not enter the mean-field Hamiltonian and thus it is effectively dimensionally reduced. Then we have indeed simplified the complicated task of calculating the eigenvalue spectrum and we need to diagonalize in coordinate space

$$\mathcal{H}_{1\text{d}} = \begin{pmatrix} \mathrm{i}\partial_z & & M_f(z) & \\ & -\mathrm{i}\partial_z & & M_f(z) \\ M_f^*(z) & & -\mathrm{i}\partial_z & \\ & M_f^*(z) & & \mathrm{i}\partial_z \end{pmatrix}. \tag{4.47}$$

Since the kinetic part of the thermodynamic potential contains only the eigenvalues of the full Hamiltonian, we need to relate the eigenvalues of the dimensionally reduced Hamiltonian to those of the full Hamiltonian. This will be accomplished by boosting the system to (in general) non-zero values of $\vec{p}_{xy}$. The full energy eigenvalues are then related by

$$E_f(\vec{p}_{xy}) = \mathrm{sign}\big(\epsilon_f\big)\,\sqrt{\epsilon_f^2 + \vec{p}_{xy}^{\,2}}, \tag{4.48}$$

to the eigenvalues ϵ_f of the dimensionally reduced Hamiltonian. Now we are able to construct the full eigenvalue spectrum from the subspace spanned by the wave functions at vanishing transverse momentum, i. e. by the set $\{\psi_{\epsilon_f,\vec{p}_{xy}=0}\}$. The kinetic part of the thermodynamic potential can be written as

$$\Omega^f_{\mathrm{kin}} = -\frac{N_c}{V_\parallel}\int \frac{d^2p_{xy}}{(2\pi)^2}\sum_{E_f(\vec{p}_{xy})}\left(\frac{E_f(\vec{p}_{xy})-\mu_f}{2} + T\log\left(1+\exp\left(-\frac{E_f(\vec{p}_{xy})-\mu_f}{T}\right)\right)\right), \tag{4.49}$$

where $E_f(\vec{p}_{xy})$ is given by Eq. (4.48).

4.5.2. Solitonic solutions

The Hamiltonian Eq. (4.47) can be further rewritten by applying an unitary transformation, bringing it in a block diagonal form [26]

$$\mathcal{H}'_{1\mathrm{d}} = \begin{pmatrix} \tilde{\mathcal{H}}'_{1\mathrm{d}}(M_f(z)) & \\ & \tilde{\mathcal{H}}'_{1\mathrm{d}}(M_f(z)^*) \end{pmatrix}, \tag{4.50}$$

where one block on the diagonal is given by

$$\tilde{\mathcal{H}}'_{1\mathrm{d}}(M_f(z)) = \begin{pmatrix} -\mathrm{i}\partial_z & M_f(z) \\ M_f(z)^* & \mathrm{i}\partial_z \end{pmatrix}. \tag{4.51}$$

These blocks are formally identical to the Hamiltonian of the Gross-Neveu model (for isospin-symmetric matter) in $1+1$ dimensions, and the quasi-particle spectrum is known (see e. g. [49, 50, 51, 52, 53]). If we focus on real ansätze for the quark masses, the eigenvalue spectrum can be expressed in terms of the quark masses given by

$$\begin{aligned} M_f(z) &= \Delta_f\nu_f\frac{\mathrm{sn}\left(\Delta_f z|\nu_f\right)\mathrm{cn}\left(\Delta_f z|\nu_f\right)}{\mathrm{dn}(\Delta_f z|\nu_f)} \\ &= \Delta_f\left(1+\sqrt{1-\nu_f}\right)\left(\frac{1-\sqrt{1-\nu_f}}{1+\sqrt{1-\nu_f}}\right)\mathrm{sn}\left(\Delta_f\left(1+\sqrt{1-\nu_f}\right)\middle|\left(\frac{1-\sqrt{1-\nu_f}}{1+\sqrt{1-\nu_f}}\right)^2\right), \end{aligned} \tag{4.52}$$

where sn, cn and dn are Jacobi elliptic functions. In the second row of Eq. (4.52), the mass function was rewritten (see e. g. the published version of [26] for details) in

terms of a single Jacobi elliptic function. Here Δ and ν are the variational parameters, characterizing the shape of the modulation. By tuning the elliptic modulus $\nu \in [0;1]$ a single kink solution at $\nu = 1$ can gradually be connected to a sinusoidal modulation at $\nu = 0$. Also here $M_u(z) = M_d(z)$ and $\nu_u = \nu_d$ holds for isospin-symmetric matter, as we will see below.

Writing the thermodynamic potential in terms of the density of states is possible since the eigenvalue spectrum is analytically known and explicitly the density of states is given by [26]

$$\begin{aligned}\rho_f^{\text{solitons}}(E) =& \frac{2E\Delta_f}{\pi^2}\Bigg\{\Theta(\sqrt{\bar{\nu}}\Delta_f - E)\left[\mathbf{E}(\tilde{\theta}|\tilde{\nu}) + \left(\frac{\mathbf{E}(\nu)}{\mathbf{K}(\nu)} - 1\right)\mathbf{F}(\tilde{\theta}|\tilde{\nu})\right] \\ &+ \Theta(E - \sqrt{\tilde{\nu}}\Delta_f)\Theta(\Delta_f - E)\left[\mathbf{E}(\tilde{\nu}) + \left(\frac{\mathbf{E}(\nu)}{\mathbf{K}(\nu)} - 1\right)\mathbf{K}(\tilde{\nu})\right] \\ &+ \Theta(E - \Delta_f)\Big[\mathbf{E}(\theta|\tilde{\nu}) + \left(\frac{\mathbf{E}(\nu)}{\mathbf{K}(\nu)} - 1\right)\mathbf{F}(\theta|\tilde{\nu}) + \frac{\sqrt{(E^2 - \Delta_f^2)(E^2 - \tilde{\nu}\Delta_f^2)}}{E\Delta_f}\Big]\Bigg\},\end{aligned} \tag{4.53}$$

where $\mathbf{E}$ is the elliptic integral of second kind and $\mathbf{F}$ is the incomplete and $\mathbf{K}$ the complete elliptic integral of first kind. For brevity we also introduced $\tilde{\nu} = 1 - \nu$, $\tilde{\theta} = \arcsin\left(E/(\sqrt{\tilde{\nu}}\Delta)\right)$ and $\theta = \arcsin\left(\Delta/E\right)$. The period of the modulation is given by

$$L_f = 4\mathbf{K}(\nu_f)/\Delta_f \tag{4.54}$$

and is related to the wave number by $q_f = 2\pi/L_f$.

For simplicity we restrict ourselves to equal variational parameters

$$\Delta_u = \Delta_d = \Delta, \quad \nu_u = \nu_d = \nu \tag{4.55}$$

for both flavors. The thermodynamic potential is then given by

$$\begin{aligned}\Omega_{\text{kin}}^f(T, \bar{\mu}, \mu_I; \Delta, \nu) = -N_c \int_{-\infty}^{\infty} dE_f \int \frac{d^2p_{xy}}{(2\pi)^2}\, \rho_{\text{sol}}(E_f)\times \\ \times \sum_{f=u,d}\left(\frac{E_f - \mu_f}{2} + T\log\left(1 + \exp\left(-\frac{E_f - \mu_f}{T}\right)\right)\right)\end{aligned} \tag{4.56}$$

with the definitions used from Eq. (4.48) and $\rho_u^{\text{solitons}} = \rho_d^{\text{solitons}} \equiv \rho_{\text{sol}}$. The condensate part is given by

$$\Omega_{\text{cond}} = \frac{1}{4GL}\int_0^L dz\, \left|M(z)\right|^2, \tag{4.57}$$

where we exploited that $M_u(z) = M_d(z) \equiv M(z)$ and $L_u = L_d \equiv L$ holds due to our restriction to equal amplitudes and elliptic moduli.

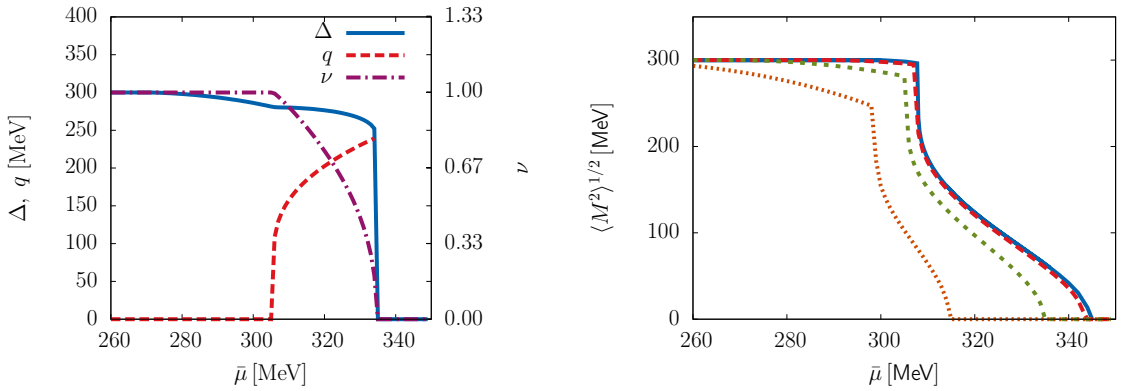

Figure 4.22.: Results after minimization of Ω allowing for a solitonic modulation with equal amplitudes and periodicities at zero temperature. *(Left):* Variational parameters for $\mu_I = 60\,\mathrm{MeV}$. *(Right):* Spatially-averaged quark mass at $\mu_I = 0$ (solid blue), $\mu_I = 20\,\mathrm{MeV}$ (dashed red), $\mu_I = 60\,\mathrm{MeV}$ (short-dashed green) and $\mu_I = 120\,\mathrm{MeV}$ (dotted orange).

At the onset of the inhomogeneous phase and at zero temperature, the elliptic modulus starts to decrease monotonously from unity and Δ begins to shrink, as shown in Fig. 4.22. From this one could also calculate the amplitude of the modulation directly, but here we show the spatially-averaged quark mass[3] $\sqrt{\langle M(z)\rangle^2}$ instead. It begins to drop rapidly, when an inhomogeneous solitonic solution becomes favored over the homogeneous broken or restored phase. For increasing $\bar{\mu}$ the spatially-averaged mass approaches zero and also ν becomes zero. If the isospin-chemical potential is increased, the size of the inhomogeneous window shrinks and the value of the spatially-averaged quark masses decreases, as seen before for the CDW. At larger μ_I the elliptic modulus and Δ become smaller; the wave number q at fixed μ_I is continuously rising with $\bar{\mu}$, starting from zero as seen in the left panel of the figure.

Comparing the free energies of different types of spatial modulations, we find that the inhomogeneous phase with a solitonic modulation is energetically favored earlier at fixed T and μ_I over the homogeneous broken solution than for the CDW, i. e.

$$\bar{\mu}_{c,1}^{\text{solitons}} < \bar{\mu}_{c,1}^{\text{CDW}},$$

as can be seen in Fig. 4.23 at $T = 0$ and $\alpha = 0.5$. From the free energies shown there it is also evident that the order of the phase transition at the onset changes between a solitonic and a plane-wave modulation. Namely, it is of second order for the solitons and thus it connects smoothly the homogeneous broken solution to the restored phase through two second order phase transitions. For increasing μ_I the difference in the free energies between the solitonic solution, the CDW and the restored phase gets smaller, until it vanishes at or above a critical isospin-chemical potential $\mu_I \geq \mu_{I,c}$. For $T = 0$ this is shown in Fig. 4.24, where the inhomogeneous phase extends along the μ_I-axis up to $\mu_I^c(T = 0) \approx 241\,\mathrm{MeV}$.

[3]This quantity also can be interpreted to characterize the amplitude of the solitonic modulation.

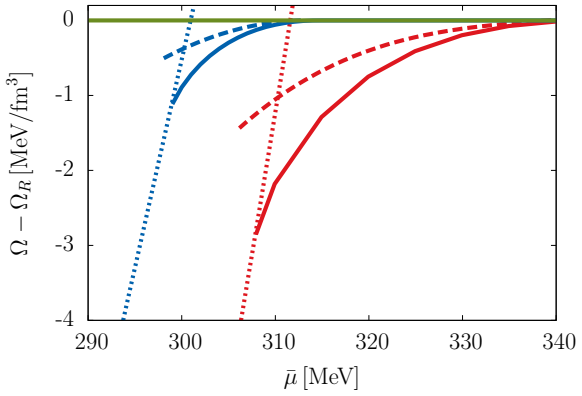

Figure 4.23.: Thermodynamic potential relative to the grand potential of the restored phase for the energetically favored phase against the flavor-averaged chemical potential at $T = 0$ and $\alpha = 0.5$ for $\mu_I = 0\,\mathrm{MeV}$ (red) and $\mu_I = 120\,\mathrm{MeV}$ (blue), where we allowed different types of modulations to appear: a solitonic solution with $\Delta_u = \Delta_d$ and $\nu_u = \nu_d$ (solid), a CDW solutions (dashed) and a solution with homogeneous chiral symmetry-breaking order-parameter (dotted) and the restored solution (solid green).

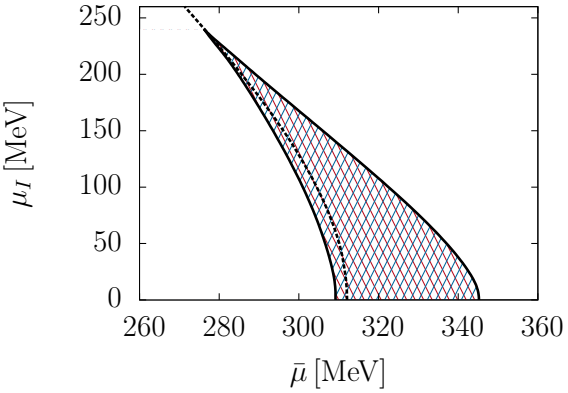

Figure 4.24.: Phase diagram in the $\bar{\mu} - \mu_I$-plane at $T = 0$ for solitonic modulations with equal amplitudes and moduli. In the shaded area an inhomogeneous solution is favored and for reference the chiral phase boundary of purely homogeneous matter is also shown (dashed).

Turning now to the phase structure in the $\bar{\mu} - T$-plane at fixed μ_I, the inhomogeneous region is basically unaltered in its size when compared to the one of the CDW case (cf. Fig. 4.11 for the CDW case), which is the reason it is not shown here separately. This is not surprising, since we have seen that the onset of the inhomogeneous region allowing for solitonic modulations, shifts only slightly to smaller flavor-averaged chemical potentials in comparison to the CDW, while the upper end is unaltered for the two kinds of modulations. This fact is also supported by a Ginzburg-Landau analysis at vanishing isospin-asymmetry [54, 55].

At this point we also should point out that it is still unclear at present, if solitonic modulations at non-vanishing isospin chemical potential are self-consistent solutions – as it is the case for $\mu_I = 0$.

4.6. Plane-wave ansatz for the condensates

If we specify a mass modulation by prescribing the shape of the quark masses $M_f(\vec{x})$ as we have done in the previous sections, the resulting condensate functions can be determined straightforwardly (see Appendix B.2 for details). For $\alpha = 0.5$ no unequal periodicities are possible, since the condensate part of the thermodynamic potential would otherwise diverge.

An interesting question we have not addressed so far very intensively is, if we also can specify the modulation of the condensates instead of the modulation of the quark masses; mainly we have only specified the modulation of the quark masses, but have not looked at the resulting spatial modulation of the condensate functions. Our interest in this section is, what changes if we reverse this procedure and instead start from the modulation of the condensates. Instead of simple shapes for the quark masses and complicated functional dependencies for the condensate functions, we then have more complicated modulations for the quark masses, but simple ones for the condensate functions. In the following we will present results for this kind of specifying ansätze for the modulations of the order parameters.

For equal amplitudes and equal wave numbers both ansätze turn out to be the same and the results for the thermodynamic potential after determining self-consistently the variational parameters are (within numerical errors) the same. Also if we require only equal periodicities, both ansätze can be related to each other.

4.6.1. Plane-wave ansatz for the condensate functions

Making the following ansatz for the condensates (which we call the "condensate ansatz")

$$S_f(\vec{x}) = -\frac{\Delta_f}{4G} \cos\left(\vec{q}_f \cdot \vec{x}\right), \tag{4.58}$$

$$P_f(\vec{x}) = -\frac{\Delta_f}{4G} \sin\left(\vec{q}_f \cdot \vec{x}\right) \tag{4.59}$$

complicates the determination of the quark energy spectrum significantly but is not restricted at $\alpha = 0.5$, as we will see later. The associated quark mass function can be

obtained by inserting Eq. (4.58) and Eq. (4.59) in Eq. (3.20) from which

$$\hat{M}_f(\vec{x}) = (1-\alpha)\Delta_f \exp\left(\mathrm{i}\gamma^5 \vec{q}_f \cdot \vec{x}\right) + \alpha\Delta_h \exp\left(-\mathrm{i}\gamma^5 \vec{q}_h \cdot \vec{x}\right) \tag{4.60}$$

follows. The mass function is a superposition of two plane waves, for which no chiral transformation of the form Eq. (B.2) can remove the space dependence completely and thus no analytical expression for the eigenenergies is known. Therefore we need to diagonalize the mean-field Hamiltonian numerically. For this, we insert Eq. (4.60) in Eq. (3.36) and arrive at

$$\left(\mathcal{H}_f\right)_{p_m,p_n} = \tag{4.61}$$
$$\begin{pmatrix} -\vec{p}_m \cdot \vec{\sigma}\, \delta_{\vec{p}_m,\vec{p}_n} & \left[(1-\alpha)\Delta_f \delta_{\vec{p}_m,\vec{p}_n+\vec{q}_f} + \alpha\Delta_h \delta_{\vec{p}_m,\vec{p}_n-\vec{q}_h}\right] \\ \left[(1-\alpha)\Delta_f \delta_{\vec{p}_m,\,\vec{p}_n-\vec{q}_f} + \alpha\Delta_h \delta_{\vec{p}_m,\,\vec{p}_n+\vec{q}_h}\right] & \vec{p}_m \cdot \vec{\sigma}\, \delta_{\vec{p}_m,\vec{p}_n} \end{pmatrix}.$$

Since only quark momenta differing by $\vec{q}_u$ or $\vec{q}_d$ are coupled through the interaction with the condensates, as can be seen by the off-diagonal elements in Eq. (4.61), the mean-field Hamiltonian can still be brought in a block-diagonal form by applying standard procedures [7, 48] due to the lattice symmetry of the problem and then the numerical diagonalization in principle becomes feasible. However, to achieve better computability, we restrict the wave vectors to be (without loss of generality) aligned along the z-direction, which enables us to make use of the boost symmetry of the problem introduced in section 4.5.1. In particular, following our requirement of periodicity for the condensate resp. mass functions, we assume that the one-dimensional modulation has an overall period of length L. This can be realized by choosing the wave number as an integer number of a fundamental wave number q,

$$q_u = n_u\, q, \quad q_d = n_d\, q, \tag{4.62}$$

with $n_u, n_d \in \mathbb{Z}$ and $q = 2\pi/L$. As a consequence of our choice for q_u and q_d also the ratio of the wave numbers $R = q_u/q_d$ becomes a rational number. Since any real number can be approximated by rational numbers to arbitrary accuracy, this is not a severe restriction in principle. Our practical calculations will of course be limited to comparing a finite number of ratios. Furthermore we assume for the evaluation of the thermodynamic potential, that the greatest common divisor (gcd) of n_u and n_d is unity, which is possible without loss of generality since any gcd unequal to 1 can be reabsorbed by re-scaling q.

The BZ is then defined by the momentum interval $[0, q]$ in z-direction while the BZ is still infinite in the x- and y-direction. The spacing between the components of Eq. (4.61) is equal to q because of Eq. (4.17). Together with $p_z = k_z + q$ the mean-field Hamiltonian can then be numerically diagonalized. In particular, since the modulation Eq. (4.60) is one-dimensional this allows to use a dimensionally reduced Hamiltonian $\mathcal{H}_{1D}$. The thermodynamic potential is given by

$$\Omega^f_{\text{kin}} = -TN_c \int \frac{d^2p_{xy}}{(2\pi)^2} \int_{BZ} \frac{dk}{2\pi} \sum_{E_{f,1D}(k)} \log\left(2\cosh\left(\frac{E_f - \mu_f}{2T}\right)\right), \tag{4.63}$$

where $E_{f,1D}(k)$ are the eigenvalues associated with the block $\mathcal{H}_{1D}(k)$ and $k \in$ BZ. The eigenvalues E_f of $\mathcal{H}$ are related to the eigenvalue spectrum of the dimensionally reduced Hamiltonian by Eq. (4.48).

The condensate part of the thermodynamic potential can be determined from Eq. (3.40) by inserting the condensate ansätze Eq. (4.58) and Eq. (4.59). In analogy to section 4.4 we need to distinguish between different cases for the wave-vectors. Formally we have

$$\Omega_{\text{cond}} = \frac{1}{8GV} \int_V d^3x \, \left((1-\alpha) \left(\Delta_u^2 + \Delta_d^2 \right) + 2\alpha \Delta_u \Delta_d \cos\left((\vec{q}_u + \vec{q}_d)\, \vec{e}_z z \right) \right) \tag{4.64}$$

which gives after the integration over the Wigner-Seitz cell

$$\Omega_{\text{cond}} = \begin{cases} \frac{1}{8G} \left[(1-\alpha) \left(\Delta_u^2 + \Delta_d^2 \right) + 2\alpha \Delta_u \Delta_d \right], & \vec{q}_u = -\vec{q}_d \\ \frac{1}{8G} (1-\alpha) \left(\Delta_u^2 + \Delta_d^2 \right), & \text{else.} \end{cases} \tag{4.65}$$

In contrast to making an ansatz for the shape of the mass modulation, here the condensate part favors unequal periodicities. Already small differences between q_u and q_d lead to the lowering of the free energy through the condensate part and thus unequal periodicities become favored by Ω_{cond}. For the kinetic part this is not obvious any more like for the case of a simple plane-wave mass modulation.

Comparing Eq. (4.33) and Eq. (4.34) with Eq. (4.58) and Eq. (4.59) for $\vec{q}_u = -\vec{q}_d$, one finds that the amplitudes of the plane-wave modulation for the condensates and for the quark masses are linked to each other by

$$\tilde{\Delta}_f = \frac{1}{1-2\alpha} \left[(1-\alpha)\, \Delta_f - \alpha \Delta_h \right], \tag{4.66}$$

where $\tilde{\Delta}_f$ refers to the amplitude of flavor f for the condensate ansatz and Δ_f to the amplitude of the mass ansatz.

For the practical implementation of the condensate ansatz, we need to numerically determine the eigenvalue spectrum of the Hamiltonian. At $\alpha = 0$ we reproduce the results of sec. 4.4.1, which is not surprising since also for prescribing the shape of the condensates the thermodynamic potential separates in two independent parts associated with the quark flavors. Furthermore for this setup, we can determine q_u and q_d directly and do not need to approximate it by using Eq. (4.62). The result is shown for $\mu_I = 20\,\text{MeV}$ in Fig. 4.25. Also for $\vec{q}_u = -\vec{q}_d$ the minimization of the thermodynamic potential with respect to the variational parameters yield the same results like for the ansatz of the quark masses and we are able to numerically confirm the relation Eq. (4.66) within numerical errors.

As a first step, we set one q_f to zero, which will be $q_u = 0$ for our discussion. With this we are able to reduce the complexity of diagonalizing the Hamiltonian and turn to a realistic degree of flavor-mixing $\alpha = 0.2$. We can map the Hamiltonian to the one of a CDW with large bare quark masses, where one element for up quarks in momentum space is given by

$$(\mathcal{H}_u)_{\vec{p}_m, \vec{p}_n} = \begin{pmatrix} -\vec{p}_m \cdot \vec{\sigma}\, \delta_{\vec{p}_m, \vec{p}_n} & \left((1-\alpha)\, \Delta_u \delta_{\vec{p}_m, \vec{p}_n + \vec{q}_u} + \alpha \Delta_d \delta_{\vec{p}_m, \vec{p}_n} \right) \\ \left((1-\alpha)\, \Delta_u \delta_{\vec{p}_m, \vec{p}_n - \vec{q}_u} + \alpha \Delta_d \delta_{\vec{p}_m, \vec{p}_n} \right) & \vec{p}_m \cdot \vec{\sigma}\, \delta_{\vec{p}_m, \vec{p}_n} \end{pmatrix}, \tag{4.67}$$

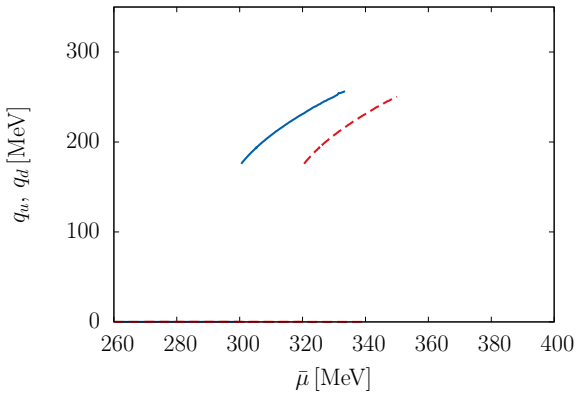

Figure 4.25.: Wave-numbers q_u (solid blue) and q_d (dashed red) for $\alpha = 0$, $\mu_I = 20\,\mathrm{MeV}$ and at $T = 0$.

and for down quarks it reads

$$(\mathcal{H}_d)_{\vec{p}_m,\vec{p}_n} = \begin{pmatrix} -\vec{p}_m \cdot \vec{\sigma}\,\delta_{\vec{p}_m,\vec{p}_n} & ((1-\alpha)\,\Delta_d \delta_{\vec{p}_m,\vec{p}_n} + \alpha\Delta_u \delta_{\vec{p}_m,\vec{p}_n-\vec{q}_u}) \\ ((1-\alpha)\,\Delta_d \delta_{\vec{p}_m,\vec{p}_n} + \alpha\Delta_u \delta_{\vec{p}_m,\vec{p}_n+\vec{q}_u}) & \vec{p}_m \cdot \vec{\sigma}\,\delta_{\vec{p}_m,\vec{p}_n} \end{pmatrix}. \tag{4.68}$$

By inspecting the diagonal entries with $\vec{p}_m = \vec{p}_n$, one recognizes that for up quarks $\alpha\Delta_d$ is at the same position as a bare quark mass term m_u would be. Analogously we find that the expression $(1-\alpha)\Delta_d$ occurs at the same position as m_d would. This suggest that the resulting modulations for up quarks happen around $\alpha\Delta_d$ with amplitude $(1-\alpha)\Delta_u$ and around $(1-\alpha)\Delta_d$ with magnitude $\alpha\Delta_u$ for down quarks. However, numerically determining the variational parameters yields no (h,i) solution. In a next step, we thus allow both q's to be non-zero at $\alpha = 0.2$ and investigate the occurrence of (i,i) solutions.

Then we need to probe different ratios (here only $n_u/n_d \in \{-1, 5/4, 4/3, 2, 5\}$ due to numerical tractability) to calculate the favored ground state and afterwards determine which solutions at a fixed ratio is energetically preferred. For isospin-symmetric matter we find that always a ratio of unity is favored throughout the $\bar{\mu} - T$ plane. The thermodynamic potential for this case is shown in the left panel of Fig. 4.26. There only an inhomogeneous solution with equal periodicities (but opposite sign in the wave-vectors) emerges. For intermediate values of the baryon chemical potential $\bar{\mu}$ the system energetically favors an inhomogeneous ground state, while at lower $\bar{\mu}$ the inhomogeneous phase is disfavored against a homogeneous solution.

If μ_I at fixed $\bar{\mu}$ is altered, a sequence of different ratios n_u/n_d is energetically favored. At small values of the isospin-asymmetry, phases with equal periodicities are most favored, while gradually for increasing μ_I phases with unequal periodicities become more and more favored against the inhomogeneous solution with equal periodicities. For ratios near unity the thermodynamic potential is slightly higher than the one for a phase with equal periodicities, i. e. $\Omega(T,\bar{\mu},\mu_I)|_{n_u/n_d\neq -1} > \Omega(T,\bar{\mu},\mu_I)|_{n_u/n_d=-1}$ for small μ_I, which is not the case any more, when we change μ_I to higher values. Larger ratios are disfavored at small μ_I and while keeping a ratio with a large value fixed, there is a second-order

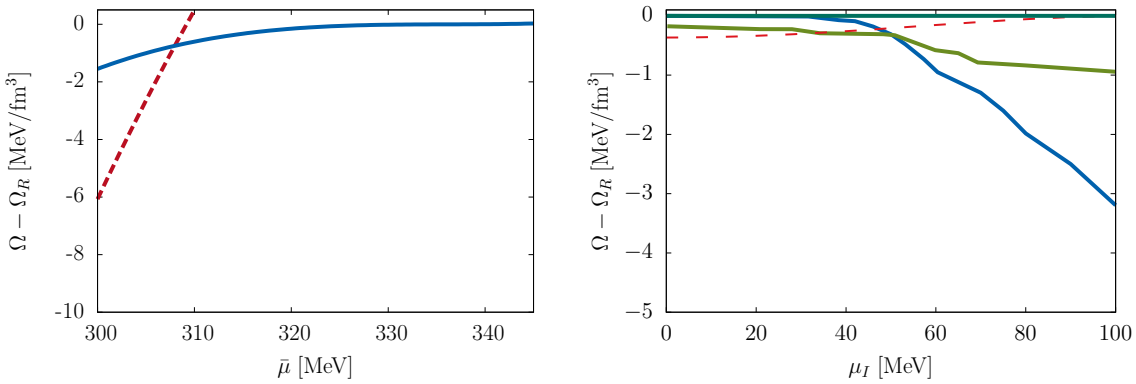

Figure 4.26.: *(Left):* Thermodynamic potential (relative to the restored phase) at $T = \mu_I = 0$ for a plane-wave modulation of the condensates (solid blue). For comparison, also the homogeneous solution is shown (dashed red). *(Right):* Thermodynamic potential (relative to the restored phase) at $T = 0$, $\alpha = 0.2$ and $\bar{\mu} = 320\,\mathrm{MeV}$ for a plane-wave modulation of the condensates with $n_u/n_d = 5$ (solid blue) and $n_u/n_d = 5/4$ (solid green). For comparison, also the CDW solution is shown (dashed red).

phase-transition from the restored to the inhomogeneous phase at non-zero μ_I as can be seen for $n_u/n_d = 5$ in the right panel of Fig. 4.26. At very large μ_I even this phase becomes disfavored against a homogeneous chiral-symmetry breaking phase (which occurs at $\mu_I \approx 200$ MeV and is thus not shown in the figure). The phase transition from the inhomogeneous to this homogeneous phase is first order. It seems plausible that the energetically favored ratio grows with increasing μ_I. For the ratio $n_u/n_d = 5/4$, which is also present in the figure, an (i, i)-solution is found, which becomes the most favored solution in some interval at intermediate values of μ_I. Subsequently also other ratios become favored, if the isospin-chemical potential is increased. At least for the ratios we considered, the growing of the energetically favored value of n_u/n_d is within numerical errors[4] supported by our calculations, since first the phase with $n_u/n_d = -1$ is energetically preferred, then the ratio $5/4$ follows and for large μ_I a ratio with a large value of 5 is energetically favored.

For $n_u/n_d = 4/3$ the amplitudes at $\bar{\mu} = 320\,\mathrm{MeV}$ are shown in Fig 4.27. For this, we find that even at $\mu_I = 0$ different amplitudes emerge, although the condensate modulation for this ratio is not the most favored phase there. Together with the unequal periodicities, the resulting mass function is a beat of two frequencies and different magnitudes in position space. In general, it seems at $\alpha \neq 0$ that simple modulations of the condensates are more preferred in comparison to simple modulations of the quark masses.

Comparing the free energies for the condensate and the mass ansatz shows that de-

[4]The relative error is below or equal to 10^{-10} in our numerical setup for the thermodynamic potential, from which the most favored set of variational parameters at fixed ratio n_u/n_d was determined and the pressures of the solutions compared.

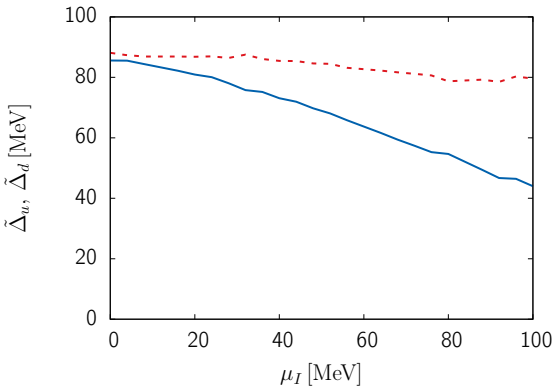

Figure 4.27.: Amplitudes $\tilde{\Delta}_u$ (blue solid) and $\tilde{\Delta}_d$ (dashed red) for the condensate ansatz at $T = 0$, $\bar{\mu} = 320\,\mathrm{MeV}$, $\alpha = 0.2$ and $n_u/n_d = 4/3$.

pendent on the ratios n_u/n_d the condensate ansatz can be favored over the mass ansatz at $\alpha = 0.2$ and thus stabilizes the inhomogeneous phase.

At fixed $\mu_I = 50\,\mathrm{MeV}$ and $\alpha = 0.2$, we determine the most favored value of the considered ratios by choosing the solution with the highest pressure, as shown in Fig. 4.28. We find for three values of $\bar{\mu}$, that relative large ratios $n_u/n_d = 2$ seem to be in general favored. For $\bar{\mu} = 320\,\mathrm{MeV}$ a phase with $n_u/n_d = 4/3$ is favored. Clearly here a solution with equal periodicities is energetically not the most preferred solution.

For $\alpha = 0.5$, we calculate the most favored ratio n_u/n_d in the whole $\bar{\mu} - T$-plane for a set $n_u/n_d \in \{-1, 4/3, 2, 5\}$, from which we determine the energetically preferred solution at given values of $T, \bar{\mu}, \mu_I$. The resulting $\bar{\mu} - T$ phase diagram for $\mu_I = 60\,\mathrm{MeV}$ is shown in Fig. 4.29. There we find that different ratios are again favored throughout different regions of the phase diagram. Moreover, allowing for unequal periodicities stabilizes the inhomogeneous phase considerably when compared to the phase structure of crystalline phases at $\mu_I = 0$, i. e. the thermodynamic potential relative to the restored phase has larger negative values than for the isospin-symmetric case. In contrast to $\alpha = 0.2$ the order of the favored ratios along the $\bar{\mu}$-axis is different; first, large values are favored until the inhomogeneous phase ends at $n_u/n_d = 4/3$ before the ratio actually reaches unity. The regions associated with different periodicities are almost parallel to the temperature axis for a large range, and bend for high temperatures for large ratios to lower $\bar{\mu}$, while for higher $\bar{\mu}$ the boundary shows an s-shape.

To summarize our findings, we note that at least for $\alpha = 0.5$, $\alpha = 0.2$ the condensate ansatz is favored over the CDW or the mass ansatz and it seems to also hold for finite temperature, which we only checked for $\alpha = 0.5$. It is still an interesting question, to investigate if more complicated shapes of the modulation are favored. For a realistic degree and maximally coupled quark flavors, we have confirmed that the occurrence of a beat in the quark masses may stabilize the system considerably.

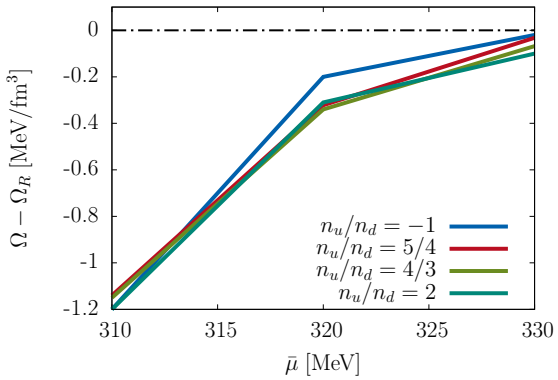

Figure 4.28.: Thermodynamic potential (relative to the restores phase) when allowing for the condensate ansatz at $T = 0$, $\mu_I = 50\,\mathrm{MeV}$, $\alpha = 0.2$ and different ratios n_u/n_d.

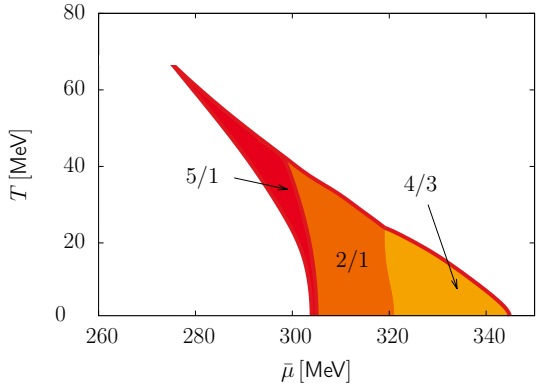

Figure 4.29.: Phase diagram in the $\bar{\mu} - T$ plane for $\mu_I = 60\,\mathrm{MeV}$. The shaded areas indicate the regions where an inhomogeneous solution for the condensate ansatz is favored over a homogeneous solution. The different colors correspond to different values of the energetically most favored ratio n_u/n_d, as indicated by the label.

5. Compact stellar matter

One interesting possibility, where our work may have significant impact, is the physics of compact stars. Although it is currently not fully clear if quark matter persists in compact stars, eventually inhomogeneous chiral symmetry-breaking condensates could have influence on astrophysical observables and thus enabling access to the QCD phase structure. Mandatory for this is electric charge-neutrality of the neutron star, from which the requirement of non-zero isospin chemical potentials arises, since the electric charge of up and down quarks are not the same.

First investigations at $\alpha = 0$ however found no significant influence of crystalline chiral-symmetry breaking phases on mass-radius relations of neutron stars [56, 57], which is also confirmed by our calculations and fully consistent with our expectations. In particular, since the energy difference of inhomogeneous chiral symmetry-breaking phases compared to homogeneous chiral symmetry-breaking phases is rather small, no significant influence on the maximum stellar radius or mass is present.

In the following we study different degrees of flavor-mixing on compact star properties. First, we study the phase structure for electric charge-neutral matter when allowing for a spatial modulation of the order-parameters. Then, we derive an equation of state for quark matter and use it as an input for mass-radius calculations for quark stars.

5.1. Electric charge neutrality

Since compact stars need to have vanishing net electric charge and be in beta equilibrium, the isospin-chemical potential is no longer an independent external parameter but is fixed by the conditions of requiring charge-neutrality. To describe such a situation, we need to introduce leptons in our model, which we will do by considering a homogeneous gas of massless electrons. Additionally we require quark matter to be in β-equilibrium with electrons, satisfying the process

$$d \rightleftharpoons u + e^- + \bar{\nu}_e. \tag{5.1}$$

For the neutrinos we assume that they leave the system as soon as they are created. Then we have baryon number conservation, a conserved electric charge and in principle three color charges, which however play no role in our setup; thus our system is characterized by two conserved charges: the net quark number and the overall electric charge. The chemical potentials for the quarks and electrons are then given in terms of a quark

number chemical potential and an electric charge chemical potential by

$$\mu_u = \mu + \frac{2}{3}\mu_Q, \tag{5.2}$$

$$\mu_d = \mu - \frac{1}{3}\mu_Q, \tag{5.3}$$

$$\mu_e = -\mu_Q. \tag{5.4}$$

The electric charge chemical potential is related by $\mu_Q = \mu_I$ to the isospin-chemical potential introduced earlier, while $\bar{\mu} = \mu + \mu_Q/6 \neq \mu$.

The thermodynamic potential Eq. (3.39) needs to be extended by the contribution of the electrons to

$$\Omega_{\text{tot}}(T, \mu, \mu_Q) = \Omega_{\text{kin}}(T, \mu, \mu_Q) + \Omega_{\text{cond}} + \Omega_e(T, \mu_Q), \tag{5.5}$$

where

$$\Omega_e(T, \mu_Q = -\mu_e) = -\frac{1}{12\pi^2}\left(\mu_e^4 + 2\pi^2 T^2 \mu_e^2 + \frac{7\pi^4}{15}T^4\right). \tag{5.6}$$

To ensure global electric charge neutrality in compact stellar matter also the number densities need to be determined, which are given on mean-field level by

$$n_\alpha(z) = \left\langle \bar{\alpha}\gamma^0\alpha \right\rangle, \tag{5.7}$$

where α are the spinors for the α-th species.

In general the number densities can also be spatially varying for inhomogeneous chiral condensates, except for the CDW and the plane-wave case where the densities are constant-in-space. For the CDW case it was shown that although the chiral condensates are modulated, the number density stays constant in space (see e. g. [47, 58, 46]) and does not follow the modulation of the quark masses $M_f(z)$. The same reasoning also applies to the plane-wave modulation of the mass functions of section 4.4, as we will argue below.

The spatially averaged number densities of the up and down quarks can be derived from inserting the corresponding spinors u and d in Eq. (5.7) and yield

$$\bar{n}_f(T, \mu, \mu_Q) = \langle n_f(z) \rangle = -\frac{\partial \Omega_{\text{tot}}(T, \mu, \mu_Q)}{\partial \mu_f}. \tag{5.8}$$

Analogously the number density for the electrons are obtained from

$$\bar{n}_e(T, \mu_Q) = \frac{\partial \Omega_e(T, \mu_Q)}{\partial \mu_Q}. \tag{5.9}$$

Although the requirement of local charge neutrality would be possible, here we require our strong-interaction matter to be only globally charge neutral and therefore we can use the spatially-averaged densities instead of the fully space-dependent densities. The

requirement of electric charge neutrality translates to the vanishing of the overall net electric-charge density

$$\bar{n}_Q(T,\mu,\mu_Q) \stackrel{!}{=} 0 \tag{5.10}$$

yielding the condition

$$\bar{n}_Q(T,\mu,\mu_Q) = -\frac{\partial\Omega_{\text{tot}}(T,\mu,\mu_Q)}{\partial\mu_Q} \tag{5.11}$$

$$= \frac{2}{3}\bar{n}_u(T,\mu,\mu_Q) - \frac{1}{3}\bar{n}_d(T,\mu,\mu_Q) - \bar{n}_e(T,\mu_Q) \stackrel{!}{=} 0, \tag{5.12}$$

from which we can determine μ_Q self-consistently at fixed (T,μ). From now on we will not distinguish for simplicity between the spatially averaged number densities $\bar{n}$ and n, but always mean the spatially-averaged number densities.

5.1.1. Constant-in-space condensates

The number densities for homogeneous condensates are shown in the left panel of Fig. 5.1 at vanishing temperature and zero isospin imbalance. When chiral symmetry is broken, also the density is zero, until it rises slowly at $\mu > M_{\text{vac}}$. Subsequently the density jumps at the phase transition to large values and the density is the same as an ideal massless Fermi gas. In general the density for a Fermi gas for particles with mass M at $T = 0$ with $N_f \times N_c$ degenerate species is given by

$$n_{\text{Fermi gas}}(\mu;M) = \frac{N_f N_c}{3\pi^2}\left(\mu^2 - M^2\right)^{\frac{3}{2}}\Theta\left(\mu - M\right). \tag{5.13}$$

Here, a non-zero effective quark mass qualitatively suppresses at fixed μ large densities, i. e. large masses counteract large densities.

Because of that and the fact that in the homogeneous phase the masses are for non-vanishing flavor mixing in general smaller around the phase transition than for isospin-symmetric matter, we expect the overall number densities n to be larger at $\mu_I \neq 0$ than for isospin-symmetric matter. For non-zero isospin chemical potentials the number densities at $T = 0$ and maximal degree of flavor mixing are shown in the right panel of Fig. 5.1. In comparison to the isospin-symmetric case, the individual contribution to the overall density of the two flavors changes. For the restored phase, both flavors are decoupled and the number densities are independent of each other, as can be seen from the figure.

The number densities for different degrees of flavor mixing are shown in Fig. 5.2. The jump from the region with broken to restored chiral symmetry is also present at $\alpha \neq 0.5$ although it can be weaker, depending on the degree of flavor mixing and μ_I. For completely decoupled quark flavors, the overall number density $\bar{n}$ jumps at the phase transition of the up quarks and jumps again while the down quarks undergo a phase transition – mirroring the fact that both densities $\bar{n}_{u,d}$ depend explicitly only on the respective flavor mass M_f and chemical potential μ_f.

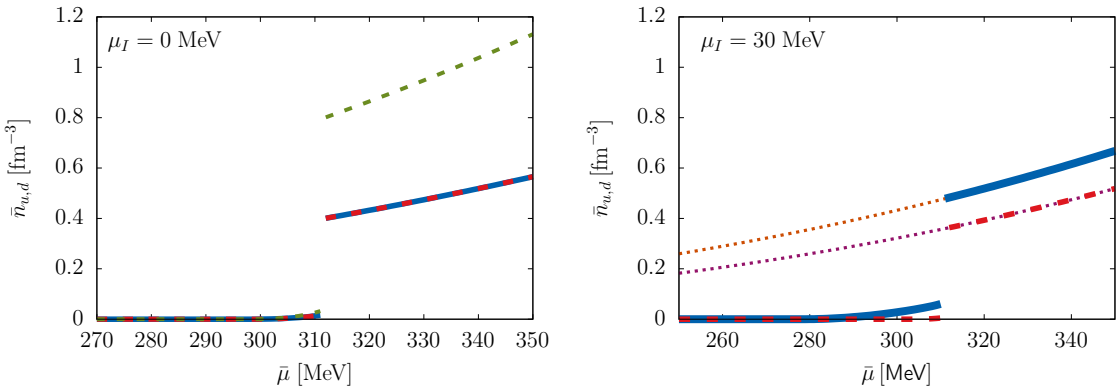

Figure 5.1.: Number densities $\bar{n}_f$ of up (solid blue) and down (dashed red) quarks against the flavor-averaged chemical potential at vanishing temperature for constant-in-space condensates, $\alpha = 0.5$ and at two values of the isospin chemical potential. For reference also the number density of an ideal massless Fermi gas at $\mu_I = 30\,\mathrm{MeV}$ (small dotted lines) and the total averaged number density $\bar{n} = \bar{n}_u + \bar{n}_d$ at $\mu_I = 0$ (dotted green) are shown.

Evaluating the condition Eq. (5.12), allows to determine μ_I self-consistently and we then get the variational parameters ($\{M_f\}$) at given (T, μ, μ_Q). The result is shown in Fig. 5.3, where at vanishing temperature the isospin-chemical potential is first zero, then drops slowly before the phase transition and finally becomes of the order of $\approx -100\,\mathrm{MeV}$ and is getting more negative for increasing μ. The quark mass does only differ slightly around the phase transition when compared to the results in isospin-symmetric matter for $\alpha = 0.2$.

5.1.2. Spatially-varying condensates

For spatially-varying condensates, we focus first on the simple case of plane-wave modulations of the quark masses. To show that also for the case of plane-wave modulations of the mass functions the number densities are constant-in-space, let us modify the basic arguments used by the authors of ref. [46] to prove that the number density also for our case of non-degenerate flavors are spatially constant: considering chiral transformations of the form $f = \exp(-i\gamma^5 q_f z_0/2) f'$ on the (space-dependent) spinor of flavor f with z_0 being a constant, one recognizes that the number densities are invariant under such transformations

$$\left\langle \bar{f}\gamma^0 f \right\rangle = \left\langle \left[\bar{f}' \exp\left(-i\gamma^5 \frac{q_f}{2} z_0\right)\right] \gamma^0 \left[\exp\left(-i\gamma^5 \frac{q_f}{2} z_0\right) f'\right] \right\rangle = \left\langle \bar{f}'\gamma^0 f' \right\rangle , \tag{5.14}$$

since γ^0 anti-commutes with γ^5. For the mass functions, the chiral transformation however leads to a phase shift resp. to a translation by z_0 in the direction of the modulation, showing that the number densities cannot be spatially varying, like reasoned for the CDW case by Carignano et al. [46] and hence also the number densities for the plane-wave case are constant in space. Then we can evaluate Eq. (5.11) with using only the

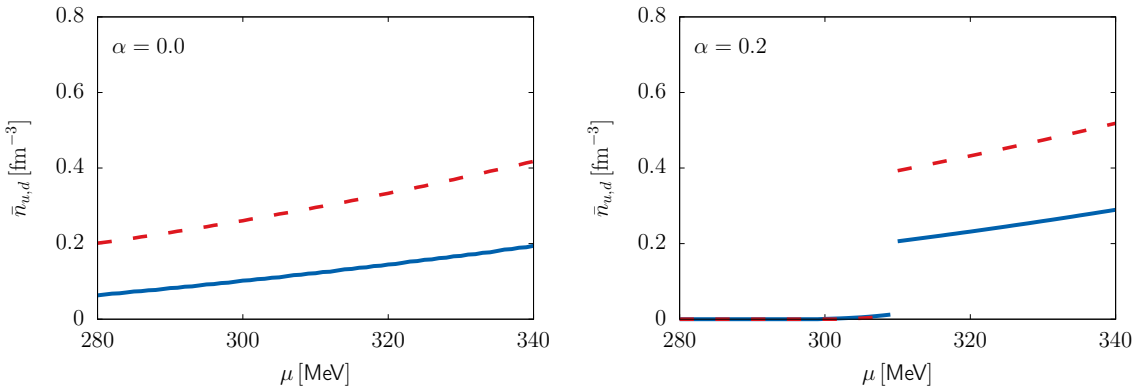

Figure 5.2.: Number densities $\bar{n}_f$ of up (solid blue) and down (dashed red) quarks for charge neutral quark matter in β-equilibrium against the flavor-averaged chemical potential and vanishing temperature for constant-in-space condensates and two different degrees of flavor mixing.

much simpler constant-in-space densities. For more complicated types of modulation this will in general not work, but this will be anyhow out of scope of the thesis (and we require $\bar{n}_Q = 0$ here).

Exemplary for a realistic degree of flavor mixing the number densities of up and down quarks are shown in Fig. 5.4 at $T = 0$, where again the suppression of the number densities due to large quark masses is seen. Around the first-order phase transition in the inhomogeneous phase the density is always smaller than for purely homogeneous condensates (as indicated by the dashed line). An asymmetry between the two quark flavor does not change this, but shifts the two number densities n_u and n_d for fixed μ_I along the y-axis apart from each other.

For a plane wave modulation of the quark masses, the self-consistently obtained isospin-chemical potential does not differ much from the homogeneous results. The resulting mass function at the self-consistently determined value of the isospin-chemical potential at zero temperature is shown in Fig. 5.5 for the special case of a chiral density wave and in Fig. 5.6 for a case where the amplitudes of the quark masses were allowed to be different. For small chemical potentials the result is a solution with homogeneous chiral condensates in charge-neutral matter, while for intermediate values of the averaged chemical potential inhomogeneous chiral symmetry breaking still occurs, but only in a smaller μ-window than for $\mu_I = 0$. The onset of the inhomogeneous phase in charge-neutral matter is slightly shifted to lower μ-values, which is also seen in strong-interaction matter with non-zero electrical net charge, when considering $\mu_I \neq 0$. For a realistic degree of flavor-mixing, the inhomogeneous window at $T = 0$ is larger than for a CDW wave (cf. Figs. 5.5 and 5.6), although the absolute numbers do not differ much. Before the phase transition, both amplitudes agree with each other and afterwards the amplitudes are not equal any more in the inhomogeneous phase. These effects are due to the self-consistently tuned values of μ_I and are the same as we have seen for inhomogeneous chiral condensates in isospin-asymmetric matter (with fixed μ_I).

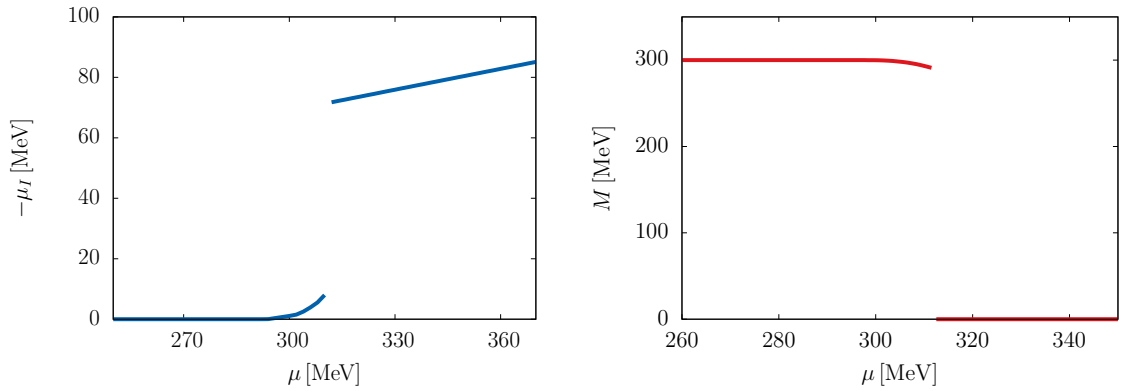

Figure 5.3.: Isospin-chemical potential $\mu_I = \mu_Q$ (left) and the quark mass $M_u = M_d = M$ (right) at $T = 0$, $\alpha = 0.5$ as a function of the quark-number chemical potential μ for charge-neutral matter in β-equilibrium, allowing for homogeneous condensates.

In the phase diagram of charge-neutral matter, regions with inhomogeneous chiral symmetry breaking are still found and coexist with areas where chiral symmetry is homogeneously broken or it becomes restored. For a chiral density wave, the phase structure is depicted on the left in Fig. 5.7, where it can be seen that the inhomogeneous region is smaller than for the case $\mu_I = 0$. Especially for large temperatures the inhomogeneous phase in charge-neutral matter becomes energetically disfavored and thus extends to lower temperatures than in electrically charged quark matter at $\mu_I = 0$.

5.2. Mass-radius relation

In this section we will consider the mass-radius relation of a pure quark star to show the influence of our equation of state on astrophysical observables. For this we need to have quark matter to be electric charge neutral and we will allow inhomogeneous chiral symmetry breaking condensates. Being aware that a compact star with solely two-flavor quark matter is not a realistic setup, our aim here is to study the influence of inhomogeneous phases on the quark level, for which a pure quark star is sufficient.

The equation of state (EoS) is required to solve the relation between the quark stars' mass and radius from the TOV equations. It provides a relation between state variables and typically links the pressure p to the energy density ϵ. To derive this relation one has to incorporate the microscopic details of the underlying theory by using a thermodynamic description for matter in equilibrium. For a grand canonical ensemble the internal energy density is related to the pressure, temperature T, entropy density s, chemical potentials μ_i and number densities n_i by

$$\epsilon = -p + Ts + \sum_i \mu_i \, n_i. \tag{5.15}$$

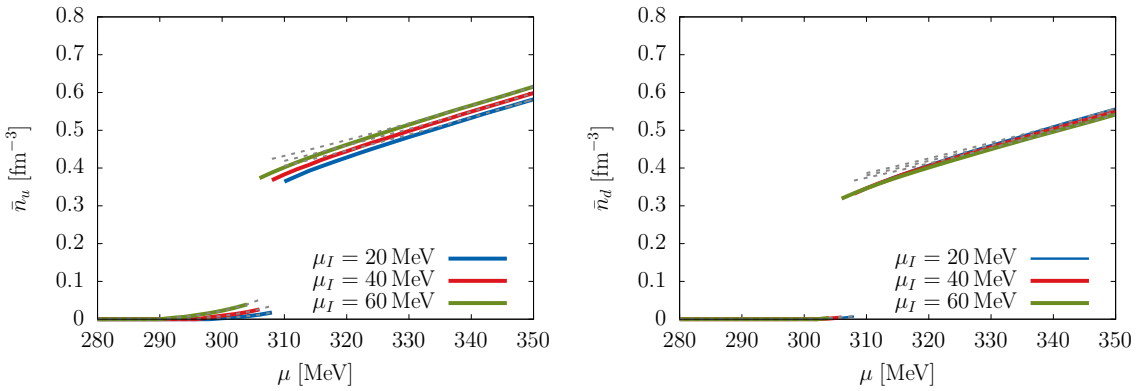

Figure 5.4.: Number densities of up (left) and down quarks (right) for different values of μ_I at $T = 0$, $\alpha = 0.2$ and a plane wave modulation of the quark masses. For reference also the results for homogeneous chiral condensates are shown (gray).

The pressure can be obtained from the thermodynamic potential as

$$p = -\left(\Omega - \Omega_0\right) \tag{5.16}$$

where Ω_0 is the thermodynamic potential in vacuum. The entropy density can be derived from the grand potential by

$$s = -\frac{\partial \Omega}{\partial T}. \tag{5.17}$$

In the following we assume that the energy density is constant-in-space and want to apply our equation of state to determine the structure of a spherical, non-rotating star. From the Einstein equations of general relativity, one can derive differential equations, specifying the radial gradient of the star's mass M_{star} and pressure p. This is accomplished by the Tolman-Oppenheimer-Volkoff (TOV) equation, which is explicitly given by [59, 60]

$$\frac{dp}{dr} = -\frac{G\left(p+\epsilon\right)\left[M_{\text{star}}(r) + 4\pi r^3 p\right]}{r\left(r - 2GM_{\text{star}}(r)\right)} \tag{5.18}$$

with $M_{\text{star}}(r)$ being the star's mass enclosed in a sphere with radius r, given by

$$M_{\text{star}}(r) = 4\pi \int_0^r dr'\, r'^2 \epsilon \tag{5.19}$$

and G denotes Newton's gravitational constant. To solve this differential equations, we use a numerical Runge-Kutta method.

The star's radius R is determined by the value of the radial coordinate, where the pressure vanishes, i. e. $p(r = R) = 0$. To determine an actual trajectory in the $M_{\text{star}}(r = R) - R$ plane, we start by solving Eq. (5.18) from the core of the star to the surface.

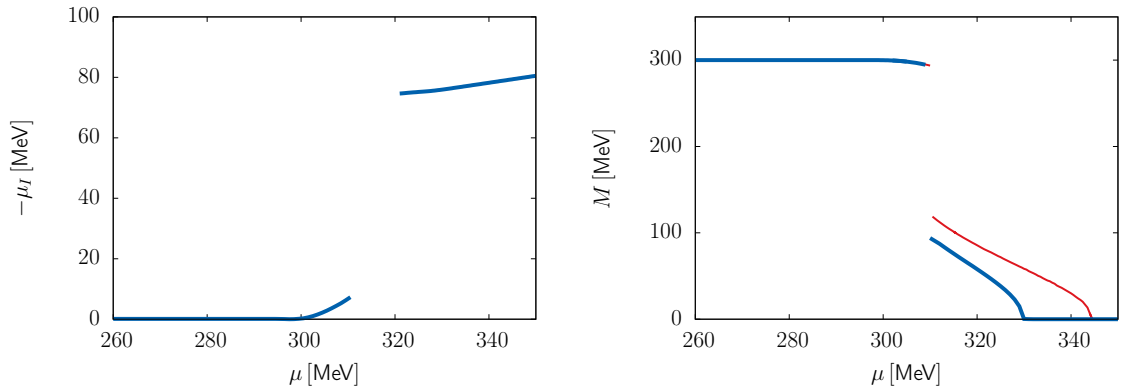

Figure 5.5.: Isospin-chemical potential $\mu_I = \mu_Q$ *(left)* and amplitude M (blue solid) on the right panel for a chiral density wave at $T = 0$ for electrical charge-neutral matter. For reference the amplitude of a CDW at $\mu_I = 0$ is also shown (red thin line).

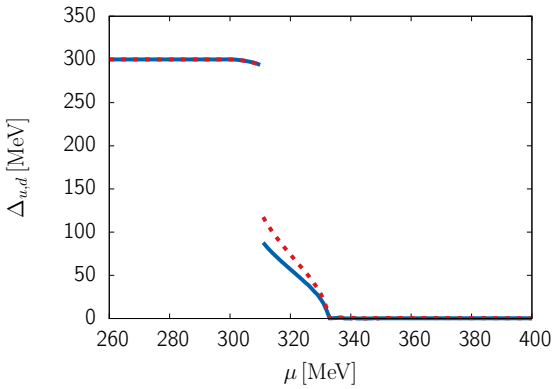

Figure 5.6.: Amplitudes of up (red dashed) and down (blue solid) quarks at $T = 0$ for charge neutral matter at $\alpha = 0.2$ and a plane-wave modulation of the quark masses.

In general we expect that there exists a maximal mass for a given equation of state. Since recently two $M_{\text{star}} = 2M_{\text{Sun}}$ neutron stars were experimentally observed [61, 62], this poses severe limitations to realistic equation of states. Furthermore, since we are dealing with cold and dense compact star matter, we restrict ourselves to vanishing temperatures.

5.2.1. Homogeneous condensates

For isospin-symmetric, homogeneous matter the EoS and the quark stars' masses and radii are shown in Fig. 5.8. The maximal mass is around 1.92 M_{Sun} at around $R = 11.25\,\text{km}$. Clearly our EoS does not meet the required mass of two solar masses, which is however not surprising since we consider only neutron stars made of pure quark matter.

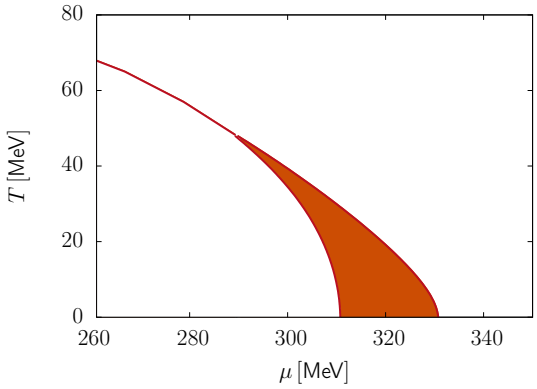

Figure 5.7.: Phase diagram for charge-neutral matter. In the shaded region a chiral density wave for the modulation of the quark masses is energetically favored over the homogeneous phase (to the left of the inhomogeneous region) and over the restored phase (to the right of the inhomogeneous phase).

It is conceivable that by allowing for nuclear matter we may reproduce mass-radius relations satisfying the two solar mass limit. Due to our choice of parameters, the quark matter is not self-bound, which therefore allows for large radii at low masses for quark stars.

In the following we first investigate the effects of an isospin-imbalance on mass-radius sequences before we turn to charge-neutral matter. For isospin-asymmetric matter, the quark star can have a larger mass, since the EoS gets stiffer. Smaller degrees of flavor mixing also stabilize the star, as can be seen in Fig. 5.9, where different α's at various values of μ_I are shown. At $\alpha = 0.5$ the stiffening has small effects on the mass-radius relation of the quark star, while for $\alpha = 0$ the maximal mass rises, being above $M_{\text{star}} = 1.95\, M_{\text{Sun}}$. At the same time the position of the maximum of the $M - R$ trajectory shifts to larger radii. For a realistic degree of flavor mixing $\alpha = 0.2$ the corresponding trajectories in the $M - R$-plane and the effects of an isospin-chemical potential are visible in the right panel of Fig. 5.9. Again at low masses an increasing isospin-chemical potential shifts the star's radius to larger values. The peaks of the curves shift slightly to larger masses for non-vanishing isospin imbalance.

By considering charge-neutral quark matter, the maximum obtainable mass is around $M_{\text{star}} \approx 1.93 M_{\text{Sun}}$, the maximum gets shifted to large radii and mainly the behavior at small star masses is affected by the self-consistently obtained μ_I required for charge neutrality, as can be seen in Fig. 5.10.

As already mentioned, one should also include nuclear matter in this discussion, but this is not in the scope of the thesis.

5.2.2. Inhomogeneous condensates

Allowing for inhomogeneous condensates instead of purely homogeneous ones, changes the EoS mainly around the former first-order phase transition. In total the effects on

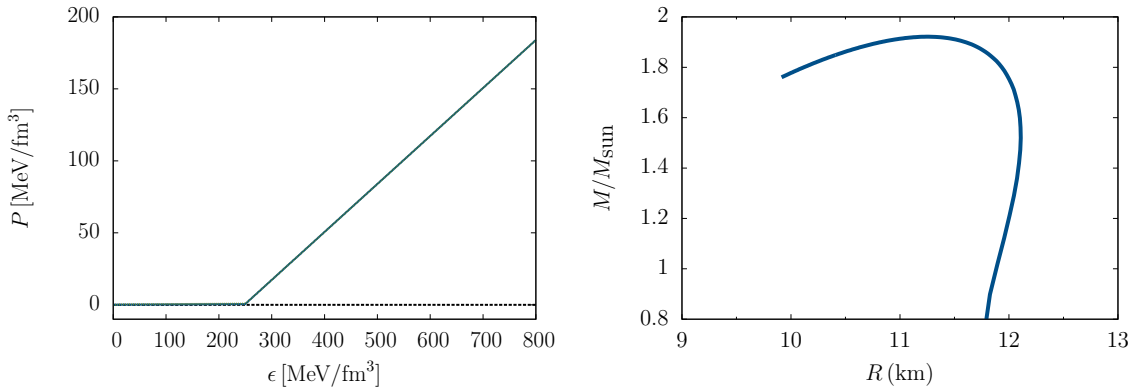

Figure 5.8.: *(Left):* Equation of state $P(\epsilon)$, which enters the TOV equation. *(Right):* Mass-radius relation for a pure quark star. Here, we neglect the charge-neutrality constraint, i. e. consider isospin-symmetric matter $\mu_I = 0$ and limit ourselves to homogeneous condensates at $T = 0$.

the thermodynamics quantities are small[1]. Therefore the anticipated effects for spatially varying condensates on the mass-radius relation are expected to also be small.

In the following we will concentrate on the simple ansatz of a plane-wave modulation of the quark masses and again consider only vanishing temperatures.

The pressure for isospin-symmetric matter for homogeneous and inhomogeneous condensates differs only around the phase transition and for high densities. Consequently also the EoS entering the TOV equation has only small variations compared to the homogeneous one and the resulting $M-R$ sequence is shown in Fig. 5.11. Compared to the sequence for homogeneous matter, the mass-radius relation does not differ much for crystalline condensates and the maximal mass is not distinguishable between homogeneous and inhomogeneous condensates, which was already found in [57].

For isospin-asymmetric matter at a realistic degree of flavor mixing the EoS becomes softer for inhomogeneous condensates (cf. Fig. 5.12, right panel) for higher densities in comparison to homogeneous condensates, while at small number densities the EoS with crystalline phases is stiffer. Thus when allowing for crystalline phases, (slightly) smaller star masses can be reached than for purely homogeneous chiral condensates, since the pressure of the quarks cannot support larger star masses and radii. This is shown in Fig. 5.13 where the mass radius sequence at $\alpha = 0.2$ and $\mu_I = 20\,\text{MeV}$ can be seen for homogeneous and inhomogeneous phases. In general there are two counteracting effects for non-zero isospin chemical potentials: first, a realistic degree of flavor mixing shifts the whole mass-radius sequence to larger radii, while the basic shapes stays nearly the same. Second, when allowing for inhomogeneous condensates the masses and radii of the quark star are shifted down again. The effects due to different shapes of the modulation on the mass-radius sequences is very small and is shown for one configuration in the

[1]The pressure, for example, changes on the sub-percent or percent level when comparing solutions with homogeneous condensates to solutions with inhomogeneous condensates for all kinds of modulations we considered.

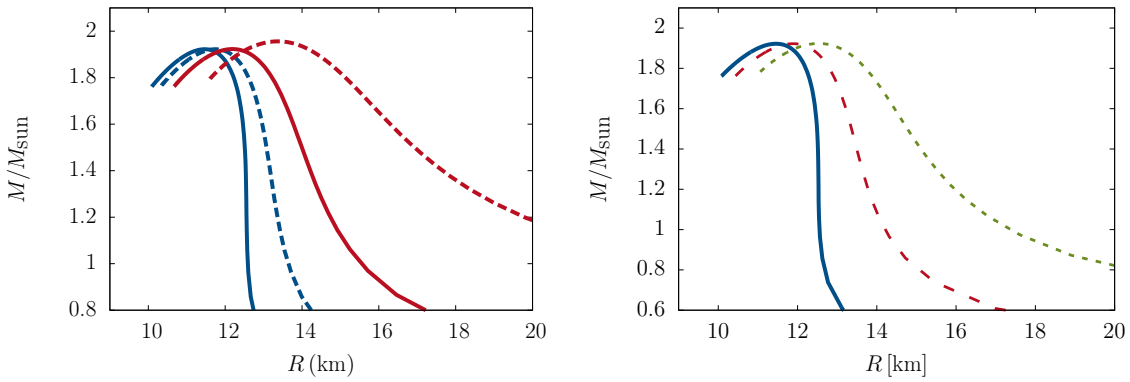

Figure 5.9.: *(Left):* Mass-radius relation at $\mu_I = 10\,\mathrm{MeV}$ (blue) and $\mu_I = 20\,\mathrm{MeV}$ (red) for $\alpha = 0$ (dashed) and $\alpha = 0.5$ (solid). *(Right):* Mass-radius relation at $\mu_I = 2\,\mathrm{MeV}$ (solid blue), $\mu_I = 10\,\mathrm{MeV}$ (dashed red) and $\mu_I = 20\,\mathrm{MeV}$ (dotted green) for $\alpha = 0.2$. For both $M - R$-relations a pure quark star was assumed and only homogeneous condensates evaluated at $T = 0$ were considered.

right panel of Fig. 5.13. For the CDW modulation the maximal star mass is smaller but situated at larger radii than for a plane-wave modulation with different amplitudes of the flavors. At the lower end of the curve in the $M - R$ plane, the CDW has in contrast smaller masses at the same radius than the solution with $\Delta_u \neq \Delta_d$.

The effects of μ_I are also visible in Fig. 5.14, where a non-zero isospin-chemical potential shifts the mass-radius sequences to larger radii. The maxima of these sequences occur at larger radii in comparison to smaller μ_I, while also the maximal attainable mass also grows with increasing μ_I. For self-consistently determined values of μ_I, the mass-radius sequence is shown in the right panel of the figure. We find that also for this configuration, the maximal star's mass is still comparable to the one for isospin-symmetric quark matter or even to purely homogeneous quark matter at $\mu_I = 0$. The maximum of the $M - R$-curve is only weakly dependent on the exact values of μ_I or the shape of the modulation for which the EoS enters the TOV calculations.

The difference between inhomogeneous and homogeneous chiral condensates in the experimentally observable area in the $M - R$–plane is very small and thus the determination of clear signatures for inhomogeneous chiral symmetry breaking in compact stellar objects seems currently not possible from this relation. This was already known for isospin-symmetric matter, but for isospin-asymmetric quark matter the occurrence of crystalline chiral condensates together with a non-maximal degree of flavor mixing could enable future experiments to find evidence of it.

On the other hand it is clear that our model is not able to realistically describe compact stellar matter, since at the densities realized in the interior of compact stars also color-superconductivity should affect the phase structure of strong-interaction matter (see e. g. [63]) or magnetic fields can play an important role (see e. g. [64]).

Since we only model a quark star, the next step would be to additionally account

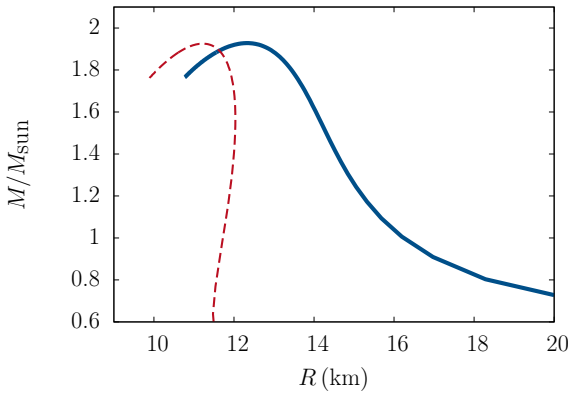

Figure 5.10.: Mass-radius relation for an electric charge-neutral quark star with homogeneous chiral-symmetry breaking condensates at $\alpha = 0.2$ and $T = 0$. For reference also the solution for charged quark matter at $\mu_I = 0$ is shown (dashed red).

for nuclear matter, which could for example result in a neutron star with a possible inhomogeneous quark core. Then, also the interplay of superconductivity with chiral symmetry breaking should be studied, where also interesting effects might arise for mass-radius sequences, if charge-neutral matter is considered. Even more important are transport properties, which should be influenced more strongly by inhomogeneous chiral symmetry breaking phases.

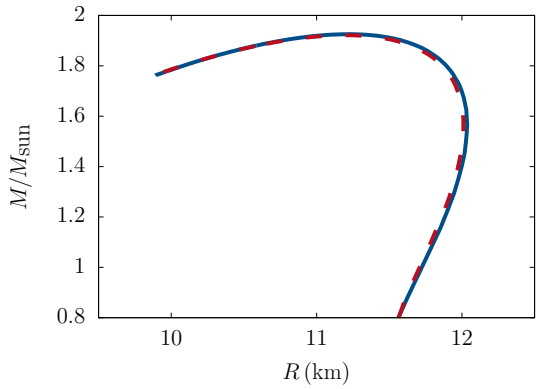

Figure 5.11.: Mass-radius sequence for a quark star for a plane-wave modulation of the chiral condensates in isospin-symmetric matter at $T = 0$. For reference also the sequence for purely homogeneous condensates is shown (dashed red).

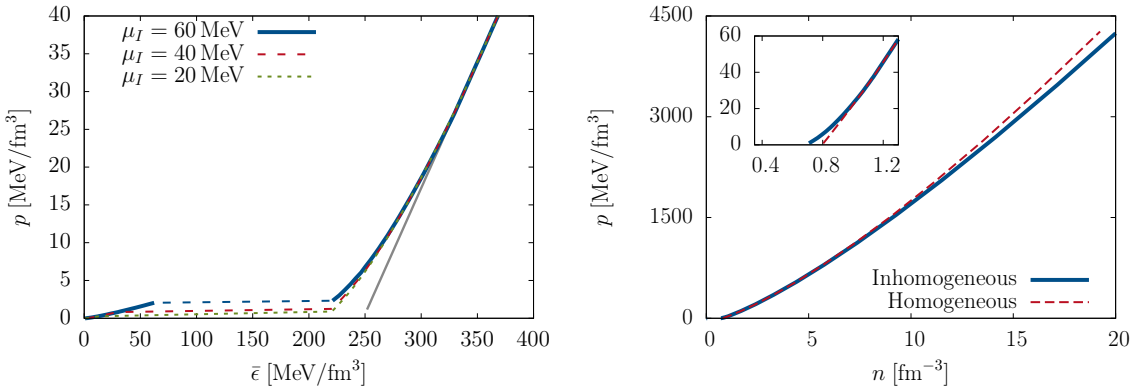

Figure 5.12.: *(Left):* Equation of state $\epsilon(p)$ for different values of μ_I at $T = 0$, $\alpha = 0.2$ and a plane wave modulation of the quark masses. For reference also the results for homogeneous chiral condensates are shown (gray). *(Right):* Pressure against the number density $n = \bar{n}_u + \bar{n}_d$ at $T = 0$, $\alpha = 0.2$ and $\mu_I = 20\,\mathrm{MeV}$ for constant-in-space and modulated chiral condensates.

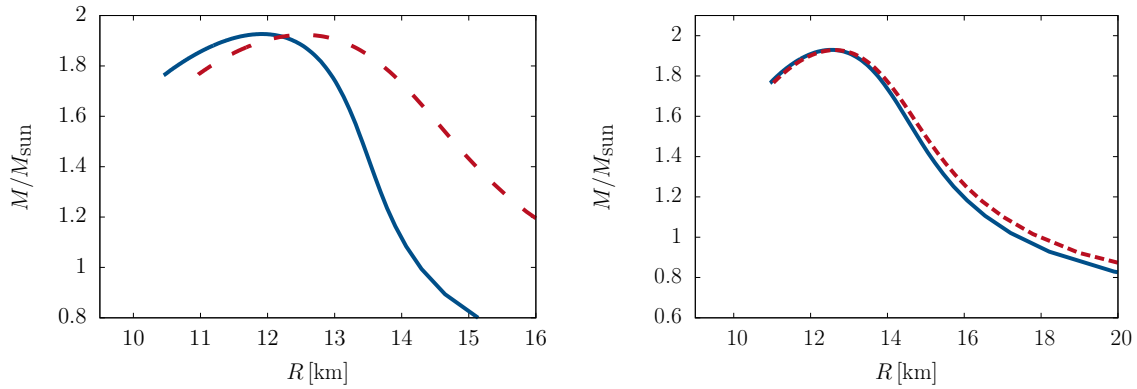

Figure 5.13.: Mass-radius relation of a quark star at $T = 0$ and $\alpha = 0.2$. *(Left):* Comparison of the $M - R$ sequence at $\mu_I = 20\,\text{MeV}$ for homogeneous chiral condensates (dashed red) and a crystalline phase with a plane-wave modulation of the quark masses (solid blue). *(Right):* $M - R$ sequence at $\mu_I = 40\,\text{MeV}$ for a CDW (dashed red) and a plane-wave modulation of the quark masses (solid blue).

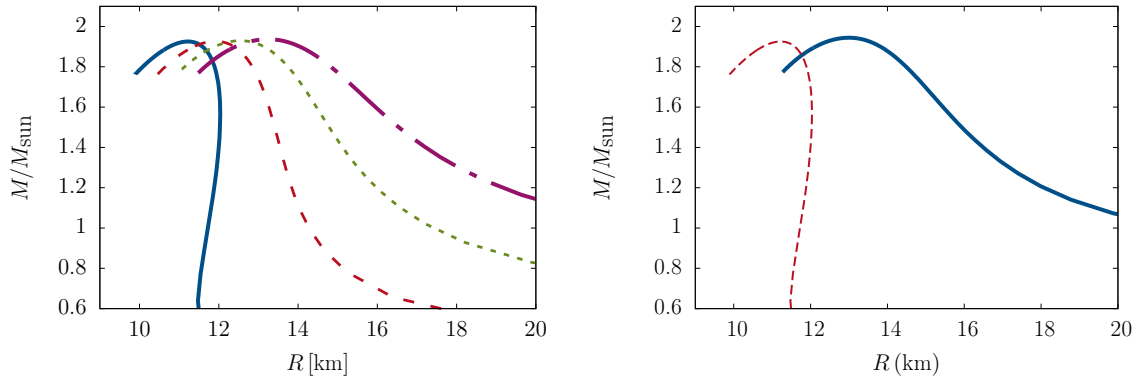

Figure 5.14.: Mass-radius sequence at $T = 0$, $\alpha = 0.2$ for a plane-wave modulation of the quark masses at different values of μ_I: *(left):* isospin-symmetric matter (solid blue), $\mu_I = 20\,\text{MeV}$ (dashed red), $\mu_I = 40\,\text{MeV}$ (dotted green) and $\mu_I = 60\,\text{MeV}$ (dash-dotted purple). *(Right):* For self-consistently determined value of μ_I for charge neutral matter. For reference also the solution for $\mu_I = 0$ is shown (dashed red).

6. Interplay with color superconductivity

Besides the occurrence of crystalline chiral symmetry breaking through quark-antiquark pairs at low temperatures and intermediate densities, also color superconductivity may be present in the region of interest. In general, according to the Cooper theorem, fermionic systems form pairs of fermions at no free energy cost in the vicinity of the highly degenerate surface of the Fermi sphere if an attractive interaction is present. In turn this leads to an instability in the normal state, favoring the state with the condensed pairs. Since for QCD there are attractive interaction-channels, the ground state of QCD may be color-superconducting [65, 66, 67, 68], i. e. forming condensates of fermion pairs. In particular, the pairs formed are (naively speaking) consisting of two quarks and are called diquarks. Since quarks have many degrees of freedom, different pairing patterns for color-superconductivity can occur (see e. g. [63] for a review), but most prominently a gap in the single-particle spectrum develops for color-superconductivity.

Currently it is not clear from first-principle calculations which phase is actually favored in the intermediate density and temperature region, but at asymptotically high densities and three colors quark matter is expected to be deconfined and forms a homogeneous color-superconductor.

The condensation at equal Fermi spheres for isospin-symmetric matter does not cost any energy, which is not the case any more, if the Fermi momenta of the fermions are unequal. Then, there is a possibility for an adaption process of the Fermi spheres to become equal and then form again diquark condensates. This process is naturally limited by the energy gain through condensation that needs to compensate the energy required to adapt the Fermi spheres [69, 70, 71].

For crystalline color-superconducting phases the system tolerates larger asymmetries between the Fermi spheres (see e. g. [8] for a review, or e. g. ref. [7]) and the quark-quark pairs do not have vanishing overall momentum. Then, crystalline color-superconducting phases can be favored in asymmetric matter over the homogeneous color-superconducting or restored phase.

Since chiral symmetry breaking and color-superconductivity are affected in different ways by an asymmetry between the quark chemical potentials and can appear at the same baryon density range, it is an interesting question to study which phase structure is actually realized when the interplay of chiral symmetry breaking and color-superconductivity is allowed. Namely, on the one hand color-superconductivity sets in as soon as the number density of the system becomes non-zero, the Fermi spheres are equal and the pairing occurs, but on the other hand chiral symmetry breaking may suppress a non-zero number density. Thus the phase structure strongly depends on the relative weight of the two

different phenomena and detailed (numerical) calculations are required to map out the actual phase structure.

It was already found that a coexistence phase with simultaneously occurring crystalline quark-antiquark pairs and homogeneous quark-quark pairs is favored over the homogeneous phases [72, 11]. For simplicity the investigation was restricted to a chiral density wave modulation for the chiral condensates and a homogeneous color-superconducting condensate at $\mu_I = 0$. For non-zero asymmetry, the possibility of a coexistence phase with simultaneous chiral symmetry-breaking and color-superconductivity was studied in our framework in Ref. [10]. In the following we will present the results (at non-zero isospin-chemical potential) for an interplay of a CDW modulation[1] of the chiral condensates and a constant-in-space diquark gap and detail the phase structure at zero temperature, which should be for example relevant for compact stars.

6.1. Extension of the model

To account for the diquark pairing the model Lagrangian, Eq. (3.1) is extended by an additional term

$$\mathcal{L}_C = H \sum_{A=2,5,7} \left(\bar{\psi} i\gamma_5 C\tau_2\lambda_A \bar{\psi}^{\mathsf{T}}\right)\left(\psi^{\mathsf{T}} C i\gamma_5\tau_2\lambda_A \psi\right) , \tag{6.1}$$

where H is another dimensionful coupling constant, λ_A are Gell-Mann matrices in color space (with color index A) and $C = i\gamma^2\gamma^0$ denotes the charge conjugation operator. In particular, we focus for this quark-quark interaction on scalar condensates of the form

$$s_{2A} = \langle \psi^{\mathsf{T}} C\gamma_5\tau_2\lambda_A\psi\rangle. \tag{6.2}$$

Since for $N_f = 2$ the diquark condensates s_{2A} (with $A = 2, 5, 7$) form a vector in color-space, that can always be rotated by global SU(3)-color transformations, we focus on the s_{22} direction and introduce the 2SC condensate

$$s_{22} = \langle \psi^{\mathsf{T}} C\gamma_5\tau_2\lambda_2\psi\rangle, \tag{6.3}$$

which consists of red and green up and down quarks, while blue quarks remain unpaired. The gap associated with this 2SC condensate is defined as

$$\Delta = -2H\, s_{22} , \tag{6.4}$$

For simplicity we assume this condensate to be spatially constant, as in [11] and consider also for simplicity a chiral density wave for the modulation of the chiral condensates

$$\hat{M}_f(\vec{x}) = M \exp\left(\mathrm{i}\gamma^5 \vec{q}_f \cdot \vec{x}\right), \tag{6.5}$$

with $\vec{q}_u = -\vec{q}_d$ like in sec. 4.3. For brevity, q will denote the magnitude of $\vec{q}_u$ and $\vec{q}_d$, while both have opposite sign.

[1] For a generalized modulation of the chiral condensates, see [10].

When dealing with diquark condensates, the Nambu-Gor'kov (NG) formalism turns out to be useful and simplifies the approach considerably. For this we assume that ψ and $\psi^C = C\bar{\psi}^T$ are formally independent fields and introduce the bispinors

$$\Psi = \frac{1}{\sqrt{2}} \begin{pmatrix} \psi \\ \psi^C \end{pmatrix} \tag{6.6}$$

to rewrite the Lagrangian as

$$\mathcal{L}_{MF} + \bar{\psi}\gamma_0\hat{\mu}\psi = \bar{\Psi}\mathcal{S}^{-1}(\vec{x})\Psi - \mathcal{V}\,. \tag{6.7}$$

Here, $\mathcal{V}$ is a field-independent term and the inverse propagator $\mathcal{S}^{-1}$ is given by

$$\mathcal{S}^{-1}(\vec{x}) = \begin{pmatrix} \mathrm{i}\partial\!\!\!/ - \hat{M}(\vec{x}) + \hat{\mu}\gamma^0 & \Delta\gamma_5\tau_2\lambda_2 \\ -\Delta^*\gamma_5\tau_2\lambda_2 & \mathrm{i}\partial\!\!\!/ - \hat{M}(\vec{x}) - \hat{\mu}\gamma^0 \end{pmatrix}. \tag{6.8}$$

Note that in contrast to Eq. (3.18) the inverse propagator is not diagonal in flavor space in presence of the 2SC condensate. But as before we can separate the inverse propagator in momentum space according to

$$\mathcal{S}^{-1}_{p_m,p_n} = \gamma^0 \left(i\omega_{p_m} - \mathcal{H}_{p_m,p_n}\right) \delta_{\omega_{p_m},\omega_{p_n}} \tag{6.9}$$

with ω_n being Matsubara frequencies. For static condensates the inverse propagator is diagonal in these frequencies and the Matsubara sum can be performed analytically, yielding

$$\Omega_{\mathrm{kin}} = -\sum_{\lambda} \left[|\lambda| + 2T\,\mathrm{Log}\left(1 + \exp\left(-\frac{|\lambda|}{T}\right)\right)\right], \tag{6.10}$$

where the trace has been expressed as a sum over the eigenvalues $\{\lambda\}$ of the Hamiltonian $\mathcal{H}$ in Nambu-Gor'kov, Dirac, color, flavor and momentum space.

The remaining problem of diagonalizing the Hamiltonian turns out to be rather tedious. To simplify the determination of the eigenvalues, we first remove the non-trivial Dirac structure in the off-diagonals of the Hamiltonian in momentum space by applying a transformation

$$U = \begin{pmatrix} 1 & \\ & \gamma^0\gamma^5 \end{pmatrix} \tag{6.11}$$

to the Hamiltonian $\mathcal{H}$ as

$$\mathcal{H}'_{\vec{p}_m,\vec{p}_n} = \left(U^\dagger \mathcal{H} U\right)_{\vec{p}_m,\vec{p}_n}\,. \tag{6.12}$$

The resulting Hamiltonian (in momentum space) is given by

$$\mathcal{H}'_{\vec{p}_m,\vec{p}_n} = \begin{pmatrix} (\gamma^0 \vec{p}\!\!\!/_n\, \delta_{\vec{p}_m,\vec{p}_n} - \hat{\mu}\,\delta_{\vec{p}_m,\vec{p}_n} + \hat{M}\gamma^0\,\delta_{\vec{p}_m,\vec{p}_n+\vec{q}}) & \tau_2\lambda_2\Delta\delta_{\vec{p}_m,\vec{p}_n} \\ \tau_2\lambda_2\Delta^*\delta_{\vec{p}_m,\vec{p}_n} & -(\gamma^0 \vec{p}\!\!\!/_n\, \delta_{\vec{p}_m,\vec{p}_n} + \hat{\mu}\,\delta_{\vec{p}_m,\vec{p}_n} + \hat{M}\gamma^0\,\delta_{\vec{p}_m,\vec{p}_n+\vec{q}}) \end{pmatrix} \tag{6.13}$$

from which we need to remove the space dependence (in position space) on the diagonal elements by applying chiral transformations, as shown before. As a complication these transformations need to be generalized to account for the NG structure by writing in position space

$$U_{\chi,\mathrm{NG}}(\vec{x}) = \frac{1}{\sqrt{2}} \begin{pmatrix} U_\chi(\vec{x}) \\ U_\chi^+(\vec{x})) \end{pmatrix} \tag{6.14}$$

with $U_\chi(\vec{x}) = \exp\left(-i\gamma^5 \vec{q}\cdot\vec{x}/2\right)$ acting on the NG components. Since no non-trivial dependence is induced by these transformations for the off-diagonal terms, we can furthermore use energy projectors of the form $\Lambda_{\vec{p}}^{\pm} = (1 \pm \gamma^0(\gamma^i p^i - \gamma^i\gamma^5 \frac{q^i}{2} + M)/\epsilon_\pm)/2$, with $\epsilon_\pm$ known from Eq. (4.26), to arrive at

$$\mathcal{H}'_{\vec{p}_m,\vec{p}_n} = \begin{pmatrix} (\hat{\epsilon}_{\vec{p}_m} - \hat{\mu})\delta_{\vec{p}_m,\vec{p}_n} & \Delta\gamma_5\tau_2\lambda_2\delta_{\vec{p}_m,\vec{p}_n} & & \\ \Delta^*\gamma_5\tau_2\lambda_2\delta_{\vec{p}_m,\vec{p}_n} & -(\hat{\epsilon}_{\vec{p}_m} - \hat{\mu})\delta_{\vec{p}_m,\vec{p}_n} & & \\ & & -(\hat{\epsilon}_{\vec{p}_m} + \hat{\mu})\delta_{\vec{p}_m,\vec{p}_n} & \Delta\gamma_5\tau_2\lambda_2\delta_{\vec{p}_m,\vec{p}_n} \\ & & \Delta^*\gamma_5\tau_2\lambda_2\delta_{\vec{p}_m,\vec{p}_n} & (\hat{\epsilon}_{\vec{p}_m} + \hat{\mu})\delta_{\vec{p}_m,\vec{p}_n}. \end{pmatrix} \tag{6.15}$$

Here the method of applying energy projectors is exact, since the Hamiltonian has no explicit space-dependence anymore. For more complicated modulations, like a sinusoidal modulation or space-dependence of the diquark condensates this would not be the case, since an explicit spatial dependence would still be present in the Hamiltonian. Note that we reordered lines and columns in Eq. (6.15) to make the diagonal structure obvious. The blocks are related to the NG structure and we have also a two-fold spin degeneracy of the problem. Due to the energy projectors, blocks associated with the eigenvalues with negative or positive signs but same magnitude can be identified, which correspond to the quarks and antiquarks of one flavor. In the end it is therefore sufficient to diagonalize only one block, which will be, without loss of generality, the block of particles (and not the antiparticles).

Due to the fact that only red and green quarks participate in the pairing but blue quarks do not, the Hamiltonian can be further decomposed in color and flavor space into two separate blocks. Then, the diagonalization of the Hamiltonian becomes feasible and we obtain the positive eigenvalues for the two quark flavors

$$\lambda^u_{r,g} = \sqrt{(\epsilon_\pm - \bar{\mu})^2 + |\Delta|^2} - \frac{\mu_I}{2} \tag{6.16}$$

$$\lambda^d_{r,g} = \sqrt{(\epsilon_\pm - \bar{\mu})^2 + |\Delta|^2} + \frac{\mu_I}{2} \tag{6.17}$$

$$\lambda^u_b = \epsilon_\pm - \bar{\mu} - \frac{\mu_I}{2} \tag{6.18}$$

$$\lambda^d_b = \epsilon_\pm - \bar{\mu} + \frac{\mu_I}{2}, \tag{6.19}$$

where

$$\epsilon_\pm = \sqrt{\vec{p}^2 + M^2 + \frac{\vec{q}^2}{4} \pm \sqrt{M^2\,\vec{q}^2 + (\vec{q}\cdot\vec{p})^2}}. \tag{6.20}$$

These are formally the same eigenvalues derived in [11]. To obtain the corresponding antiquark energies, it is sufficient to invert the sign of $\bar{\mu}$ in Eqs. (6.16) - (6.19) and for $|\Delta| \to 0$ we naturally recover the thermodynamic potential of the CDW.

Since also here the thermodynamic potential is formally divergent, we use a Pauli-Villars-like scheme by replacing $\epsilon_\pm$ by its regularized form according to

$$\epsilon_\pm \to \sum_j c_j \sqrt{\epsilon_\pm^2 + j\Lambda^2} \tag{6.21}$$

in the above eigenvalues.

The condensate part of the thermodynamic potential reads

$$\Omega_{\text{cond}} = \frac{1}{V}\int_V d^3x\, \mathcal{V} = \frac{M^2}{4G} + \frac{|\Delta|^2}{4H}\,. \tag{6.22}$$

The diquark coupling H is treated as a free parameter and will be parameterized in terms of the coupling G.

6.2. Results

Already for a pure CDW in our setup[2] it is well known that the inhomogeneous solution first becomes disfavored against the restored phase for increasing densities, as exemplary seen in the previous chapters. At even higher chemical potentials then an inhomogeneous solution becomes favored again [73], which is also called the 'continent'. The continent seems to extend to infinitely high densities and temperatures. Currently it is not clear if the phase with spatially-modulated order-parameters really extend to infinitely high densities, although there are clear hints for that [74] but also results suggesting the opposite [75]. Anyhow, restricting our discussion to $\mu \leq 550\,\text{MeV}$ is sufficient for our purposes and both references agree on the appearance of such an inhomogeneous continent in this range. Furthermore the exact phase structure allowing for spatially-modulated order-parameters of chiral symmetry at intermediate values of the chemical potential depends also on the exact regularization parameters in our Pauli-Villars scheme. In particular, the inhomogeneous solution at intermediate densities is connected to the continent at high densities when requiring $M_{\text{vac}} = 330\,\text{MeV}$ and no restored solution is found for low temperatures between the "first" inhomogeneous region and the continent. For $T = 0$, $\mu_I = 0$ and $H = 0$ this is shown in Fig. 6.1 (again for $m = 0$), where the inhomogeneous chiral-symmetry breaking phase is always favored over the restored phase as soon as $\bar{\mu} \geq \bar{\mu}_{c,1}$.

This may not be true as soon as color-superconducting phases are considered. Since it is expected that 2SC condensation plays an important role for this region of intermediate to large densities, we allow color-superconducting phases as a next step in our system. A priori it is not clear which type of phase is favored in this region and the detailed

[2] Still for the parameter set of $M_{\text{vac}} = 300\,\text{MeV}$ given in Tab. A.1 for our model.

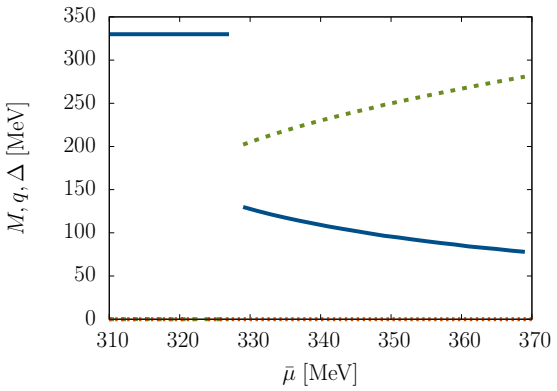

Figure 6.1.: Energetically favored values of the amplitude M (solid blue), the wave-number q (dashed green) for inhomogeneous chiral condensates and the diquark gap Δ (dotted orange) for $T = 0$, $M_{\text{vac}} = 330\,\text{MeV}$, $\mu_I = 0$ and $H = 0$.

structure needs to be calculated numerically. Before coming to studying the simultaneous appearance of the color-superconducting and chiral-symmetry breaking phases, the properties of homogeneous 2SC condensation only are investigated.

An asymmetry between the two quark chemical potentials does not only affect chiral-symmetry breaking phases but also has influence on the quark-quark condensates by disfavoring this BCS pairing mechanism and eventually leading to the breakup of the diquark condensate once it surpasses a critical value. In Fig. 6.2 this is visible at fixed $\bar{\mu}$ and $H = 0.5\,G$ (which will be our standard value for the diquark coupling if not stated otherwise), where the gap Δ drops to zero at a critical $\mu_I \approx 1.42\,\Delta_0$ with Δ_0 being the gap at $\mu_I = 0$. In the weak coupling limit this critical value has been calculated by Chandrasekhar and Clogston and is given by $\mu_I = \sqrt{2}\Delta$ [69, 71] which is also known as the Chandrasekhar-Clogston limit (CC limit) and we expect the critical value of the isospin-chemical potential for our calculations to be of this order. Indirectly the breakup of diquark condensation for $\mu_I \geq \mu_I^c$ is also present in the right panel of Fig. 6.2, since $\bar{\mu}$ fixes the value of Δ_0 and thus in turn determines the critical value μ_I^c. Thus at increasing $\bar{\mu}$ and fixed μ_I the gap Δ_0 reaches large enough values so that the isospin-chemical potential is below the CC limit and the gap Δ becomes non-zero. Although the free energy associated with the color-superconducting condensates changes with altering μ_I at fixed $\bar{\mu}$, the value of the order-parameter needs to remain unchanged below μ_I^c [70]. For two different values of μ_I this is also present in Fig. 6.2, where the 2SC solution with a larger asymmetry between the quark chemical potentials becomes favored at larger increasing values of $\bar{\mu}$.

As seen in Fig. 6.3, allowing for the simultaneous appearance of color-superconducting and chiral symmetry-breaking condensates in isospin-symmetric matter replaces the inhomogeneous chiral symmetry breaking phase at intermediate densities by a phase where both a crystalline chiral condensate and a nonzero diquark gap occur. The onset of this coexistence phase is first-order and occurs at a slightly lower chemical potential

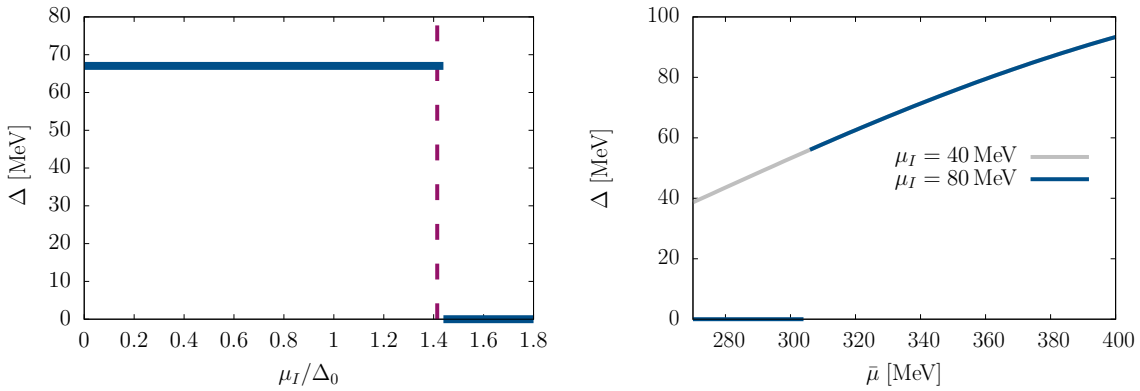

Figure 6.2.: Diquark gap Δ at $T = 0$, $M_{\text{vac}} = 330\,\text{MeV}$ for a 2SC phase only (with $M = 0$). *(Left):* For $\bar{\mu} = 330\,\text{MeV}$ against μ_I and *(right):* at various μ_I against the flavor-averaged chemical potential. For the left panel the isospin chemical potential on the x-axis was rescaled with $\Delta_0 = \Delta(\mu_I = 0)$ and the CC limit is indicated by the vertical line.

compared to the case with no or with only diquark condensation. Furthermore the inhomogeneous chiral-symmetry breaking solution does not extend up to large chemical potentials anymore and instead the amplitude of the chiral condensate decreases to zero. There the system undergoes a second-order transition from the coexistence phase to a pure 2SC phase by the 'melting' of the chiral condensate, i. e. the amplitude of the chiral condensate smoothly reaches zero and the diquark gap does not jump. In the absence of a non-zero chiral condensate the 2SC gap is slightly larger than in the coexistence phase, as can be seen in the right panel of Fig. 6.3 where the gap in the coexistence phase smoothly approaches the pure 2SC result for increasing $\bar{\mu}$. By allowing such a coexistence phase, the inhomogeneous continent does not extend to very large densities and is replaced by a homogeneous 2SC phase. Under the assumption of no mixing of chiral-symmetry breaking and color-superconducting phases this was already found earlier [76].

At moderate values of the isospin-chemical potential the coexistence phase shrinks marginally as μ_I grows. This is due to the pairing stress caused by $\mu_I \neq 0$, on which the phases react differently. The variational parameters can be seen in Fig. 6.4 at vanishing temperature. Basically the values of the diquark gap Δ remains unchanged for low μ_I and the amplitude M gets slightly smaller when comparing the results for $\mu_I = 0$, $\mu_I = 40\,\text{MeV}$ and $\mu_I = 80\,\text{MeV}$. The size of the coexistence region shrinks for increasing μ_I and the onset of a pure 2SC phase, replacing the coexistence phase, shifts down to lower values of $\bar{\mu}$. For even higher values of the isospin-asymmetry, the homogeneous chiral-symmetry breaking, the CDW and the pure 2SC solutions emerge besides the restored phase with $\Delta = M = 0$, but no coexistence region exists.

The free energies of the different phases can be seen in Fig. 6.5. There the free energies are shown at four values of μ_I, which allows to discuss the influence of μ_I on the different pairing mechanisms. One recognizes that the thermodynamic potential for a CDW with

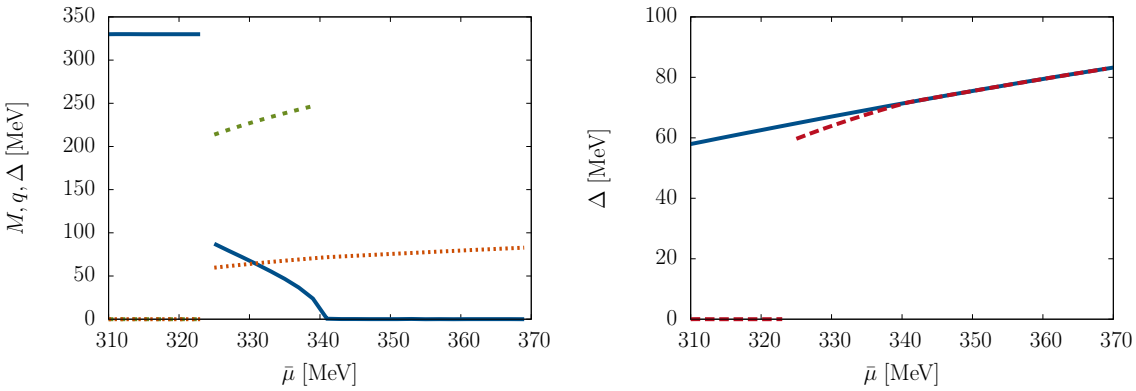

Figure 6.3.: *(Left):* Energetically favored values of the amplitude M (solid blue), the wave-number q (dashed green) for inhomogeneous chiral condensates and the diquark gap Δ (dotted orange); *(Right):* Value of the diquark gap without (solid blue) and with (dashed red) inhomogeneous chiral symmetry breaking condensates at $T = 0$, $M_{\text{vac}} = 330\,\text{MeV}$, $\mu_I = 0$ and $H = 0.5\,G$.

no color-superconductivity is only mildly affected by the increasing isospin-chemical potential, which we already found before. The free energy of the phase with only 2SC condensation is in contrast strongly influenced by an isospin-asymmetry and eventually the phase disappears at fixed $\bar{\mu}$ for sufficiently large values of μ_I, as can be seen for $\mu_I = 100\,\text{MeV}$ in the lower right panel of the figure. At the same time also no coexistence phase is found any more. This does not happen at smaller values of μ_I, where the coexistence phase is in some interval more favored than the pure 2SC or CDW phase, but also shrinks for increasing μ_I. The value of the diquark gap remains unchanged for sufficiently low μ_I, while the amplitude of the CDW gets slightly smaller. In general the phase structure remains almost unaltered for $\mu_I = 40\,\text{MeV}$ and $\mu_I = 80\,\text{MeV}$, as can also be seen in Fig. 6.4 for vanishing temperatures. There, a coexistence phase is still present in some interval and gets replaced by a pure 2SC phase for larger $\bar{\mu}$.

If the isospin-chemical potential is increased further, the phase structure changes. Namely, there are different type of phase transitions possible, dependent on the value of $\bar{\mu}$. Exemplary for $\bar{\mu} = 330\,\text{MeV}$ this can be seen very well at $T = 0$ in Fig. 6.6, where one observes the occurrence of a coexistence phase up to the critical isospin chemical potential $\mu_I^C = \sqrt{2}\Delta_0 \approx 90\,\text{MeV}$. Interestingly the gap in the coexistence phase has a weak dependence on μ_I and grows by $\approx 2\,\text{MeV}$ from $\mu_I = 0$ to μ_I^c, which does not occur if a pure 2SC solution is considered where Δ stays constant, as expected for homogeneous 2SC condensates [70].

The phase structure at $T = 0$ in the $\bar{\mu} - \mu_I$ plane is shown in Fig. 6.7. For low $\bar{\mu}$, a phase with homogeneous chiral symmetry breaking and no color superconductivity is favored over the other condensation patterns. The coexistence phase is adjacent to the homogeneous chiral-symmetry breaking phase and exists in a range of $\bar{\mu} \approx 324 - 341\,\text{MeV}$ at $\mu_I = 0$ and extends up to intermediate values of the isospin-chemical potentials. For higher μ_I's the coexistence phase is disfavored against a phase with inhomogeneous

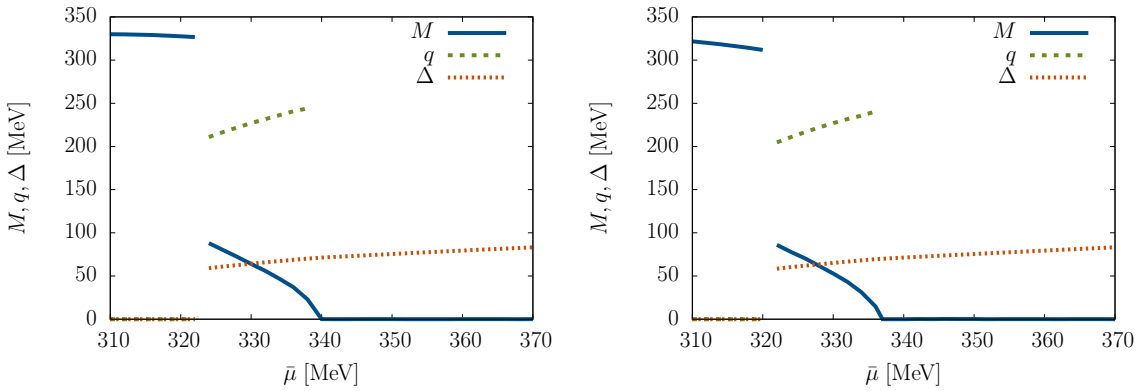

Figure 6.4.: Energetically favored values of the amplitude M (solid blue), the wavenumber q (dashed green) for inhomogeneous chiral condensates and the diquark gap Δ (dotted orange) at $T = 0$, $M_{\text{vac}} = 330\,\text{MeV}$ and $H = 0.5\,G$ for $\mu_I = 40\,\text{MeV}$ (left) and $\mu_I = 80\,\text{MeV}$ (right).

chiral-symmetry breaking and no color superconductivity. Also the pure 2SC phase is disfavored there. For higher $\bar{\mu}$ the coexistence phase undergoes a second order phase transition to the pure 2SC phase for low μ_I, while for large values of μ_I the diquark gap in the coexistence phase jumps discontinuously and one arrives at a purely inhomogeneous chiral symmetry breaking phase with no 2SC condensates. For large values of μ_I (close to the value where charged pion condensation should set in) and large $\bar{\mu}$ also the inhomogeneous chiral symmetry breaking phase becomes disfavored against the asymmetry in the occupation numbers and the system reaches the restored phase with $M = \Delta = 0$.

Although we restricted our analysis to homogeneous diquark condensates, it is interesting that also for our simplified ansatz, the inhomogeneous continent disappears and a coexistence region where inhomogeneous chiral symmetry breaking and a nonzero homogeneous 2SC gap are simultaneously present, appears. It seems that for sufficiently high densities and low μ_I the pure 2SC phase is always favored over the chiral symmetry-breaking phase. The size of the coexistence and 2SC region depends on the strength of the diquark coupling, and for larger values such as $H = 3/4\,G$ the pure 2SC phase becomes thermodynamically favored over all inhomogeneous solutions, since the 2SC phase alone is by large numbers favored over a large interval over chiral symmetry-breaking phases. Only for vanishing or small chemical potentials, chiral symmetry-breaking phases are still energetically favored over 2SC phases. Since there, inhomogeneous condensation is not favored over homogeneous condensation for chiral symmetry breaking, no coexistence phase can emerge there.

In general one would expect that the real ground state of dense matter for large isospin-asymmetries is a coexistence phase where both the chiral condensate and the diquark gap are spatially modulated. This will be clearly out of the scope of this thesis and further investigations are needed. Furthermore it is known that if the chiral condensate becomes inhomogeneous, a spatial dependence on the density of the system may be

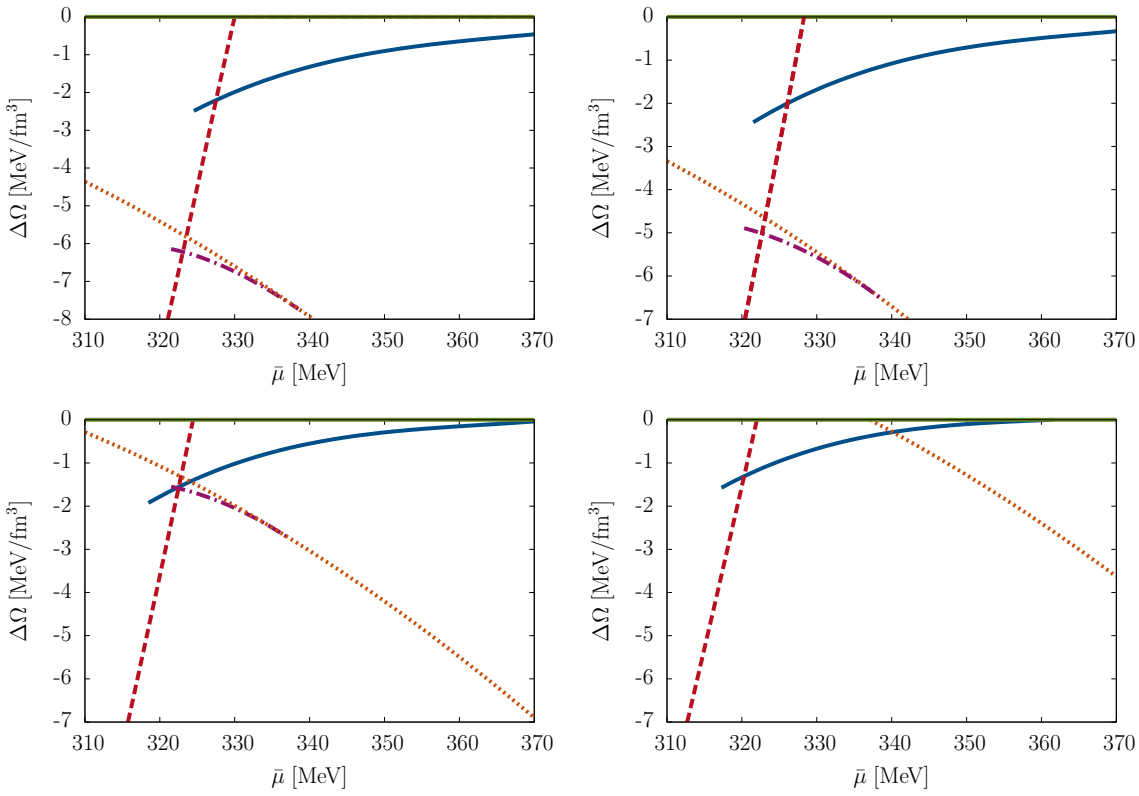

Figure 6.5.: Thermodynamic potential relative to the restored phase as a function of the average quark chemical potential at $T = 0$ and $H = G/2$ for homogeneous chiral condensates (dashed red), inhomogeneous chiral condensates (solid blue), only diquark condensation (dotted orange) and the coexistence phase with simultaneous inhomogeneous chiral symmetry breaking and homogeneous color-superconductivity (dash-dotted purple) at $\mu_I = 0$ (top left), $\mu_I = 40\,\mathrm{MeV}$ (top right), $\mu_I = 80\,\mathrm{MeV}$ (bottom left) and $\mu_I = 100\,\mathrm{MeV}$ (bottom right).

induced and in turn this allows to form color-superconducting islands in the (space-dependent) regions of high density of the system. A first, simple step would be to generalize the results to non-zero temperatures and study the phase structure. Another possible extension would be to investigate the influence of the coexistence phase on the properties of compact stellar matter.

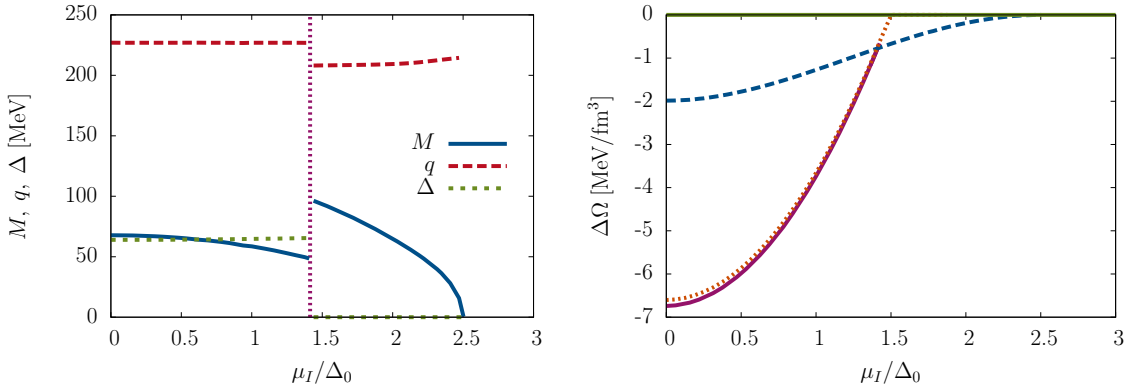

Figure 6.6.: *(Left):* Energetically favored variational parameters at $\bar{\mu} = 330$ MeV and $H = G/2$, $T = 0$, as a function of μ_I. The vertical line indicates the CC limit. *(Right):* Thermodynamic potential corresponding to the different solutions: coexistence phase (solid purple) with simultaneous occurrence of inhomogeneous chiral symmetry breaking and homogeneous color-superconductivity, inhomogeneous chiral condensates (dashed blue) and the pure 2SC phase (dotted orange).

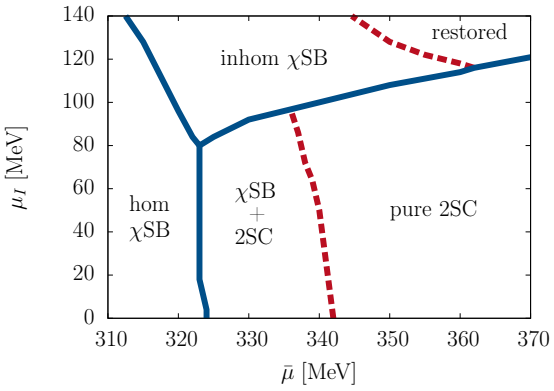

Figure 6.7.: Phase diagram in the $\bar{\mu}$-μ_I plane at $T = 0$ and for $H = G/2$. Solid blue lines denote first-order phase transitions, while dashed red lines indicate second-order ones. The label "hom χSB" characterizes a region where $M \neq 0$, $q = \Delta = 0$, "χSB+2SC" denotes a region with $M \neq 0$, $q \neq 0$, $\Delta \neq 0$, while "inhom χSB" corresponds to a region characterized by $M \neq 0$, $q \neq 0, \Delta = 0$ and "pure 2SC" labels a domain where $M = 0$, $\Delta \neq 0$.

7. Conclusions

In this work we have investigated inhomogeneous phases in isospin-asymmetric matter within the NJL model.

First, we developed a framework for allowing spatially modulated order-parameters associated with chiral symmetry breaking in our model, extending the existing formalism for inhomogeneous phases to isospin-asymmetric matter and allowing a more general interaction, that permits to control the degree of flavor mixing between up and down quarks. On the mean-field level we were able to derive an explicit expression for the grand potential for different shapes of the modulation of the chiral condensates. Because of the required diagonalization of an effective Hamiltonian, we assumed a crystalline structure for the order-parameters, namely periodicity and time-independence for the condensates, which then, together with limiting to simple types of modulations and / or lower-dimensional modulations, allowed us to determine the energy spectrum of the system from the Hamiltonian. For simplicity this was mainly done for plane-wave modulations. With this, the favored ground state of the system was determined numerically by addressing the stationary constraint of the grand potential.

We confirmed earlier results [25, 26, 55, 73] indicating that inhomogeneous chiral-symmetry breaking phases does occur in isospin-symmetric matter, but also found that such crystalline phases occur in isospin-asymmetric matter, where also a region with inhomogeneous chiral condensates emerges at low temperatures. Exemplarily we confirmed that solitonic modulations are energetically favored against our simple plane-wave modulations, but it turned out that these changes have only mild influence on the phase structure in our model; a fact, which has been already known for isospin-symmetric matter. Thus we still used our simple ansatz in specifying the modulation of the quark masses or condensates, but aimed to gain insight in a more generic phase structure.

While for isospin-symmetric matter the degree of flavor mixing does not affect the phase structure of the model, it has significant influence on the phase structure if the two quark flavors become non-degenerate. For completely decoupled quark flavors two separate inhomogeneous phases associated with up and down quarks are found, where the phase structure of our two-flavor model can be mapped to the phase structure of a one-flavor model. Here, the detailed phase structure is almost independent of the exact shape of the modulation and the connection to a one-flavor model is a generic feature of the grand potential, which separates in two independent parts for no flavor-mixing. From this it was found that unequal wave-vectors or equivalently unequal periodicities per quark flavor are energetically favored, while in contrast enforcing equal periodicities for the flavor-dependent quark masses at very small degrees of flavor mixing resulted in the phase to be disfavored against the homogeneous or restored phase. In this sense allowing for unequal periodicities can energetically stabilize the inhomogeneous phase in

isospin-asymmetric matter and the wave number is also here approximately proportional to the respective quark flavor chemical potential, which was first found for $\mu_I = 0$.

For non-vanishing degrees of flavor-mixing and non-zero isospin-chemical potentials there were two possible ansätze for the plane-wave modulation available. On the one hand we could make the plane-wave ansatz for the modulation of the quark masses per flavor or on the other hand impose a plane wave for the modulations of the up and down quark condensates, which then together specify the particular modulation of the quark mass. Since the two quark flavors are non-degenerate, the resulting thermodynamic potential is in general different for the two cases and we were able to study different characteristics of the system linked to the two ansätze.

By focusing on the plane-wave modulations on the quark mass-level, we found that the inhomogeneous region at fixed isospin-chemical potential is smallest for a maximal degree of flavor mixing. There, only plane waves with equal amplitudes and wave numbers are possible, which is in isospin-symmetric matter commonly known as the CDW, where we also adopted this term for non-zero isospin-asymmetries. The resulting phase structure is very similar to the one in isospin-symmetric matter, where an 'inhomogeneous island' emerges around the usual chiral restoration transition of homogeneous chiral condensates. For the CDW in isospin-asymmetric matter, the dependence on the degree of flavor mixing dropped out and therefore this type of solution may occur independently on the degree of flavor-mixing at $\mu_I \neq 0$. By allowing different amplitudes for the modulation of the quark masses, an explicit dependence on α was introduced and such inhomogeneous phases were found to be energetically more favored than the CDW. For very small degrees of flavor mixing, non-equal periodicities are energetically favored over inhomogeneous phases with equal periodicities, but already at relatively small degrees of flavor mixing they become disfavored against inhomogeneous phases with equal wave-vectors and disappear when approaching a maximal degree of flavor-mixing. Especially for an assumed realistic degree of flavor-mixing, no inhomogeneous phase with unequal periodicities is favored.

To check if the disappearance of unequal periodicities at a realistic degree of flavor-mixing is attributed to our particular choice of ansatz, we turned to specify ansätze on the level of the chiral condensates. By this, also inhomogeneous phases with unequal periodicities could be favored at a realistic degree of flavor-mixing. In particular, we showed that for large enough values of the isospin-chemical potential modulations of the condensates with unequal periodicities are more favored than modulations of the quark masses. Already for small differences between the periodicities of up and down quarks, an energy gain caused by the condensate part was observed. Furthermore, the overall energy gain enabled the inhomogeneous phase to be more stable against the effects of the additional pairing stress caused by $\mu_u - \mu_d \neq 0$ and thus could possibly provide observable consequences. To determine the phase structure, we were actually limited by the need of numerical calculations, since the Hamiltonian needed to be diagonalized by brute-force methods. In combination with our formalism, we therefore considered only rational ratios for the ratio of the two wave-numbers. We confirmed that different ratios are energetically favored in different regions of the parameter range. Also for a maximal degree of flavor-mixing it is found that specifying the condensate modulations rather

than the mass modulations allows to stabilize the inhomogeneous phase. In general the pressure differences between the two types of ansätze is up to a few MeV/fm^3, which is however small if compared to the restored phase's or homogeneous phase's (absolute) pressures.

Naturally an isospin-asymmetry arises for compact stars due to the requirement of charge neutrality. Therefore we studied the possibility of inhomogeneous phases in charge-neutral matter. To allow a 'realistic' description, we needed to additionally introduce electrons as the only leptons present in our system and required the isospin-chemical potential to be self-consistently determined from the grand potential. We found that inhomogeneous phases occur also for electrically charge-neutral matter, even when a CDW modulation is considered for the grand potential. In comparison to inhomogeneous phases at $\mu_I = 0$, the inhomogeneous region for matter with vanishing net-charge is smaller in the $\mu - T$-plane. At the self-consistently determined value of μ_I the differences in the pressure for a modulation on the mass or condensate level is only up to 10 % and thus we considered for simplicity only the mass ansatz for charge-neutral matter.

In a next step, the equation of state was determined for charge-neutral inhomogeneous matter at various degrees of flavor-mixing to serve as an input for mass-radius sequence calculations for compact stars. We were able to show that visible differences in mass-radius sequences of pure quark stars are present, if charge-neutral matter is compared to electrically charged matter at $\mu_I = 0$. However, the difference between only homogeneous and spatially modulated phases for mass-radius sequences is weakly observable for chiral-symmetry breaking and thus such static astrophysical observables may not allow to distinguish if homogeneous or inhomogeneous phases are realized in neutron stars. Especially since the determination of the stars' radii is currently a very hard task and only mass measurements are sufficiently precise, our results do not help to constrain quark matter properties from astrophysical observations. Since we only considered configurations, where the star is completely made out of quarks, it is also not surprising that our model does not reproduce observations of two-solar mass neutron stars. To allow a more realistic description, it would be good to also account for nuclear matter with electric net-charge zero and consider a hybrid configuration of nuclear and quark matter for the neutron star. Studying transport properties, like the cooling of the neutron star, might also allow insight on the properties of neutron star matter and could possibly allow to investigate the effects of inhomogeneous phases on compact stellar matter.

Currently there is no common agreement on how the QCD phase structure looks like at intermediate densities. On the one hand crystalline chiral condensates may be the favored ground state in this region, but on the other hand also color-superconductivity should become important for non-zero densities and low temperatures. Therefore as a final step we also introduced color-superconducting phases to our two-flavor model and considered a 2SC phase besides inhomogeneous chiral-symmetry breaking. For numerical reasons we allowed only a CDW solution for the modulation of the quark masses for chiral-symmetry breaking and considered only a homogeneous 2SC condensate. In this configuration we confirmed the relevance of a phase at zero temperature, where chiral-symmetry breaking and color-superconducting condensates coexist. For intermediate

densities the inhomogeneous continent, which occurs if one focuses on chiral symmetry breaking condensates only, disappears and the inclusion of color-superconductivity renders the purely chiral-symmetry breaking phase disfavored against phases with color-superconducting condensates. For larger baryon densities chiral-symmetry breaking gets disfavored and a purely 2SC phase persists. For non-zero isospin-asymmetries, the details of the phase structure depend on the relative weight of the couplings associated with color-superconductivity and chiral-symmetry breaking. Since both phases react differently to the pairing stress caused by $\mu_I \neq 0$, it was interesting to study the phase structure at various values of the isospin-chemical potential. Up to intermediate isospin-densities at vanishing temperatures, we found that the phase structure is basically unaltered compared to the isospin-symmetric case. For vanishing baryon densities a homogeneous chiral-symmetry breaking phase is favored, then a transition to the coexistence phase follows at increasing baryon density and finally we arrive at a 2SC phase for even higher values of the flavor-averaged chemical potential. At large values of the isospin-chemical potential, the coexistence phase at intermediate baryon number densities and the 2SC phase cease to exist, since the color-superconducting phases cannot account any more for the pairing stress through a BCS-like pairing. Since the inhomogeneous chiral-symmetry breaking phase is more stable against the effects of the isospin-asymmetry, it exists up to larger asymmetries and then becomes energetically disfavored. Of course, the analysis performed, serves only as a first step, since it is known that inhomogeneous phases can also occur for color-superconductivity but this was neglected here. It is however known that these types of condensation are less prone to an isospin-asymmetry than the spatially constant ones. It is thus conceivable that the most favored type of the coexistence phase is one, where inhomogeneous color-superconducting and chiral-symmetry breaking phases are allowed at the same time. This investigation would however require more work to do and was clearly out of the scope of this work. Another possibility is to study more complicated modulations of the chiral condensates, which might imply spatially modulated number densities. Then, color-superconductivity might occur in a narrow peak region with high densities, while adjacent to that region only chiral-symmetry breaking is energetically favored. At least for solitonic modulations this should be straight-forward in our formalism, but requires more intensive numerical analyses.

Although being favored in mean-field approximation, it is worth noting that strictly speaking modulations of the order parameters in one dimension are unstable at finite temperature, since the modulations are destroyed by thermal fluctuations [77]. Recent calculations also have addressed the effects of the mean-field approximation and the question how the regularization affects the results [78] by studying inhomogeneous phases in a two-flavor chiral quark-meson model. Going to account for the Dirac-sea contributions of the quarks, it is found that inhomogeneous phases still occur. In general it is also not clear, if the solutions in our model are self-consistent ones in isospin-asymmetric matter and deserves further work to be done.

The extension of our calculations is possible in many ways. First, instead of assuming a simple plane-wave modulation for the quark masses or the condensate functions, studying more complicated shapes for the order-parameters of chiral symmetry could

be possible to generalize our results in isospin-asymmetric matter. As a next step, one could allow for two-dimensional modulations and analyze the phase structure of inhomogeneous chiral symmetry breaking in isospin-asymmetric matter. On the other hand considering more complicated modulations, together with the requirement of only locally charge neutrality, could lead to interesting consequence, like for example that the leptons set a characteristic length scale of the system by coupling through the Coulomb interaction with the spatially modulated quark phase. Also charged-pion condensation, which we have neglected so far, is relevant for a non-zero isospin-asymmetry. Even for this type of condensation, the emergence of crystalline phases could be a valid option and the simultaneous appearance of inhomogeneous chiral-symmetry breaking phases and inhomogeneous charged-pion condensation is worth investigating. On the other hand it is also very interesting to study the interplay of inhomogeneous chiral symmetry breaking and inhomogeneous color-superconductivity, since it was shown for each phase that they are present in isospin-asymmetric matter, but so far the simultaneous occurrence was never explicitly considered.

A. Thermodynamic of the NJL model

A.1. Thermodynamic potential for $G_1/G_2 < 1$

Here we will show that for $G_1/G_2 < 1$ the thermodynamic potential is unbounded from below, since the term Eq. (3.16) entering the grand potential is in turn not bounded from below. Concentrating on the vacuum for now, where we can safely neglect the pseudo-scalar condensates – and assuming that the condensates as physical quantities are real, we get

$$
\begin{aligned}
&G_1 \left(S_u(\vec{x})^2 + S_d(\vec{x})^2\right) + 2G_2 \left(S_u(\vec{x}) S_d(\vec{x})\right) = G_1 \left(\left(S_u(\vec{x})^2 + S_d(\vec{x})^2\right) + 2\frac{G_2}{G_1} \left(S_u(\vec{x}) S_d(\vec{x})\right) \right) \\
&= G_1 \left(\left(S_u(\vec{x}) + \frac{G_2}{G_1} S_d(\vec{x}) \right)^2 + \left(1 - \left(\frac{G_2}{G_1} \right)^2 \right) S_d(\vec{x})^2 \right) \\
&= G_1 \left(\left(S_u(\vec{x}) + \frac{G_2}{G_1} S_d(\vec{x}) \right)^2 + \left(\frac{G_1^2 - G_2^2}{G_1^2} \right) S_d(\vec{x})^2 \right) .
\end{aligned}
$$

The first term

$$
\left(S_u(\vec{x}) + \frac{G_2}{G_1} S_d(\vec{x}) \right)^2 \geq 0 \tag{A.1}
$$

is always larger than or equal zero. The second term is, dependent on the ratio of G_1 to G_2, smaller, equal or larger than zero; namely

$$
\left(\frac{G_1^2 - G_2^2}{G_1^2} \right) S_d(\vec{x})^2 \begin{cases} \leq 0, & \text{for} \quad G_1 \leq G_2 \\ \geq 0, & \text{for} \quad G_1 \geq G_2 \end{cases} . \tag{A.2}
$$

Together, Eqs. (A.1) and (A.2) show that $\mathcal{L}_{\text{cond}}$ is unbounded from below for $G_1 < G_2$ resp. for $G_1/G_2 < 1$, if the condensates are sent to large values. The same is true for non-zero temperatures or non-vanishing densities.

A.2. Matsubara formalism

For finite-temperature field theory it is common to perform the Matsubara summation, where one sums over discrete imaginary frequencies, the so called Matsubara frequencies (see e. g. [44] for details). Essentially the summation can be replaced by a contour

integral in the complex plane. For example during the derivation of the thermodynamic potentials, one often encounters expressions like

$$T\sum_n \log\left(\frac{\omega_n^2+x^2}{T^2}\right) \tag{A.3}$$

with fermionic Matsubara frequencies given by $\omega_n = (2n+1)\pi T$. To solve this we rewrite the logarithm

$$\sum_{n=-\infty}^{\infty} \log\left(\frac{\omega_n^2+x^2}{T^2}\right) = \sum_{n=-\infty}^{\infty}\int_1^{x^2/T^2} du\,\frac{1}{u+(2n+1)^2\pi^2} + \log\left(1+(2n+1)^2\pi^2\right) \tag{A.4}$$

and interchange the order of summation and integration

$$\sum_{n=-\infty}^{\infty} \log\left(\frac{\omega_n^2+x^2}{T^2}\right) = \int_1^{x^2/T^2} \sum_{n=-\infty}^{\infty}\frac{1}{u+(2n+1)^2\pi^2}\,du + \sum_{n=-\infty}^{\infty}\log\left(1+(2n+1)^2\pi^2\right). \tag{A.5}$$

Applying the residue summation formula for the first part of Eq. (A.5) yields after using the third binomial formula

$$\sum_{n=-\infty}^{\infty}\frac{1}{u+(2n+1)^2\pi^2} = \frac{1}{4\pi^2}\sum_{n=-\infty}^{\infty}\frac{1}{\left(n-\frac{\pi-\mathrm{i}\sqrt{u}}{2\pi}\right)\left(n-\frac{\pi+\mathrm{i}\sqrt{u}}{2\pi}\right)} \tag{A.6}$$

$$= \frac{1}{4\pi^2}\frac{\pi\left(\cot\left(\frac{\pi-\mathrm{i}\sqrt{u}}{2}\right)-\cot\left(\frac{\pi+\mathrm{i}\sqrt{u}}{2}\right)\right)}{4\mathrm{i}\sqrt{u}\frac{1}{\pi}} = \frac{1}{\sqrt{4u}}\tanh\left(\frac{\sqrt{u}}{2}\right) = \frac{1}{\sqrt{u}}\left(\frac{1}{2}-\frac{1}{\exp\left(\sqrt{u}\right)+1}\right). \tag{A.7}$$

Inserting this into Eq. (A.5), we arrive at

$$\int_1^{x^2/T^2}\frac{1}{\sqrt{u}}\left(\frac{1}{2}-\frac{1}{\exp\left(\sqrt{u}\right)+1}\right)du + \sum_{n=-\infty}^{\infty}\log\left(1+(2n+1)^2\pi^2\right) \tag{A.8}$$

and after integration with respect to u we obtain

$$-\frac{|x|}{T}+2\log\left(1+\exp\left(\frac{|x|}{T}\right)\right)+1-2\log\left(1+\exp\left(1\right)\right)+\sum_{n=-\infty}^{\infty}\log\left(1+(2n+1)^2\pi^2\right) \tag{A.9}$$

$$\begin{aligned}&=-\frac{|x|}{T}+2\log\left(\exp\left(\frac{|x|}{T}\right)\left(1+\exp\left(-\frac{|x|}{T}\right)\right)\right)+1-2\log\left(1+\exp\left(1\right)\right)\\&\qquad+\sum_{n=-\infty}^{\infty}\log\left(1+(2n+1)^2\pi^2\right)\\&=\frac{|x|}{T}+2\log\left(1+\exp\left(-\frac{|x|}{T}\right)\right)+\left(1-2\log\left(1+\exp\left(1\right)\right)+\sum_{n=-\infty}^{\infty}\log\left(1+(2n+1)^2\pi^2\right)\right).\end{aligned} \tag{A.10}$$

With this the overall expression is given by

$$T\sum_n\log\left(\frac{\omega_n^2+x^2}{T^2}\right)=|x|+2T\log\left(1+\exp\left(-\frac{|x|}{T}\right)\right). \tag{A.11}$$

A.3. Separating vacuum and medium contributions

To derive an expression for the vacuum and medium parts of the thermodynamic potential, we start with the r.h.s. of Eq. (A.11) by inserting eigenvalues of the form $\pm\epsilon-\mu_f$ for the quarks and antiquarks of flavor f, where the exact form of the eigenvalues is not specified but we require the ϵ's to be symmetric around zero. Depending on the values of ϵ and μ_f in the expression (which occurs in Ω^f_{kin})

$$\sum_{\epsilon\gtrless0}\left(|x|+2T\ln\left(1+\exp\left(-\frac{|x|}{T}\right)\right)\right) \tag{A.12}$$

$$=\sum_{\epsilon\gtrless0}\left\{|\epsilon-\mu_f|+|\epsilon+\mu_f|+2T\left[\ln\left(1+\exp\left(-\frac{|\epsilon-\mu_f|}{T}\right)\right)+\ln\left(1+\exp\left(-\frac{|\epsilon+\mu_f|}{T}\right)\right)\right]\right\}$$

we need to distinguish between the cases

$$\begin{aligned}&2\left(\mu_f+T\ln\left(1+\exp\left(-\tfrac{-\epsilon+\mu_f}{T}\right)\right)+T\ln\left(1+\exp\left(-\tfrac{\epsilon+\mu_f}{T}\right)\right)\right),\quad \epsilon<\mu_f\\&2\left(\epsilon+T\ln\left(1+\exp\left(-\tfrac{-\epsilon+\mu_f}{T}\right)\right)+T\ln\left(1+\exp\left(-\tfrac{\epsilon+\mu_f}{T}\right)\right)\right),\quad \epsilon>\mu_f\end{aligned} \tag{A.13}$$

for the integrand. Explicitly this yields

$$\begin{aligned}2\sum_{\epsilon>0}\Bigg\{&\epsilon+\mu_f+T\Bigg(\ln\left[\left(1+\exp\left(-\frac{-\epsilon+\mu_f}{T}\right)\right)\left(1+\exp\left(-\frac{\epsilon-\mu_f}{T}\right)\right)\right]\\&+2\ln\left(1+\exp\left(-\frac{\epsilon+\mu_f}{T}\right)\right)\Bigg)\Bigg\},\end{aligned} \tag{A.14}$$

which can be rearranged to give

$$2\sum_{\epsilon>0}\left\{-2\left(\epsilon+\mu_f\right)+2T\log\left(\exp\left(\frac{\mu_f}{T}\right)\left(1+\exp\left(\frac{\epsilon-\mu_f}{T}\right)\right)\left(1+\exp\left(\frac{\epsilon+\mu_f}{T}\right)\right)\right)\right\}$$
$$=4\sum_{\epsilon>0}\left\{\epsilon+T\ln\left(1+\exp\left(-\frac{\epsilon+\mu_f}{T}\right)\right)+T\ln\left(1+\exp\left(-\frac{\epsilon-\mu_f}{T}\right)\right)\right\}, \tag{A.15}$$

for which we made use of the assumption of ϵ to be symmetric around zero. Since now no medium dependence is present for the first term in Eq. (A.15), but for the other terms, we can identify the vacuum and medium parts from this result as $\omega_{\mathrm{vac}}(\epsilon)=\epsilon$ and $\omega_{\mathrm{med}}(\epsilon)=T(\ln\left(1+\exp\left(-(\epsilon+\mu_f)/T\right)\right)+T\ln\left(1+\exp\left(-(\epsilon-\mu_f)/T\right)\right))$, as already quoted in Eq. (3.49) and Eq. (3.50).

A.4. Regularization

Here we will show, how to regularize the quartically divergent thermodynamic potential of our model by presenting different regularization schemes.

A.4.1. Three-momentum cutoff

An often used regularization scheme is the O(3) cutoff scheme, where the restriction of momenta fulfilling $|\vec{p}|\leq\Lambda$ is imposed on the integration over quark momenta in the thermodynamic potential, i.e.

$$\int\frac{d^3p}{(2\pi)^3}\,T\log\left(2\cosh\left(\frac{E_f(\vec{p})-\mu_f}{2T}\right)\right)\rightarrow\int_{|\vec{p}|\leq\Lambda}\frac{d^3p}{(2\pi)^3}\,T\log\left(2\cosh\left(\frac{E_f(\vec{p})-\mu_f}{2T}\right)\right). \tag{A.16}$$

It turns out that this scheme violates Lorentz-symmetry and is not well suited if one deals with inhomogeneous condensates, since the quark momenta are not fixed and the eigenstates of the mean-field Hamiltonian cannot be labeled by a single momentum; thus a O(3) cutoff would suppress the coupling of momenta $\vec{p}_m$ and $\vec{p}_n$ with a difference larger than the cutoff; potentially leading to cutoff artifacts, like shown in the context of spatially-varying condensates in color-superconducting quark matter [7].

A.4.2. Pauli-Villars regularization

To circumvent (obvious) regularization artifacts in our region of interest, we choose a Pauli-Villars regularization scheme [79] which we apply to the vacuum contributions of the thermodynamic potential. The basic idea of both authors was to introduce heavy, unphysical masses in the (inverse) propagator to overcome divergent terms by adding enough counter terms, so that together the original function and the function with the added regulator masses cancel the divergences.

In particular, following the arguments of reference [7] for a suited regularization in the context of inhomogeneous condensates we need to modify the approach slightly. Going back to the thermodynamic potential and replacing the logarithm in the thermodynamic potential Eq. (3.26) by its Schwinger proper-time representation yields

$$\log A \to -\int_0^\infty \frac{d\tau}{\tau}\, f(\tau) \exp\left(-\tau A\right) \tag{A.17}$$

with a blocking function $f(\tau)$ which serves as a regulator.

Specifying this function also defines the details of the regularization scheme. For the sake of performing the Matsubara sum analytically we use

$$f(\tau) = c_0 + c_1 \exp\left(-1\tau\Lambda^2\right) + c_2 \exp\left(-2\tau\Lambda^2\right) + \ldots + c_{n_{PV}} \exp\left(-n_{PV}\tau\Lambda^2\right). \tag{A.18}$$

The coefficients c_i are determined by the conditions $\sum_j c_j = 0$ and $\sum_j c_j(M^2 + j\Lambda^2) = 0$, where we have a freedom to choose c_0.

For the following discussion, we proceed with our discussion for $n_{PV} = 3$. Inserting Eq. (A.18) into Eq. (A.17) yields with $c_0 = 1 = -c_3, c_1 = -c_2 = -3$

$$\log A \to \log A - 3\log\left(A + 1\Lambda^2\right) + 3\log\left(A + 2\Lambda^2\right) - \log\left(A + 3\Lambda^2\right), \tag{A.19}$$

from which we can carry out the summation over Matsubara frequencies as usual. The regularized version of the kinetic part of the thermodynamic potential then reads[1]

$$\Omega^f_{\text{kin}}(T, \mu_f) \propto \sum_{E_{\lambda_f}} \Bigg\{ \Bigg(\sum_{j=0}^{n_{PV}} c_j E_{\lambda_f, j} + T\log\left(1 + \exp\left(-\frac{E_{\lambda_f} - \mu_f}{T}\right)\right) + T\log\left(1 + \exp\left(-\frac{E_{\lambda_f} + \mu_f}{T}\right)\right)\Bigg)\Bigg\} \tag{A.20}$$

with

$$E_{\lambda_f, j} = \sqrt{E_{\lambda_f} + j\Lambda^2} \tag{A.21}$$

and we assumed that the spectrum is symmetric around zero. Here E_{λ_f} are the eigenvalues of the mean-field Hamiltonian $\mathcal{H}_f$. If we had allowed for an explicit μ-dependence of the eigenenergies, i. e. considering $\mathcal{H}_f - \mu_f$ instead, then unphysical regularization artifacts would have been picked up in the thermodynamic potential due to the regularization procedure which violate the Silver-Blaze property[2]. Since we also cannot reproduce the correct Stefan-Boltzmann limit if we also regularize temperature-dependent parts of Eq. (A.20), we only regularize the first term that encodes the vacuum contributions.

Also it should be noted, that we replace the free energies in our regularization scheme instead of the masses, as originally done by Pauli and Villars.

[1] Formally all eigenvalues in the expression for the kinetic part would be regularized, but for reasons becoming clear later only the vacuum contributions are regularized.

[2] In general observables "derived" from the unregularized NJL model respect this property, which does not hold if this regularization scheme is used.

Table A.1.: Model parameters in the Pauli-Villars regularization scheme obtained by fitting to vacuum phenomenology for given quark masses.

n_{PV}	M_{vac} [MeV]	Λ [MeV]	$G\Lambda^2$
3	300	757.048	6.00214
	330	728.368	6.5994

Fitting of parameters

To fix (G, Λ) within the Pauli-Villars regularization scheme, we fit the parameters to match vacuum phenomenology in our mean-field model. We require to reproduce the pion decay constant in the chiral limit $f_\pi = 88\,\text{MeV}$ [80] and require a fixed value of the quark mass in vacuum of M_{vac} instead of the conventionally used chiral condensate. This is necessary, since covariant regularization schemes like the Pauli-Villars one, yield rather small, unphysical values of the quark mass ($M_{\text{vac}} \approx 200\,\text{MeV}$) if a realistic value of the chiral condensate is used to determine the model parameters (see [26] for a discussion). Thus the fitting procedure is reversed and we determine the model parameters by prescribing the vacuum quark mass. From this, the coupling G and Λ and also indirectly the value of the quark condensate is accessible.

In particular, for fixed constituent quark mass in vacuum M_{vac} we determine the Pauli-Villars cutoff Λ from fitting it to reproduce the pion decay constant in our regularization scheme, which is given by [32]

$$f_\pi^2 = -\frac{N_c M_{\text{vac}}^2}{4\pi^2} \sum_{j=0}^{n_{PV}} c_j \log\left(\frac{M_{\text{vac}}^2 + j\Lambda^2}{M_{\text{vac}}^2}\right). \tag{A.22}$$

In a next step the coupling G is determined at known Λ and fixed M_{vac} from the gap equation in vacuum [32]

$$M_{\text{vac}} = -\frac{2}{3} G N_c N_f \left\langle \bar{\psi}\psi \right\rangle \tag{A.23}$$

with

$$\left\langle \bar{\psi}\psi \right\rangle = -\frac{3 M_{\text{vac}}}{4\pi^2} \sum_{j=0}^{n_{PV}} c_j \left(M_{\text{vac}}^2 + j\Lambda^2\right) \log\left(\frac{M_{\text{vac}}^2 + j\Lambda^2}{M_{\text{vac}}^2}\right) \tag{A.24}$$

for given M_{vac} and Λ.

Mainly we will use $n_{PV} = 3$ Pauli-Villars regulators and require a quark mass of $M_{\text{vac}} = 300\,\text{MeV}$ in vacuum, yielding the parameters given in Tab. A.1.

B. Inhomogeneous condensates

B.1. Local chiral transformations for a CDW-like modulation

To remove any spatial dependence from the effective mean-field Hamiltonian for a CDW-like modulation of the quark masses, we rewrite the Dirac equation

$$\mathcal{H}_f\varphi(\vec{x}) = E_f\varphi(\vec{x}) \tag{B.1}$$

in terms of a rotated field $\varphi(\vec{x}) = U_f(\vec{x})\varphi'(\vec{x})$, where $U_f(\vec{x})$ is the unitary, local chiral transformation (see also [47, 81, 58]) given by

$$U_f(\vec{x}) = \exp\left(-i\gamma^5\frac{\vec{q}_f}{2}\cdot\vec{x}\right). \tag{B.2}$$

Inserting the rotated field in Eq. (B.1) yields

$$\mathcal{H}_f U_f(\vec{x})\varphi'(\vec{x}) = E_f U_f(\vec{x})\varphi'(\vec{x}) = U_f(\vec{x})E_f\varphi'(\vec{x}). \tag{B.3}$$

which gives after multiplying the expression with $U_f^\dagger(\vec{x})$ from the left

$$U_f^\dagger(\vec{x})\mathcal{H}_f U_f(\vec{x})\varphi'(\vec{x}) = E_f\varphi'(\vec{x}). \tag{B.4}$$

With this, we can identify the rotated mean-field Hamiltonian as

$$\mathcal{H}'_f(\vec{x}) = U_f^\dagger(\vec{x})\mathcal{H}_f U_f(\vec{x}), \tag{B.5}$$

which reads explicitly

$$\mathcal{H}'_f(\vec{x}) = \mathcal{H}'_f = \exp\left(\mathrm{i}\gamma^5\frac{\vec{q}_f}{2}\cdot\vec{x}\right)\Big[-\mathrm{i}\gamma^0\gamma^i\partial_i + \gamma^0\Delta_f\exp\left(\mathrm{i}\gamma^5\vec{q}_f\cdot\vec{x}\right)\Big]\exp\left(-\mathrm{i}\gamma^5\frac{\vec{q}_f}{2}\cdot\vec{x}\right) \tag{B.6}$$

$$= -\mathrm{i}\gamma^0\gamma^i\partial_i - i\gamma^0\gamma^i\left(\frac{\partial}{\partial x^i}\exp\left(-\mathrm{i}\gamma^5\frac{\vec{q}_f}{2}\cdot\vec{x}\right)\right) + \gamma^0\Delta_f \tag{B.7}$$

$$= -\mathrm{i}\gamma^0\gamma^i\partial_i - \gamma^0\gamma^i\,\gamma^5\frac{q_f^i}{2} + \gamma^0\Delta_f. \tag{B.8}$$

To determine the eigenvalues of the Hamiltonian, we first make a standard plane-wave ansatz for the fields, like e. g. in [58],

$$\varphi'(\vec{x}) = \phi'_f(\vec{p})\exp\left(-\mathrm{i}\,p^\mu x_\mu\right) \tag{B.9}$$

which gives

$$\mathcal{H}_f'\varphi'(\vec{x}) = \left(-i\gamma^0\gamma^i\partial_i - \gamma^0\gamma^i\gamma^5\frac{q_f^i}{2} + \gamma^0\Delta_f\right)\phi_f'(\vec{p})\exp\left(-\mathrm{i}\,p^\mu x_\mu\right) \tag{B.10}$$

$$= \left(\gamma^0\gamma^i p^i - \gamma^0\gamma^i\gamma^5\frac{q_f^i}{2} + \gamma^0\Delta_f\right)\phi_f'(\vec{p})\exp\left(-\mathrm{i}\,p^\mu x_\mu\right). \tag{B.11}$$

Identifying the first part as the Hamiltonian in momentum space, for which the eigenvalues are needed, the diagonalization is straightforward and the eigenvalues are given by

$$E_f^{\pm 2} = \vec{p}^2 + \Delta_f^2 + \frac{\vec{q}_f^2}{4} \pm \sqrt{\Delta_f^2\vec{q}_f^2 + \left(\vec{p}\cdot\vec{q}_f\right)^2}. \tag{B.12}$$

The corresponding density of states can be identified by inserting the eigenvalues Eq. (B.12) in the kinetic part of the thermodynamic potential

$$\Omega_{\mathrm{kin}}^f = -N_c\sum_{s=\pm}\int\frac{d^3p}{(2\pi)^3}\left[E_f^s + T\,\ln\left(1+\exp\left(-\frac{E_f^2-\mu_f}{T}\right)\right)\right. \tag{B.13}$$
$$\left. + T\,\ln\left(1+\exp\left(-\frac{E_f^2+\mu_f}{T}\right)\right)\right]$$

by introducing a delta function as

$$\Omega_{\mathrm{kin}}^f = -N_c\sum_{s=\pm}\int\frac{d^3p}{(2\pi)^3}\int_0^\infty dE\;\delta\left(E_f^s - E\right)\left[E + T\,\ln\left(1+\exp\left(-\frac{E-\mu_f}{T}\right)\right)\right.$$
$$\left. + T\,\ln\left(1+\exp\left(-\frac{E+\mu_f}{T}\right)\right)\right]$$

which should agree with

$$\Omega_{\mathrm{kin}}^f \stackrel{!}{=} -\int_0^\infty dE\;\rho_f(E)\;\left[E + T\,\ln\left(1+\exp\left(-\frac{E-\mu_f}{T}\right)\right) + T\,\ln\left(1+\exp\left(-\frac{E+\mu_f}{T}\right)\right)\right]. \tag{B.14}$$

Comparing both expressions shows, that for the density of states

$$\rho_f(E) = N_c\sum_{s=\pm}\int\frac{d^3p}{(2\pi)^3}\delta(E_f^s - E) \tag{B.15}$$

holds. Next, by inserting the eigenvalues Eq. (B.12) in Eq. (B.15), the expression can be evaluated further to obtain an explicit expression for ρ_f. For a CDW-like modulation of the quark masses our derived expression is formally identical to the one in [26] and can be evaluated (by identifying $Q \equiv q_f$ and $\Delta \equiv \Delta_f$) to yield the expression Eq. (4.28).

B.2. Condensate functions from mass functions

In the following we show how to derive an expression for the condensate functions, if a shape for the modulation of the quark masses was specified.

Interpreting Eq. (4.22) as a linear combination Eq. (4.32) with real (X_f) and imaginary (Y_f) part, the condensates $S_f(\vec{x})$ and $P_f(\vec{x})$ and $X_f(\vec{x})$ and $Y_f(\vec{x})$ can be related to each other; first, we identify $X_f(\vec{x})$ and $Y_f(\vec{x})$ using Eq. (3.20) as

$$X_f(\vec{x}) = (1-\alpha)\, S_f(\vec{x}) + \alpha S_h(\vec{x}), \tag{B.16}$$

$$Y_f(\vec{x}) = (1-\alpha)\, P_f(\vec{x}) - \alpha P_h(\vec{x}). \tag{B.17}$$

Since the scalar and pseudoscalar part decouple, this can also be written as a block-diagonal matrix

$$\begin{pmatrix} X_f \\ X_h \\ Y_f \\ Y_h \end{pmatrix} = \begin{pmatrix} 1-\alpha & \alpha & 0 & 0 \\ \alpha & 1-\alpha & 0 & 0 \\ 0 & 0 & 1-\alpha & -\alpha \\ 0 & 0 & -\alpha & 1-\alpha \end{pmatrix} \cdot \begin{pmatrix} S_f \\ S_h \\ P_f \\ P_h \end{pmatrix}, \tag{B.18}$$

where we dropped the space dependence of the functions for brevity. To determine the actual shape of S_f and P_f in dependence on X_f and Y_f we invert the matrix (which is possible for $\alpha \neq 0.5$) in Eq. (B.18) and obtain by multiplying out

$$\begin{pmatrix} S_f \\ S_h \\ P_f \\ P_h \end{pmatrix} = \frac{1}{1-2\alpha} \begin{pmatrix} 1-\alpha & -\alpha & 0 & 0 \\ -\alpha & 1-\alpha & 0 & 0 \\ 0 & 0 & 1-\alpha & \alpha \\ 0 & 0 & \alpha & 1-\alpha \end{pmatrix} \cdot \begin{pmatrix} X_f \\ X_h \\ Y_f \\ Y_h \end{pmatrix} \tag{B.19}$$

an expression for the condensate functions

$$S_f(\vec{x}) = \frac{1}{1-2\alpha} \left((1-\alpha) X_f(\vec{x}) - \alpha X_h(\vec{x}) \right), \tag{B.20}$$

$$P_f(\vec{x}) = \frac{1}{1-2\alpha} \left((1-\alpha) Y_f(\vec{x}) + \alpha Y_h(\vec{x}) \right). \tag{B.21}$$

For $\alpha = 0.5$ these expressions diverge, which is also the reason to restrict ourselves to $0 \leq \alpha < 0.5$ in the first step. However, by doing so we are still able to evaluate the thermodynamic potential and only after arriving at an expression for Ω discuss the limit $\alpha \to 0.5$.

Bibliography

[1] J. von Goethe, *Faust: Eine Tragödie. Erster Theil*. Hermann Passarge, 1841.

[2] M. Fukugita and A. Ukawa, "Deconfining and Chiral Transitions of Finite Temperature Quantum Chromodynamics in the Presence of Dynamical Quark Loops," *Phys. Rev. Lett.* **57** (1986) 503.

[3] A. W. Overhauser, "Structure of nuclear matter," *Phys. Rev. Lett.* **4** (Apr, 1960) 415–418.

[4] P. Fulde and R. A. Ferrell, "Superconductivity in a strong spin-exchange field," *Phys. Rev.* **135** (Aug, 1964) A550–A563.

[5] A. I. larkin and Y. N. Ovchinnikov, "Nonuniform state of superconductors," *Zh. Eksp. Teor. Fiz.* **47** (1964) 1136–1146. [Sov. Phys. JETP20,762(1965)].

[6] M. Alford, J. A. Bowers, and K. Rajagopal, "Crystalline color superconductivity," *Phys. Rev. D* **63** (Mar, 2001) 074016.

[7] D. Nickel and M. Buballa, "Solitonic ground states in (color-) superconductivity," *Phys. Rev.* **D79** (2009) 054009, `arXiv:0811.2400 [hep-ph]`.

[8] R. Casalbuoni and G. Nardulli, "Inhomogeneous superconductivity in condensed matter and QCD," *Rev. Mod. Phys.* **76** (2004) 263–320, `arXiv:hep-ph/0305069 [hep-ph]`.

[9] R. Anglani, R. Casalbuoni, M. Ciminale, N. Ippolito, R. Gatto, M. Mannarelli, and M. Ruggieri, "Crystalline color superconductors," *Rev. Mod. Phys.* **86** (2014) 509–561, `arXiv:1302.4264 [hep-ph]`.

[10] D. Nowakowski and S. Carignano, "Color-superconductivity and inhomogeneous chiral symmetry breaking in isospin-asymmetric quark matter," in *3rd Conference on The Modern Physics of Compact Stars and Relativistic Gravity Yerevan, Armenia, September 30-October 3, 2015*. 2016. `arXiv:1602.04798 [hep-ph]`.

[11] M. Sadzikowski, "Coexistence of pion condensation and color superconductivity in two flavor quark matter," *Phys. Lett. B* **553** (2003) 45–50, `arXiv:hep-ph/0210065 [hep-ph]`.

[12] **Particle Data Group** Collaboration, K. A. Olive *et al.*, "Review of Particle Physics," *Chin. Phys.* **C38** (2014) 090001.

[13] M. A. Stephanov, "QCD phase diagram: An Overview," *PoS* **LAT2006** (2006) 024, arXiv:hep-lat/0701002 [hep-lat].

[14] Y. Aoki, Z. Fodor, S. D. Katz, and K. K. Szabo, "The QCD transition temperature: Results with physical masses in the continuum limit," *Phys. Lett.* **B643** (2006) 46–54, arXiv:hep-lat/0609068 [hep-lat].

[15] **Wuppertal-Budapest** Collaboration, S. Borsanyi, Z. Fodor, C. Hoelbling, S. D. Katz, S. Krieg, C. Ratti, and K. K. Szabo, "Is there still any Tc mystery in lattice QCD? Results with physical masses in the continuum limit III," *JHEP* **09** (2010) 073, arXiv:1005.3508 [hep-lat].

[16] A. Bazavov *et al.*, "The chiral and deconfinement aspects of the QCD transition," *Phys. Rev.* **D85** (2012) 054503, arXiv:1111.1710 [hep-lat].

[17] Y. Nambu, "Quasiparticles and Gauge Invariance in the Theory of Superconductivity," *Phys. Rev.* **117** (1960) 648–663.

[18] J. Goldstone, "Field Theories with Superconductor Solutions," *Nuovo Cim.* **19** (1961) 154–164.

[19] G. 't Hooft, "Symmetry breaking through Bell-Jackiw anomalies," *Phys. Rev. Lett.* **37** (1976) 8–11.

[20] G. 't Hooft, "How Instantons Solve the U(1) Problem," *Phys. Rept.* **142** (1986) 357–387.

[21] J. B. Kogut and D. K. Sinclair, "Lattice QCD at finite isospin density at zero and finite temperature," *Phys. Rev.* **D66** (2002) 034505, arXiv:hep-lat/0202028 [hep-lat].

[22] D. Müller, M. Buballa, and J. Wambach, "Dyson-Schwinger study of chiral density waves in QCD," *Phys. Lett.* **B727** (2013) 240–243, arXiv:1308.4303 [hep-ph].

[23] T. Kojo, Y. Hidaka, L. McLerran, and R. D. Pisarski, "Quarkyonic Chiral Spirals," *Nucl. Phys.* **A843** (2010) 37–58, arXiv:0912.3800 [hep-ph].

[24] W. Broniowski, A. Kotlorz, and M. Kutschera, "Quarks with a pion condensate. A new phase of matter," *Acta Phys. Polon.* **B22** (1991) 145–166.

[25] E. Nakano and T. Tatsumi, "Chiral symmetry and density wave in quark matter," *Phys. Rev.* **D71** (2005) 114006, arXiv:hep-ph/0411350 [hep-ph].

[26] D. Nickel, "Inhomogeneous phases in the Nambu-Jona-Lasino and quark-meson model," *Phys. Rev.* **D80** (2009) 074025, arXiv:0906.5295 [hep-ph].

[27] A. N. Sissakian, A. S. Sorin, and for the NICA Collaboration, "The nuclotron-based ion collider facility (nica) at jinr: new prospects for heavy ion collisions and spin physics," *Journal of Physics G: Nuclear and Particle Physics* **36** no. 6, (2009) 064069.

[28] N. Cabibbo and G. Parisi, "Exponential Hadronic Spectrum and Quark Liberation," *Phys. Lett.* **B59** (1975) 67–69.

[29] M. Asakawa and K. Yazaki, "Chiral Restoration at Finite Density and Temperature," *Nucl. Phys.* **A504** (1989) 668–684.

[30] M. G. Alford, K. Rajagopal, and F. Wilczek, "Color flavor locking and chiral symmetry breaking in high density QCD," *Nucl. Phys.* **B537** (1999) 443–458, `arXiv:hep-ph/9804403 [hep-ph]`.

[31] U. Vogl and W. Weise, "The Nambu and Jona Lasinio model: Its implications for hadrons and nuclei," *Prog. Part. Nucl. Phys.* **27** (1991) 195–272.

[32] S. P. Klevansky, "The Nambu-Jona-Lasinio model of quantum chromodynamics," *Rev. Mod. Phys.* **64** (1992) 649–708.

[33] T. Hatsuda and T. Kunihiro, "QCD phenomenology based on a chiral effective Lagrangian," *Phys. Rept.* **247** (1994) 221–367, `arXiv:hep-ph/9401310 [hep-ph]`.

[34] M. Buballa, "NJL-model analysis of dense quark matter," *Phys. Rept.* **407** (2005) 205–376, `arXiv:hep-ph/0402234 [hep-ph]`.

[35] Y. Nambu and G. Jona-Lasinio, "Dynamical Model of Elementary Particles Based on an Analogy with Superconductivity. 1.," *Phys. Rev.* **122** (1961) 345–358.

[36] Y. Nambu and G. Jona-Lasinio, "Dynamical Model of Elementary Particles Based on an Analogy with Superconductivity. 2.," *Phys. Rev.* **124** (1961) 246–254.

[37] K. Fukushima, "Chiral effective model with the Polyakov loop," *Phys. Lett.* **B591** (2004) 277–284, `arXiv:hep-ph/0310121 [hep-ph]`.

[38] M. Hempel, V. Dexheimer, S. Schramm, and I. Iosilevskiy, "Noncongruence of the nuclear liquid-gas and deconfinement phase transitions," *Phys. Rev.* **C88** no. 1, (2013) 014906, `arXiv:1302.2835 [nucl-th]`.

[39] J. Steinheimer, J. Randrup, and V. Koch, "Non-equilibrium phase transition in relativistic nuclear collisions: Importance of the equation of state," *Phys. Rev.* **C89** no. 3, (2014) 034901, `arXiv:1311.0999 [nucl-th]`.

[40] I. Iosilevskiy, "Entropic and enthalpic phase transitions in high energy density nuclear matter," in *Compact Stars in the QCD Phase Diagram IV Prerow, Germany, September 26-30, 2014*. 2015. `arXiv:1504.05850 [nucl-th]`.

[41] M. Frank, M. Buballa, and M. Oertel, "Flavor mixing effects on the QCD phase diagram at nonvanishing isospin chemical potential: One or two phase transitions?," *Phys. Lett.* **B562** (2003) 221–226, arXiv:hep-ph/0303109 [hep-ph].

[42] G. 't Hooft, "Computation of the Quantum Effects Due to a Four-Dimensional Pseudoparticle," *Phys. Rev.* **D14** (1976) 3432–3450. [Erratum: Phys. Rev.D18,2199(1978)].

[43] M. Buballa and S. Carignano, "Inhomogeneous chiral condensates," *Prog. Part. Nucl. Phys.* **81** (2015) 39–96, arXiv:1406.1367 [hep-ph].

[44] J. I. Kapusta and C. Gale, *Finite-temperature field theory: Principles and applications*. Cambridge University Press, 2011.

[45] D. Nowakowski, M. Buballa, S. Carignano, and J. Wambach, "Inhomogeneous chiral symmetry breaking phases in isospin-asymmetric matter," in *Compact Stars in the QCD Phase Diagram IV Prerow, Germany, September 26-30, 2014*. 2015. arXiv:1506.04260 [hep-ph].

[46] S. Carignano, D. Nickel, and M. Buballa, "Influence of vector interaction and Polyakov loop dynamics on inhomogeneous chiral symmetry breaking phases," *Phys. Rev.* **D82** (2010) 054009, arXiv:1007.1397 [hep-ph].

[47] F. Dautry and E. M. Nyman, "Pion condensation and the sigma model in liquid neutron matter," *Nucl. Phys.* **A319** (1979) 323–348.

[48] S. Carignano and M. Buballa, "Two-dimensional chiral crystals in the NJL model," *Phys. Rev.* **D86** (2012) 074018, arXiv:1203.5343 [hep-ph].

[49] O. Schnetz, M. Thies, and K. Urlichs, "Phase diagram of the Gross-Neveu model: Exact results and condensed matter precursors," *Annals Phys.* **314** (2004) 425–447, arXiv:hep-th/0402014 [hep-th].

[50] M. Thies, "From relativistic quantum fields to condensed matter and back again: Updating the Gross-Neveu phase diagram," *J. Phys.* **A39** (2006) 12707–12734, arXiv:hep-th/0601049 [hep-th].

[51] G. Basar and G. V. Dunne, "A Twisted Kink Crystal in the Chiral Gross-Neveu model," *Phys. Rev.* **D78** (2008) 065022, arXiv:0806.2659 [hep-th].

[52] F. Correa, G. V. Dunne, and M. S. Plyushchay, "The Bogoliubov/de Gennes system, the AKNS hierarchy, and nonlinear quantum mechanical supersymmetry," *Annals Phys.* **324** (2009) 2522–2547, arXiv:0904.2768 [hep-th].

[53] G. Basar, G. V. Dunne, and M. Thies, "Inhomogeneous Condensates in the Thermodynamics of the Chiral NJL(2) model," *Phys. Rev.* **D79** (2009) 105012, arXiv:0903.1868 [hep-th].

[54] D. Nickel, "How many phases meet at the chiral critical point?," *Phys. Rev. Lett.* **103** (2009) 072301, arXiv:0902.1778 [hep-ph].

[55] D. Nickel, "Inhomogeneous phases near the chiral critical point in NJL-type models," *PoS* **CPOD2009** (2009) 019, arXiv:0908.3711 [hep-ph].

[56] S. Carignano, E. J. Ferrer, V. de la Incera, and L. Paulucci, "Crystalline chiral condensates as a component of compact stars," *Phys. Rev.* **D92** no. 10, (2015) 105018, arXiv:1505.05094 [nucl-th].

[57] M. Buballa and S. Carignano, "Inhomogeneous chiral symmetry breaking in dense neutron-star matter," 2015. arXiv:1508.04361 [nucl-th].

[58] M. Kutschera, W. Broniowski, and A. Kotlorz, "Quark Matter With Pion Condensate in an Effective Chiral Model," *Nucl. Phys.* **A516** (1990) 566–588.

[59] R. C. Tolman, "Static solutions of einstein's field equations for spheres of fluid," *Phys. Rev.* **55** (Feb, 1939) 364–373.

[60] J. R. Oppenheimer and G. M. Volkoff, "On massive neutron cores," *Phys. Rev.* **55** (Feb, 1939) 374–381.

[61] P. Demorest, T. Pennucci, S. Ransom, M. Roberts, and J. Hessels, "Shapiro Delay Measurement of A Two Solar Mass Neutron Star," *Nature* **467** (2010) 1081–1083, arXiv:1010.5788 [astro-ph.HE].

[62] J. Antoniadis *et al.*, "A Massive Pulsar in a Compact Relativistic Binary," *Science* **340** (2013) 6131, arXiv:1304.6875 [astro-ph.HE].

[63] M. G. Alford, A. Schmitt, K. Rajagopal, and T. Schäfer, "Color superconductivity in dense quark matter," *Rev. Mod. Phys.* **80** (2008) 1455–1515, arXiv:0709.4635 [hep-ph].

[64] I. E. Frolov, V. C. Zhukovsky, and K. G. Klimenko, "Chiral density waves in quark matter within the Nambu-Jona-Lasinio model in an external magnetic field," *Phys. Rev.* **D82** (2010) 076002, arXiv:1007.2984 [hep-ph].

[65] B. C. Barrois, "Superconducting Quark Matter," *Nucl. Phys.* **B129** (1977) 390.

[66] D. Bailin and A. Love, "Superfluidity and Superconductivity in Relativistic Fermion Systems," *Phys. Rept.* **107** (1984) 325.

[67] M. G. Alford, K. Rajagopal, and F. Wilczek, "QCD at finite baryon density: Nucleon droplets and color superconductivity," *Phys. Lett.* **B422** (1998) 247–256, arXiv:hep-ph/9711395 [hep-ph].

[68] R. Rapp, T. Schäfer, E. Shuryak, and M. Velkovsky, "Diquark bose condensates in high density matter and instantons," *Phys. Rev. Lett.* **81** (Jul, 1998) 53–56.

[69] B. S. Chandrasekhar, "A note on the maximum critical field of high-field superconductors," *Appl. Phys. Lett.* **1** no. 1, (1962) 7–8.

[70] P. F. Bedaque, "Color superconductivity in asymmetric matter," *Nucl. Phys.* **A697** (2002) 569–577, arXiv:hep-ph/9910247 [hep-ph].

[71] A. Clogston, "Upper Limit for the Critical Field in Hard Superconductors," *Phys. Rev. Lett.* **9** (1962) 266–267.

[72] M. Sadzikowski, "Comparison of the non-uniform chiral and 2SC phases at finite temperatures and densities," *Phys. Lett.* **B642** (2006) 238–243, arXiv:hep-ph/0609186 [hep-ph].

[73] S. Carignano and M. Buballa, "Inhomogeneous islands and continents in the Nambu–Jona-Lasinio model," *Acta Phys. Polon. Supp.* **5** (2012) 641–658, arXiv:1111.4400 [hep-ph].

[74] S. Vereeken, "Chiral symmetry breaking phases at high chemical potential in the NJL model," bachelor thesis, TU Darmstadt, 2015.

[75] A. Heinz, F. Giacosa, M. Wagner, and D. H. Rischke, "Inhomogeneous condensation in effective models for QCD using the finite-mode approach," *Phys. Rev.* **D93** no. 1, (2016) 014007, arXiv:1508.06057 [hep-ph].

[76] D. Nowakowski, "Inhomogeneous phases and color superconductivity in the NJL model," master thesis, TU Darmstadt, 2012.

[77] G. Baym, B. L. Friman, and G. Grinstein, "Fluctuations and long range order in finite temperature pion condensates," *Nucl. Phys.* **B210** (1982) 193–209.

[78] S. Carignano, M. Buballa, and B.-J. Schaefer, "Inhomogeneous phases in the quark-meson model with vacuum fluctuations," *Phys. Rev.* **D90** no. 1, (2014) 014033, arXiv:1404.0057 [hep-ph].

[79] W. Pauli and F. Villars, "On the Invariant regularization in relativistic quantum theory," *Rev. Mod. Phys.* **21** (1949) 434–444.

[80] J. Gasser and H. Leutwyler, "Low energy theorems as precision tests of QCD," *Physics Letters B* **125** no. 4, (1983) 325 – 329.

[81] M. Kutschera, W. Broniowski, and A. Kotlorz, "Quark Matter With Neutral Pion Condensate," *Phys. Lett.* **B237** (1990) 159.

Acknowledgments

At this point I want to thank all the people, who have supported me throughout this PhD project and allowed me to carry out this research.

First of all, I would like to thank Prof. Jochen Wambach for giving me the opportunity to work on this interesting topic in his group, for the interest in my work, and for his continuous support in all possible ways, which was always of great help.

I am especially grateful to Priv.-Doz. Dr. Michael Buballa for his assistance, support and guidance throughout the last years. He was always patient, interested in my work and on every single occasion I had questions or problems he was able to help me and had valuable advices. He has always been a great supervisor and friend. Without him, substantial parts of this work would not be possible.

Special thanks also goes to Dr. Stefano Carignano, who always contributed to my work and supported me, provided suggestions and with him I discussed interesting physics questions.

I very much enjoyed the good working environment at the Theory Center of the Institute for Nuclear Physics at the TU Darmstadt and I'd like to thank all of my colleagues. In particular, I'd like to thank Dr. Piotr Piasecki, Dr. Daniel Müller, Dr. Pascal Büscher, Dr. Ralf-Arno Tripolt, Marco Schramm, Phillip Scior, Lukas Holicki and Dr. David Scheffler for an inspiring and stimulating atmosphere and their help. Special thanks also goes to Philipp and Marco for proof-reading the draft of my thesis. Another thanks also goes to Prof. Dr. Dirk Rischke for many helpful advises and interesting discussions during all the held PhD committees and beyond.

Finally, I want to thank my family for their invaluable and ongoing support during all my life.

Diese Arbeit widme ich, in stillem Gedenken, Wilma Kadel.

Lebenslauf

Name	Daniel Nowakowski
Geburtsdatum	2. Mai 1986
Geburtsort	Heidelberg
Staatsangehörigkeit	Deutsch
Familienstand	Ledig

08/2014 - 03/2016	Wissenschaftlicher Mitarbeiter am Institut für Kernphysik der Technischen Universität Darmstadt
SS 2012 - WS 2015	Promotionsstudium in Physik an der Technischen Universität Darmstadt
02/2012	Abschluss “M. Sc. in Physics” Thesis: “Inhomogeneous phases and color superconductivity in the NJL model”
11/2009 - 02/2012	Masterstudium Physik an der Technischen Universität Darmstadt
10/2009	Abschluss “B. Sc. in Physik” Thesis: “CAST - Skysurvey: Stellar Axion Models”
10/2006 - 10/2009	Bachelorstudium Physik an der Technischen Universität Darmstadt
08/2005 - 04/2006	Zivildienst im Kreiskrankenhaus Heppenheim
1996 - 2005	Schulbesuch Martin-Luther-Schule, Rimbach Abschluss: Allgemeine Hochschulreife

Erklärung zur Dissertation

Hiermit versichere ich, die vorliegende Dissertation ohne Hilfe Dritter nur mit den angegebenen Quellen und Hilfsmitteln angefertigt zu haben. Alle Stellen, die aus Quellen entnommen wurden, sind als solche kenntlich gemacht. Diese Arbeit hat in gleicher oder ähnlicher Form noch keiner Prüfungsbehörde vorgelegen.

Darmstadt, den 06.04.2016

_____

(Daniel Nowakowski)